

**Characterizing the distribution of microbial sulfate reduction in
Loki's Castle hydrothermal system of the Arctic Mid-Ocean
Ridge (AMOR)**

Jan-Kristoffer Landro



Master of Science Thesis

Department of Earth Science
University of Bergen

June 2016

Abstract

Studies on the distribution of microbial sulfate reduction, and its impact on the global carbon and sulfur cycle, have mostly been conducted in shallow and deep-marine sediments. Little is therefore known about the ecological impact that sulfate reducing bacteria have on element cycling in ecosystems that is associated with the nutrient rich hydrothermal sediments. The chemical disequilibrium created by the mixing of hydrothermal fluids and seawater, nourish a diversity of primary producers that provide nutrients for the anaerobic heterotrophic community. Diffuse venting areas, such as the barite field on the eastern flank of the hydrothermal mound at Loki's Castle, are promising target sites for exploring the impact of biogenic processes as temperatures are within the biological window. This study aims to characterize the distribution of sulfate reducing bacteria at this diffuse venting area by integrating direct measurement of sulfate reduction rates with geochemical analyses of pore fluids and microbiological methods. The spatial distribution of the fluid compositions and flow patterns seems to determine the distribution of the metabolically functional groups in the barite field, and functions as a geochemical constraint on the chemoautotrophic primary production. Hence, the divergent fluid pattern and energy supply determines the organic carbon production, which in turn determines the distribution of the heterotrophic community. This is reflected in the distribution of sulfate reduction, where sulfate reduction rates varied between 6-132 pmol/cm³ d in substrate-poor parts of the mound to 110 nmol/cm³ d in substrate-rich sediments. Sulfate reduction rate were also measured in a barite chimney, which was associated with effluent that was characterized by elevated concentrations of methane and H₂. The geochemical measurements show a high correlation between the hydrothermal fluid signature, organic carbon production and the distribution of the mesophilic heterotrophic sulfate reducing bacteria. The diffuse venting area displays temperatures that vary between 7.8 °C in the sediments with low activity, to ~20 °C in the chimney effluent. This provides habitable conditions for mesophilic and psychrotolerant members of Desulfobacterales, Desulfarculales and Desulfuromonadales order, which were all affiliated with the Deltaproteobacteria phylum. One psychrophilic sulfate reducing bacteria, *Desulfofaba gelida*, was detected in sediments that were associated with the lowest rates. The variable CH₄ and H₂ concentration between areas with high flow rate and low flow rate give strong indications for an additional deep sub-surface sulfate reduction zone, where anaerobic oxidation of methane coupled with sulfate reducing bacteria are an important sulfate sink, in addition to H₂ consumption by chemoautotrophic sulfate reducers and/or methanogens at more elevated temperatures.

Acknowledgment

Several people have contributed to this thesis. I would first of all like to thank my supervisor Desiree Roerdink for always being available. This would be a painful process without your tips and structuring. I also have to thank my other supervisor, Ingunn H. Thorseth, for keeping the stress level high enough. I also want to thank Steffen L. Jørgensen, which is always disposable even though he doesn't have to. I would also like to thank Anita-Elin Fedøy and Håkon Dahle for for their contribution to the DNA extraction, PCR and DNA sequencing, in addition to Ingeborg Økland for the geochemical data and help with the TOC measurement.

Contents

1. Introduction	1
2. Background	3
2.1. Dissimilatory sulfate reduction.....	3
2.2. Remineralization and geochemical zonation.....	5
2.3. Hydrothermal systems	10
3. Geological settings	14
4. Materials and methods.....	18
4.1. Sample locations.....	18
4.2. Pore fluid sampling and analysis.....	18
4.3.1. Sample preparation.....	18
4.3.2. Onboard incubation	19
4.3.3. Lab-based analyses	21
4.4. TIC/TOC	23
4.5. DNA extraction and PCR	23
5. Results	25
5.1. Background sediments	25
5.1.1. Pore fluid geochemistry.....	25
5.1.2. Sulfate reduction rates	25
5.1.3. Organic and inorganic carbon	25
5.1.4. Composition of the microbial community.....	29
5.2. The inactive sulfide mound	32
5.2.1. Pore fluid geochemistry.....	32
5.2.2. Sulfate reduction rates	32
5.2.3. Organic and inorganic carbon	32
5.2.4. Microbial community	35
5.3. Surface sediments from the barite field.....	37
5.3.1. Pore fluid geochemistry.....	37
5.3.2. Sulfate reduction rates	37
5.3.3. Organic and inorganic carbon	37
5.3.4. Composition of the microbial community.....	37
5.4. Active barite chimney from the barite field.....	40
5.4.1. Pore fluid geochemistry.....	40

5.4.2.	Sulfate reduction rates	40
5.4.3.	Organic and inorganic carbon	40
5.5.	Sediments from barite field	44
5.5.1.	Pore fluid geochemistry.....	44
5.5.2.	Sulfate reduction rates	45
5.5.3.	Organic and inorganic carbon	45
5.5.4.	Composition of the microbial community.....	50
6.	Discussion	52
6.1.	Geochemistry of hydrothermal and non-hydrothermal sediments	52
6.1.1.	Geochemistry of the background sediments.....	52
6.1.2.	Geochemistry of the barite field	53
6.2.	Distribution of SRB in the barite field	56
6.3.	Comparing LCVF with equivalent sites	58
6.3.1.	Rate differences	58
6.3.2.	Effect of temperature on sulfate reduction rates.....	59
6.3.3.	Effect of substrate availability on sulfate reduction rates.....	60
6.4.	The potential for an additional deep sulfate reduction zone.....	63
6.4.1.	Anaerobic oxidation of methane (AOM).....	63
6.4.2.	H ₂ consumption	66
7.	Conclusion.....	69
8.	Future work	70
9.1.	References	71
9.2.	weblink.....	77
Appendix 1	78

1. Introduction

For decades, deep-sea sediments were assumed to be almost biologically inert due to their low energy flux, distance from the euphotic zone, high pressure and low temperature. Even so, drilling programs during the last decades have shown a highly diverse microbial community throughout the whole sediment column (*e.g. D'Hondt et al, 2002; Jørgensen and D'Hondt, 2006; Jørgensen and Boetius, 2007; Robador et al, 2015*), that accounts for about 55-85 % of the prokaryotic biomass, and 30% of the total living biomass (*D'Hondt et al, 2002; Jørgensen and D'Hondt, 2006*). However, the lack of liable substrates limits the metabolic rates and the prokaryotic density in the deep sediments. Research has shown that these organisms, living in an energy-depleted environment, experience substrate levels that barely sustain minimum metabolic requirements, and may therefore be dormant or dead (*Jørgensen and D'Hondt, 2006*). These conditions contrast the sediment conditions on the continental shelf, where the proximity to the euphotic zone causes high energy fluxes and carbon supply from primary production. The energy flux leads to increasing activity within the diverse population of microorganisms and the subsequent consumption of a variety of electron acceptors during remineralization of organic carbon. In these areas, the oxygen is consumed in the top mm to cm of the sediments, making most of the sediment column anoxic. For this reason, anoxic respiration by the reduction of sulfate dominates the continental shelf and coastal areas. However, while microbial communities in both deep-sea sediments and epi-continental ocean areas depend on photosynthetic primary production, deep-sea hydrothermal vent systems represent biological “hot-spots” where the food web is more or less independent from the surface activity. The reduced fluids emanating through conduits create a contrast in redox conditions between the vent field and the surroundings that forms a chemical disequilibrium, which is utilized by chemoautotrophic primary producers. This chemical disequilibrium links the lithosphere to the biosphere and transforms a desert-like environment to an oasis of life with its own food web.

Accordingly, high concentrations of reduced components in hydrothermal fluids from the sediment-influenced Lokis Castle Vent Field (LCVF) on the Mohns-Knipovich Ridge, Norwegian Sea (*Pedersen et al, 2010; Baumberger, 2011*), nourish a diversity of primary producers that provide nutrients for the anaerobic heterotrophic community (*e.g. Govenar, 2012*). Moreover, low-temperature diffuse venting areas (≤ 110 °C) in hydrothermal systems, such as the barite field on the eastern flank of the hydrothermal mound at Loki's Castle, are promising target sites for exploring the impact of biogenic processes as temperatures are within the biological window. Here, the seawater mixing provides the subsurface community with sulfate, which creates a metastable disequilibrium that can sustain microbial sulfate reduction. The utilization of sulfate by autotrophic or heterotrophic microorganisms plays a major role in both the sulfur and carbon cycle in these habitats (*McCollom & Shock, 1997*), as microbial sulfate reducers can be responsible for up to 80% of carbon oxidation in

modern marine systems (*Canfield et al. 1993*). In addition, microbial sulfate reduction may represent one of the oldest metabolisms on Earth, and evidence from the ancient rock record suggests early microbial activity in analogous hydrothermal settings (*e.g. Shen et al., 2001; Ueno et al., 2008; Roerdink et al., 2012, 2013*). Thus, understanding the roles and distribution of microbial sulfate reducers in these hydrothermal environments is essential for our understanding and quantification of sulfur and carbon cycles in the ancient and modern deep sea.

Yet, only a few studies have been conducted on the measurement of *in situ* metabolic rates and the distribution of microbial sulfate reduction in hydrothermal systems (*e.g. Jørgensen et al., 1992; Elsgaard et al., 1994a, b; Weber and Jørgensen, 2002; Kallmeyer and Boetius, 2004; Frank et al., 2013*). This can be attributed to the challenges with recreating artificial hydrothermal conditions and difficulties with sampling (*Frank, et al 2013*). However, previous studies of the LCVF have shown indications of microbially induced sulfate reduction (*Jaeschke et al., 2012; Eickmann et al., 2014; Steen et al., 2016*) in sediments and chimneys in the active barite field. This thesis will be the first to directly quantify the rates of microbial sulfate reduction and the distribution of sulfate reducing microorganisms in the Loki's Castle Vent Field. The main objectives of this thesis are to:

- Determine the lateral and vertical distribution and activity of sulfate reducers
- Determine the influence of electron donors (hydrogen, methane, organic carbon) on the distribution and activity of sulfate reducers
- Determine the phylogeny of the sulfate reducers.

Samples were obtained by gravity coring and using the Ægir 6000 remotely operated vehicle (ROV) during the Centre for Geobiology summer cruises of 2014 and 2015 on the R/V G. O. Sars. Gravity core GS14-GC14 was sampled by Desiree Roerdink during the cruise in 2014. Geochemical analyses pH and alkalinity were conducted by Ingunn H. Thorseth, Desiree Roerdink and Ingeborg Økland, respectively, while dissolved methane was measured by Tamara Baumberger.

2. Background

2.1. Dissimilatory sulfate reduction

Dissimilatory sulfate reduction (DSR) is one of the most prevalent metabolic pathways in anoxic marine sediments, and serves as a major sink for marine sulfur and organic carbon (*Knoblauch et al, 1999; Kasten and Jørgensen, 2006; Bowles et al, 2014*). Members of some deeply branched phylogenetic groups perform this pathway in both prokaryotic domains, which reflects the antiquity of the metabolic pathway (*Shen and Buick, 2003*). The archaeal sulfate reducers comprise of two lineages, while five belong to the bacterial domain (*Muyzers and Stam, 2008*). The archaeal sulfate reducers belong to the *Archaeaoglobus* genus in the Euryarchaeal phylum and the *Thermocladium* and *Caldivirga* genus in the Crenarchaeota phylum. All archaeal sulfate reducers are thermophilic/hyperthermophilic, where some can grow at 105°C (*Stetter, 1996; Rabus et al, 2004; Kasten and Jørgensen, 2006*). Thermophiles and hyperthermophiles are also found amongst three bacterial lineages, including Nitrospirae (*Thermodesulfovibrio* genus), Thermodesulfobacteria (*Thermodesulfobacterium* genus) and Thermodesulfobiaceae (*Muyzer and Stam, 2008*). However, since the majority (95%) of the ocean is below 4 °C (*Sawicka et al, 2012*), most taxa from the bacterial domain are mesophilic/psychrotolerant and reside in marine sediments (*Isaksen and Jørgensen, 1996; Konhauser, 2007*). All of them use SO₄²⁻ as the primary electron acceptor, and either organic carbon or H₂ as electron donor (*e.g. Madigan et al, 2013*) according to the simplified formula:



Or



While all sulfate reducing bacteria (SRB) can utilize H₂ as an electron donor (*Madigan et al, 2013*), their ability to degrade organic carbon differs. Hence, SRB are divided into two groups; those that degrade organic carbon completely to CO₂ (complete oxidizers) and those that degrade organic carbon incompletely to acetate (incomplete oxidizers) (*e.g. Konhauser, 2007; Muyzer and Stam, 2008; Madigan et al, 2013*). Most marine SRB degrade acetate to CO₂ and depend on fermenters to degrade the organic carbon to short-chained carbon molecules (*e.g. Madigan et al, 2013*).

The importance and ubiquity of the SRB in the marine sediments are mostly attributed to the abundance of sulfate in the oceans (~29 mM), along with their metabolic flexibility (*e.g. Plugge et al, 2011*). The range of different electron acceptors they can utilize varies amongst the different groups, where some SRB can substitute sulfate with iron, nitrate and uranium (VI) if necessary (*Konhauser, 2007, Muyzers and Stam, 2008*). Some sulfate reducers, like *Desulfobacter postgatei*, and some *Desulfovibrio* strains, have demonstrated the ability to survive 3 to 20 hours of oxygen exposure in well-aerated biotopes (*Jonkers et al, 2003*). One species, *Desulfovibrio oxycliniae*, can even grow

using oxygen as an electron acceptor (Hansen, 1994; Jonkers et al, 2003, Rabus et al, 2004). Since organic matter produced from primary production in the euphotic zone is their primary nutrient source, the distribution of sulfate reducers in marine sediments are commonly regulated by sedimentation rates and burial fluxes of organic matter (Konhauser, 2007; D`Hondt et al, 2009; Bowles et al, 2014), which are controlled by water depth and distance from land (fig. 1). Consequently, the deep-sea biosphere has a very low nutrient and energy flux (Jørgensen, 2012) since most of the organic matter needed for DSR is remineralized during the upper 100-200 m of the water column (Sarmiento and Gruber, 2006). Despite this, DSR is still one of the most dominating metabolism controlling organic carbon remineralization. In addition, some sulfate reducing bacteria have been shown to form consortia with anaerobic methane oxidizing archaea (ANME) in the transition zone between sulfate reduction and methane production in marine sediments and cold seeps (e.g. Knittel and Boetius, 2009; de Beer et al, 2006; Plugge et al, 2011). The methane consuming archaea belong to three distinct groups of Euryarchaeota (ANME-1, 2 and 3) that are phylogenetically affiliated with some methanogens related to the orders Methanosarcinales and Methanomicrobiales (e.g. Knittel and Boetius, 2009). The ANME mediate the anaerobic oxidation of methane (AOM) in the marine sediments with the aid of sulfate where the reaction can be written as:



ANME always co-occurs with SRB where AOM occurs (Orphan et al, 2002; Martin et al, 2008; Brazelton et al, 2006). The SRB belong to the Deltaproteobacteria lineages that include *Desulfosarcina/Desulfococcus* where ANME-1 and ANME-2 are often associated with group in the Desulfobacterales order.

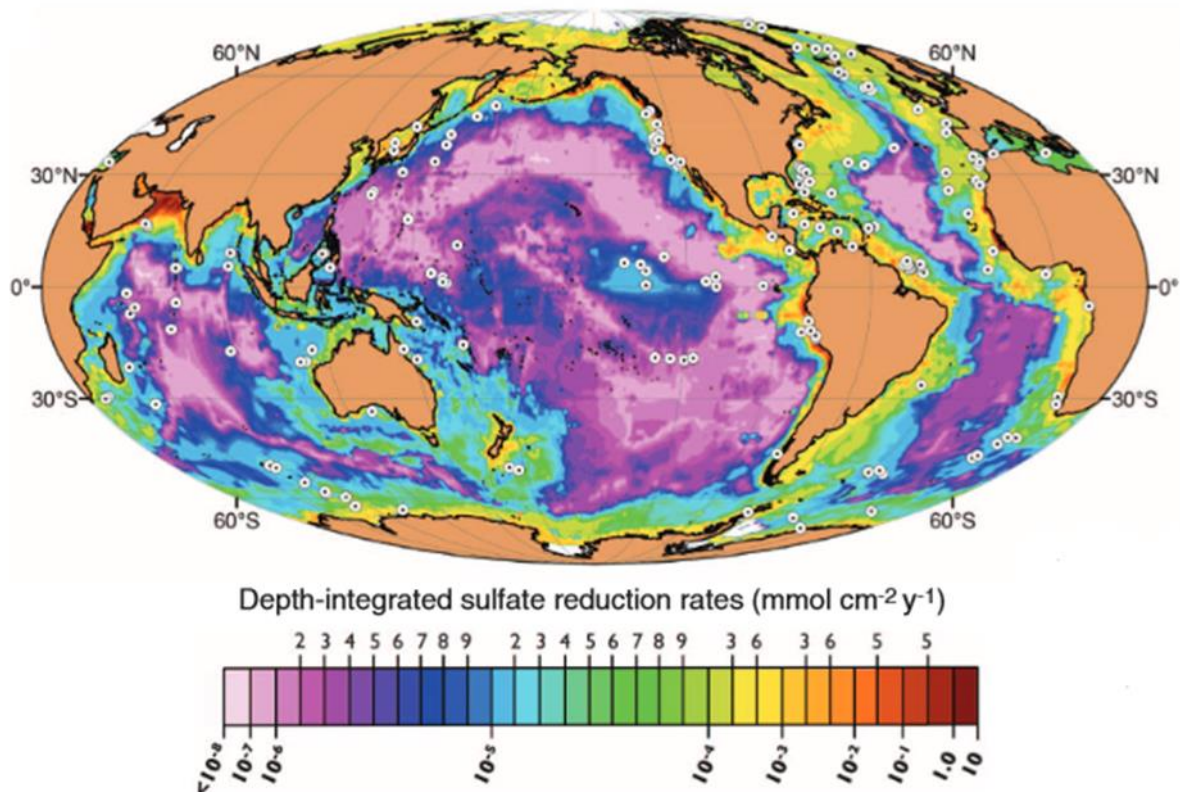


Figure 1. Distribution of SRR in marine habitats. The red areas represents high activity zones and are characterized by high sedimentation rates and high supply of marine and terrigenous organic carbon. Open ocean areas display lower sedimentation rate and lower organic carbon flux to the deep-marine sediments, hence, lower SRR (Bowles et al, 2014).

2.2. Remineralization and geochemical zonation

The geochemical composition of the seawater results from a balance between external inputs and removal rates, where microbial respiration plays an important role as a source and sink for carbon compounds. Yearly, 4040 Tmol carbon is fixed in marine biomass, whereas only 190 Tmol organic carbon is deposited on the sea floor. 82 % is precipitated in shallow areas like continental shelves, and 16% is deposited on the continental slope (Kasten and Jørgensen, 2006; Wallmann and Aloisi, 2013). The most labile (e.g. easily degraded) organic matter transported from the euphotic zone is re-oxidized in the first hundred meters of the water column, leaving the refractory carbon compounds as precipitates on the seafloor (Sarmiento and Gruber, 2006; Konhauser, 2007). This renders aerobic microbial communities in deep-sea sediments with a larger fraction of recalcitrant (stable) carbon compounds, which hampers their respiration rates in the sediment-water interface, and causes oxygen to penetrate deeper into the sediment (e.g. D'Hondt et al, 2002; Sarmiento and Gruber, 2006; Orcutt et al, 2011; Bowles et al, 2014). The efficiency of the aerobic remineralization process in the water column leaves the oligotrophic deep ocean sediments almost biologically inert compare to habitats in contact with the primary production in the euphotic zone (e.g. Burdige, 2002; Sarmiento and Gruber,

2006; Bowles *et al*, 2014). Consequentially, the low accumulation rates ($<0.001 \text{ g C cm}^{-2} \text{ yr}^{-1}$), and low sedimentation rates in the deep ocean (0.01 mm y^{-1}) makes the precipitated organic matter exposed to oxygen over a longer time until the most labile compounds are degraded (Konhauser, 2007 and fig. 2). In these areas the aerobic respiration accounts for $>90\%$ of the remineralization in the subsurface sediments, displacing the anaerobic respiration $>1.5 \text{ mbsfl}$. In contrast, shallow areas gain 25-50% of the primary production as deposits on the sea floor (Jørgensen, 2006), with a higher fraction of the labile carbon accessible to the anaerobic microbes. The high sedimentation rates in the shallow areas bury the organic carbon, shield it from the oxygen, and decrease the vertical distribution of terminal electron acceptors (TEA) in the pelagic sediments. Thus, oxygen only extends mm's to cm's into the sediment column. Therefore, anaerobic respiration accounts for a significant amount of the remineralization in coastal areas and continental margins (*e.g.* Sarmiento and Gruber, 2006; Bowles *et al*, 2014).

In the subsurface sediments, where oxygen is depleted, a cascade of potential electron acceptors is consumed according to the thermodynamically favorability, which creates a distinct zonation of microbial activity. The different heterotrophic communities continues to remineralize the organic matter aided by fermenters (*fig. 2 and table 1*). As mentioned above, the organic matter that is still preserved in the anoxic sediments represent the residual pool that was not consumed by aerobic respiration, which is why fermenters have to degrade the carbon to make it available for the other TEA's (Sarmiento and Gruber, 2006; Konhauser, 2007). In addition, the metabolic rates are significantly lower due to subsequently lower redox potential (*e.g.* D'hondt *et al*, 2002; Jørgensen and Boetius, 2007). When O_2 is depleted from the sediments, NO_3^- is the electron acceptor with the highest redox potential, followed by MnIV, FeIII, SO_4^{2-} and CO_2 (*table 1 and fig.3*) (*e.g.* Sarmiento and Gruber, 2006; Jørgensen, 2006; Konhauser, 2007; Canfield and Thamdrup, 2009).

NO_3^- is a product of aerobic microbial oxidation of NH_4^+ , where the rate of nitrate produced is dependent of the (i) depth of the oxic layer, (ii) amount of organic matter and (iii) rate of denitrification (Konhauser, 2007). The energy gain from this denitrification pathway is close to oxic remineralization and, like aerobe respirers, denitrifiers are capable of degrading organic carbon completely to CO_2 , making this one of the most important respiratory processes on the continental slope and rise.

The denitrification zone is underlain by the manganese zone. Here, manganese oxide becomes unstable and the most energetically favorable electron acceptor. These two zones may overlap, in which case the Mn^{2+} diffuses upwards and reduces nitrate to N_2 . In some cases, NH_4^+ can react with MnO_2 to produce N_2 and significantly affect the nitrification-denitrification process (Konhauser, 2007). The Mn-oxides scarcity in the sediments limits its importance in the remineralization process ($<10\%$), and in some settings it is insignificant (Sarmiento and Gruber, 2006; Konhauser, 2007).

The iron reduction zone is, like the manganese reduction zone, limited in comparison to the more volatile TEA's (O_2 , NO_3^-). Iron is immobile in oxic environments and is therefore scarce in the sediments far away from any potential source (continents, hydrothermal systems). The iron in the sediments is present in the form of iron hydroxides and is easy to reduce. The product of iron reduction also plays an important role in the sulfur cycle, where it acts as a sink for sulfide. The production of sulfide by sulfate reduction takes place in highly reduced environment where sulfate is the most energetic TEA and is, due to the abundance of dissolved sulfate in the ocean (~29 mM), one of the most important respiratory processes in marine sediments and strongly linked to carbon and iron cycles. According to Bowles et al (2014), 11.3 Tmoles of sulfate are reduced per year in the global oceans, where the highest rates can be found in shallow, epicontinental ocean areas, and the lowest rates in nutrient poor deep-sea sediments (*fig.1*) (*See also table. 6.3.1 in Sarmiento and Gruber, 2006*). It is estimated that only 7% of the sulfate reduction takes place below 2000 mbsfl (*Kasten and Jørgensen, 2006*). Considering the C:S stoichiometric ratio of 2:1 (Eq. 1), 11.3 Tmol sulfate should oxidize 22.6 Tmole organic carbon globally per year. Despite its relative insignificance in the vast regions of the deep sea, DSR is estimated to account for a large amount of the remineralization of organic carbon globally, with estimates ranging from 30 to 80% of the total annual remineralization flux (*Canfield et al, 1993; Kasten and Jørgensen, 2006; Bowles et al, 2014*). SRB therefore affect the carbon cycle significantly through remineralization in the the largest carbon reservoir on the planet. When sulfate is depleted, CO_2 becomes the most energetically favorable TEA. Methane is produced by methanogenic archaea that couple CO_2 with H_2 or acetate if the temperature conditions are suitable (*Reeburgh, 2007*). Since there is no subsequent electron donor after CO_2 , the methanogenic zone can continue until the carbon is unavailable.

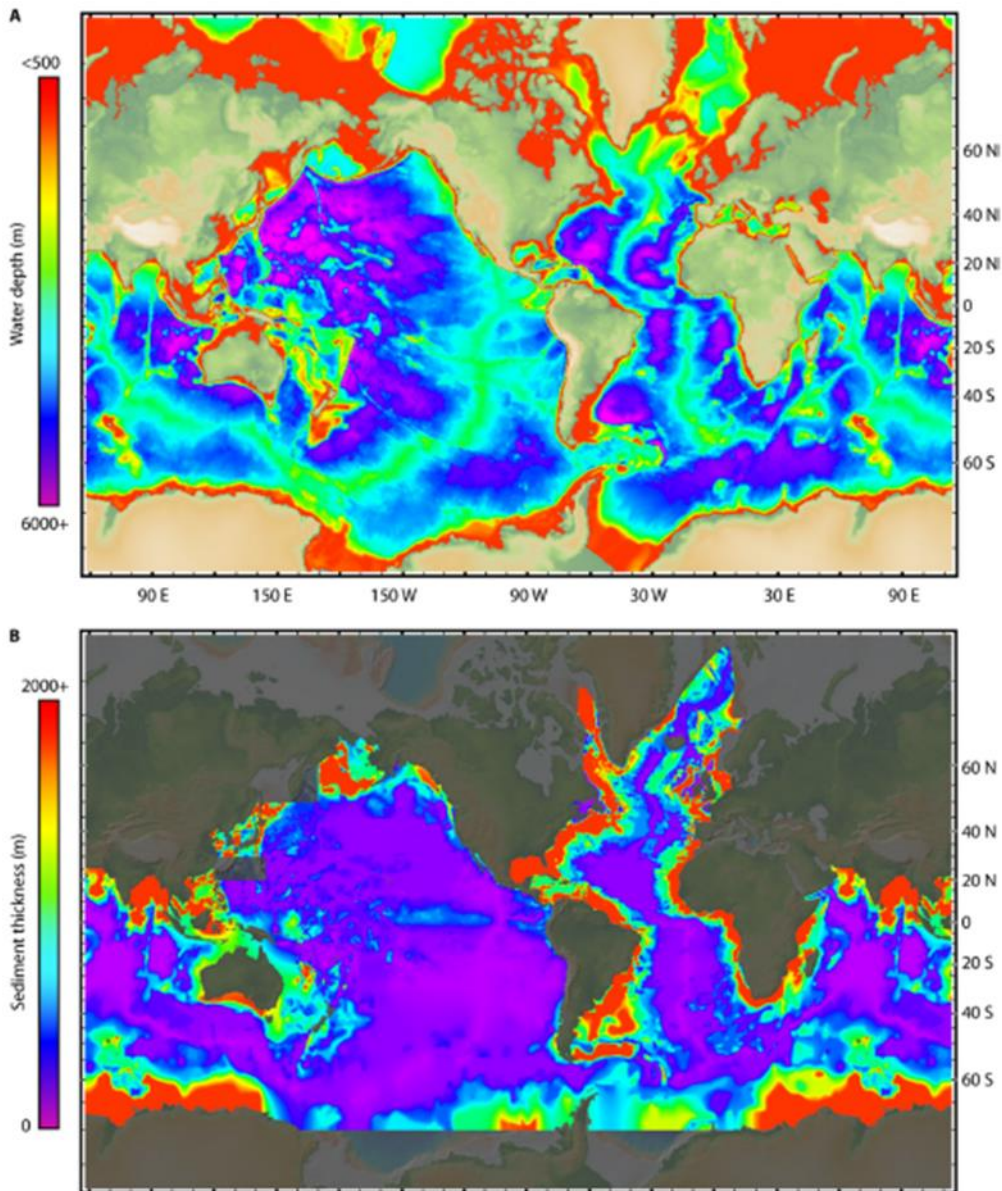


Figure 2. Overview of ocean depth (A) and sedimentation thickness (B). The sediment thickness increase close to the sediment source on the continental shelf's, while the sediments supply to the open oceans are scarce (Orcutt et al, 2011)

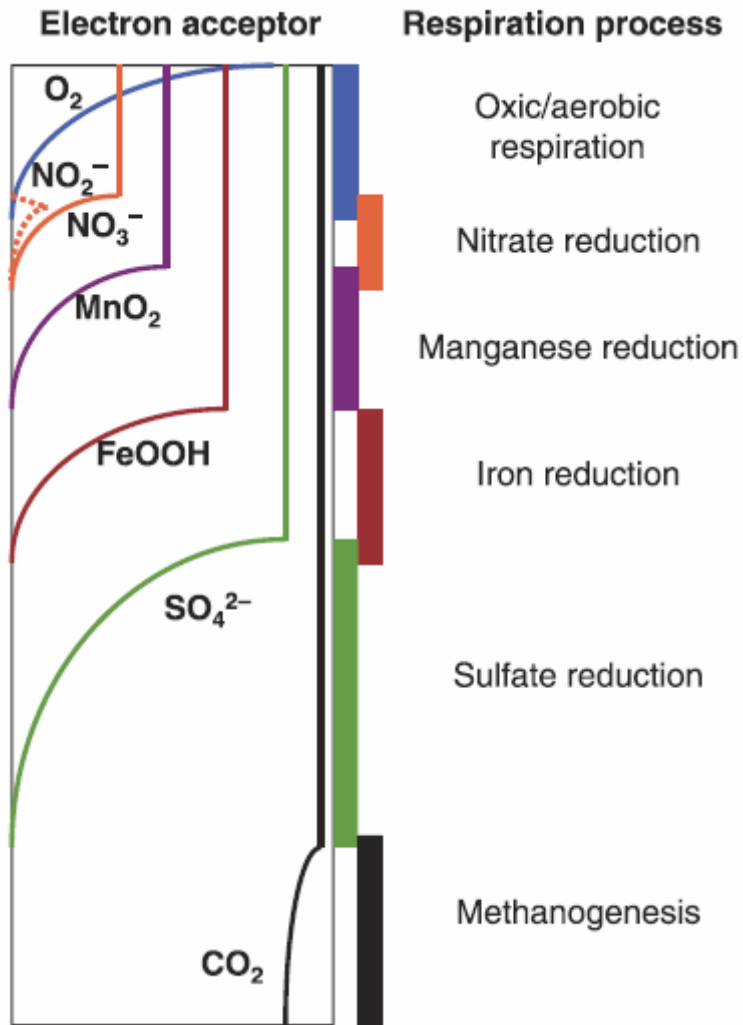


Figure 3. Simplified cartoon over the different geochemical zones based on respiration processes (Canfield and Thamdrup, 2009).

Table 1. Change in free energy during remineralization of organic matter by different respiratory processes down the sediment column (Sarmiento and Gruber, 2006).

Zone	Reactions	Free energy change (kJ mol ⁻¹)
Aerobic respiration	$\text{CH}_2\text{O} + \text{O}_2 \rightarrow \text{CO}_2 + \text{H}_2\text{O}$	-473
Denitrification	$5\text{CH}_2\text{O} + 4\text{NO}_3^- \rightarrow 2\text{N}_2 + 4\text{HCO}_3^- + \text{CO}_2 + 3\text{H}_2\text{O}$	-452
Manganese reduction	$\text{CH}_2\text{O} + 3\text{CO}_2 + \text{H}_2\text{O} + 2\text{MnO}_2 \rightarrow 2\text{Mn}^{2+} + 4\text{HCO}_3^-$	-388
Iron reduction	$\text{CH}_2\text{O} + 7\text{CO}_2 + 4\text{Fe}(\text{OH})_3 \rightarrow 4\text{Fe}^{2+} + 8\text{HCO}_3^- + 3\text{H}_2\text{O}$	-187
Sulfate reduction	$2\text{CH}_2\text{O} + \text{SO}_4^{2-} \rightarrow \text{H}_2\text{S} + 2\text{HCO}_3^-$	-82
Methanogenesis	$\text{CH}_2\text{O} \rightarrow \text{CO}_2 + \text{CH}_4$	-71

2.3. Hydrothermal systems

In contrast to the surrounding marine environments, deep-sea hydrothermal vents are characterized by flourishing life that is sustained by the steep redox and temperature gradients generated by the reduced hydrothermal fluids. The fluids often represent modified seawater that is depleted in Mg, sulfate and alkalinity and enriched in metals, such as Fe, Cu and Zn (*German and Seyfried, 2014*). This composition is the result of chemical reactions occurring during their movement through the oceanic basement, generated by conductive cooling of the crust, and contributes to the chemical alteration of the seafloor (*Alt, 1995*). The oceanic crust can roughly be divided into 3 main layers (*fig. 4*), as recognized from seismic surveys, ophiolites and direct sampling from the oceanic basement (*Alt, 1995*). The top layer comprises a porous volcanic section that mainly consists of pillow lava, breccia and lava flows, and is 0.1 – 1 km thick. Below this volcanic section, a higher density, less permeable sheeted dike section occurs that functioned as feeders to the overlying volcanic section. A several km thick layer of gabbro (*Alt, 1995*) underlies the sheeted dike section. Important physical parameters such as permeability, porosity, temperature and pressure changes through each section due to consecutive chemical reactions, and an increase in temperature with depth.

The hydrothermal circulation system can be categorized into three different zones (*fig. 5*): the *recharge zone*, *reaction zone* and *discharge zone*. During the movement of fluids through these zones, seawater is modified through processes including, water-rock reactions, phase separation and magmatic degassing (*e.g. German and Seyfried, 2014*). The recharge zone is located off-axis from the spreading ridge, and is part of the general circulation of seawater in the volcanic section. The circulation taking place in the volcanic section can be divided into open and restricted circulation. The

open circulation initiates the chemical alteration of the seawater, where oxidation of basaltic glass, olivine, plagioclase and primary sulfide minerals occurs (Alt, 1995; Tivey, 2007; German and Seyfried, 2014). The weathering causes the formation of celadonite and nontronite that fixate the alkali metals K, Rb, Cs and B (Alt, 1995, Von Dam, 1995). As the modified fluid descend, OH⁻ reacts with Mg and precipitates as smectite and chlorite, a process that consumes Mg in exchange for Na⁺, Ca⁺ and H⁺ (Tivey, 2007). This reaction takes place in the lower volcanic section at elevated temperatures (≤ 200 °C). The fluid that reaches the sheeted dikes section has obtained a more reducing character, and is depleted in Mg and alkalis. When the temperature increases above 150 °C, seawater sulfate reacts with Ca to form anhydrite. This reaction consumes all the Ca from the fluids in addition to ca 1/3 of the sulfate (Alt, 1995; Tivey, 2007; German and Seyfried, 2014). In addition, smectite formation lowers the pH and causes the leaching of alkalis. At temperatures above 250 °C, sulfate can be reduced abiotically through reactions with pyrrhotite, which leads to a small increase in $\delta^{34}\text{S}$ for the sulfide (Alt, 1995; German and Seyfried, 2014).

The fluid composition in the reaction zone differs somewhat from the original seawater composition with lower pH, Mg-depletion, and reduced compounds. It is assumed that the hydrothermal fluids get their chemical signature in this section, which occurs in the base of the sheeted dike section (German and Seyfried, 2014). The hot fluid contribute to leaching of S, Zn, Fe, Mn from the lower sheeted dikes, in addition to contribution of magmatic volatiles like H₂, CO₂, H₂O, CH₄ and ³He (Alt, 1995, Tivey, 2007). Other chemical changes to the rock include Ca, K, Rb and Ti-depletion. The fluid temperature at this depth can exceed 400 °C, which creates physical conditions close to the critical point of water. When reaching the critical point, water density and viscosity decrease, and the limit of thermal expansion and heat capacity is reached. This creates enough buoyancy to displace the overlaying seawater and transported fluids through the crust at ca. 0.7 – 5 m s⁻¹ (Alt, 1995). At this point the Fe and Mn are enriched relative to Cl. Cl is generally very conservative in hydrothermal systems and is not gained or lost during the circulation (e.g. Elderfield and Schultz, 1996; German and Seyfried, 2014).

The section where fluids starts to rise is called the discharge zone (Alt, 1995), and can roughly be divided into *focused* and *diffuse* up-flow zones, depending on the degree of channelling of the fluids. Focused up-flow zones often leads to the formation of black smoker vent systems and massive sulfide deposits. The fluids in these channelled flows will be enriched in Li, K, Rb, Cs, SiO₂, Fe, H₂S, CO₂, He, H₂ and CH₄ (e.g. Kelly et al, 2002). At temperatures over 300 °C, the fluid is hot enough to transport dissolved components like silica, Ca²⁺ and SO₄²⁻ (>150 °C) and Ba that precipitate when entering the surface. The first minerals to precipitate is silica and barite, creating a barrier between the fluid and seawater. This lead to precipitation of sulfides and anhydrite as the insulation provides progressively hotter fluids to precipitate ZnS and Fe (Hannington et al, 1995). When the fluids are sufficiently insulated to penetrate the seafloor without mixing with the seawater, black smokers are

formed. The fluid represents an end-member composition and can reach temperatures of $>300\text{ }^{\circ}\text{C}$. This allows for transportation of metals and sulfides, and precipitation of anhydrite when reacted with seawater. In contrast to the focused flow, the diffuse flow is not isolated from the surrounding environment, and will eventually mix with down welling seawater in the subsurface (Alt, 1995). Subsurface mixing with cold seawater causes precipitation of sulfides and dissolved metals. When entering the surface, these fluids have a temperature of $<10\text{-}50\text{ }^{\circ}\text{C}$ and are too cold to sustain dissolved metals, but they are enriched in gases like CH_4 and the remaining sulfide (Hannington et al, 1995). Fe-oxide and Mn-oxide can in some settings precipitate as crusts along fractures on the surface, although they are commonly scavenged by sulfide deeper into the mound. Thus, the low-temperature diffuse flow is the product of complex subsurface processes that include; seawater-hydrothermal fluid mixing, conductive cooling, various redox reactions, and mineral precipitation (Nakamura and Takai, 2014). Habitable temperatures together with a mixture of oxidized and reducing fluids can turn the inert seafloor into a flourishing ecosystem that is often characterized by the endemic character of specialized organisms (Schander et al, 2010; Tarasov et al, 2005).

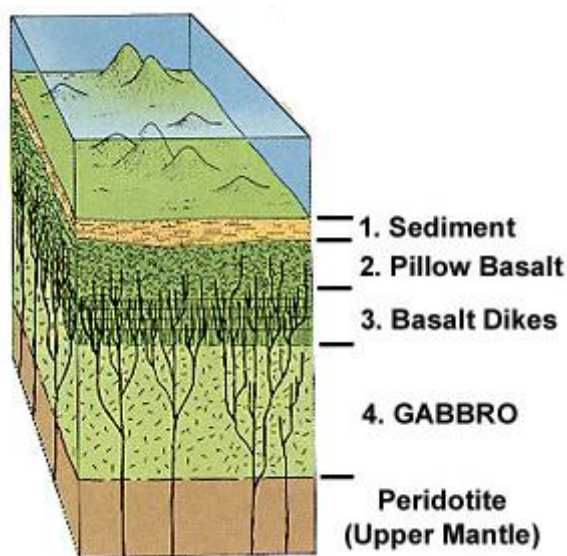


Figure 4. Schematic profile of the oceanic crust (weblink 1). Under the sediment, a volcanic layer consist of basaltic pillow lava, breccia and massive flows, which are ca. 0.1-1 km thick. This is followed by a sequence of sheeted dikes at ca 1 km. The lowermost sequence consist of several kilometres of gabbro. The average thickness of the oceanic crust is 7 km, depending on the tectonic regime (Alt, 1995).

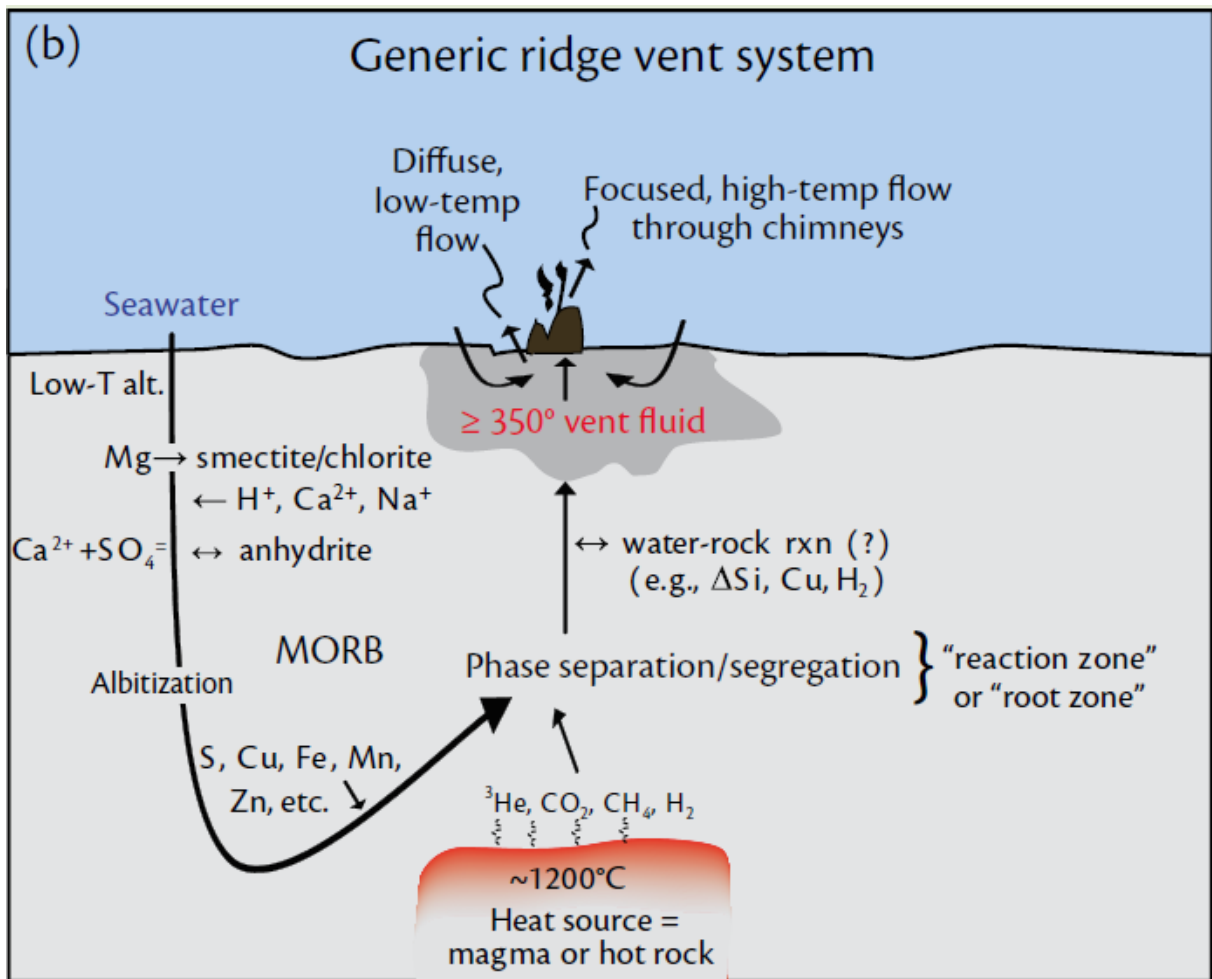


Figure 5. Schematic overview of the hydrothermal system (Tivey, 2007). Recharge zone is situated off-axis, where Mg, Ca and most of the sulfate are consumed. Reduced metals and sulfur are enriched in the reaction zone, along with ³He, CO₂, CH₄, and H₂ from magma leaching. Hot water with low density ascends to the surface in the discharge zone, where precipitation of metals occurs when mixed with seawater close to the surface.

3. Geological settings

Hydrothermal vent systems were long considered to be restricted to fast spreading ridges associated with high heat and magma supply (*Pedersen et al, 2010*). However, after the discovery of the Trans-Atlantic Geotraverse (TAG) vent field on the Mid-Atlantic Ridge, it was clear that hydrothermal vent fields were more prevalent in slow and ultra-slow spreading ridges than expected. The section of the Mid-Atlantic Ridge north of 66 °N, the Arctic Mid-Ocean Ridge (AMOR), is one of the slowest spreading ridges on the planet ($< 20 \text{ mm yr}^{-1}$). The AMOR extends from the shelf of Iceland to the Laptev Sea in Siberia and is subdivided into 6 sections: the Kolbeinsey Ridge, Mohns Ridge, the Knipovich Ridge, The Molly Ridge, the Lena Trough and the Gakkel Ridge (*Pedersen et al, 2010*) (*fig. 6*). These sections show large variations in morphology, with magmatically robust spreading ridges and shallow vent sites south of Jan Mayen, and gradually deeper and magmatically starved sections north of Jan Mayen. The Iceland hotspot influences the southern part of AMOR with increased supply of magma, leading to shallowing of the ridge and faster spreading rates than further north ($\sim 20 \text{ mm yr}^{-1}$). The AMOR starts to deepen north of Jan Mayen, where it transitions into the 550 km long Mohns Ridge in the Norwegian-Greenland Sea. The spreading rates at this section is $\sim 15 \text{ mm yr}^{-1}$ and is characterized by an average crustal thickness of $4.0 \pm 0.5 \text{ km}$, that is well below the global average for oceanic crust (*Klingelhøfer et al, 2000*). The topography displays morphological traits typical of ultra-slow spreading ridges, where the tectonics surpass the magma supply. In general, ultra-slow spreading ridges display a rough topography created by large listric faults that form deep fractures that bound the deep axial valleys and a negative depth profile (*Kelley et al, 2002; Bruvoll et al, 2009*). The Jan Mayen hot spot influences the Mohns Ridge in the southern end, which shows increasing thinning of the crust along with increasing depth towards the north. Accordingly, the deepest part ($\sim 3400 \text{ mbsl}$) is situated in the north where the Mohns Ridge transitions into the Knipovich Ridge (*Pedersen et al, 2010*). This part also hosts the Lokis Castle vent field (LCVF) which is situated $\sim 2400 \text{ mbsl}$ on a 30 km long axial volcanic ridge (AVR) that rises 1300 m above the axial valley floor (*Pedersen et al, 2010*) (*fig. 7*).



Figure 6. Overview of the AMOR. The ridge is an extension of the MAR that start at the north coast of Iceland and continue through the Norwegian-Greenland sea and through the Eurasian basin to the Laptev sea outside Siberia. Mohns ridge starts just east of Jan Mayen and ends at the Mohns-Knipovich transition.

The vent field was discovered during H₂DEEP-08 expedition with the R/V G.O. Sars (Pedersen *et al*, 2010), and is situated west of the distal parts of the Bear Island Fan at 73°30N and 8°E. The composition of the 317 °C black smoker fluid is characterized by high concentrations of CO₂ (23.8 mM), CH₄ (13.5 mM), H₂ (4.9 mM), NH₄⁺ (1.6-4.1 mM) and H₂S (2.6-4.7 mM). The vent field is basalt hosted but displays a CH₄/H₂ ratio and NH₄⁺ concentrations consistent with a sedimentary influence, which originates from the Bear Island Fan sediments that enrich the fluids with bicarbonate, methane and ammonia (Pedersen *et al*, 2010). LCVF consists of two vent sites that are coupled by two coalescing hydrothermal mounds. The mounds are 20-30 m high and 150-200 m across (Eickmann *et al*, 2014). Associated with the eastern mound is an active diffuse venting area containing multiple dead and active barite chimneys (BaSO₄) up to 1 m tall. Microbial mats cover the active chimneys and barite crust in the sediments that occur along lines, which probably reflects the flow rate and pattern of the fluid flow (Eickmann *et al*, 2014). The fluid composition and temperature (~20 °C) of the active chimneys reveals that the fluids are diluted hydrothermal fluid with a seawater/hydrothermal fluid mixing ratio of 10 % end-member fluid and 90 % seawater. (Eickmann *et al*, 2014; Steen *et al*, 2016).

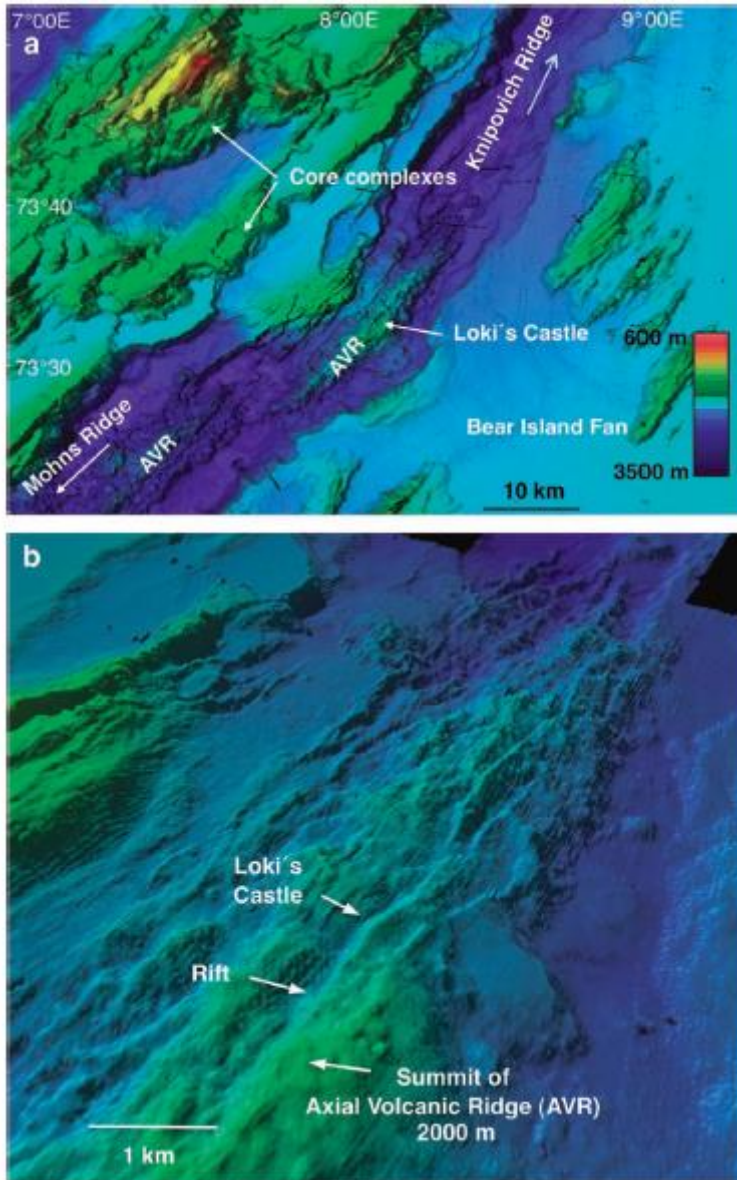


Figure 7. Bathymetric picture over the axial volcanic ridge that host LCVF (A). LCVF is associated with a rift close to the top of the AVR (B) (Pedersen et al, 2010).

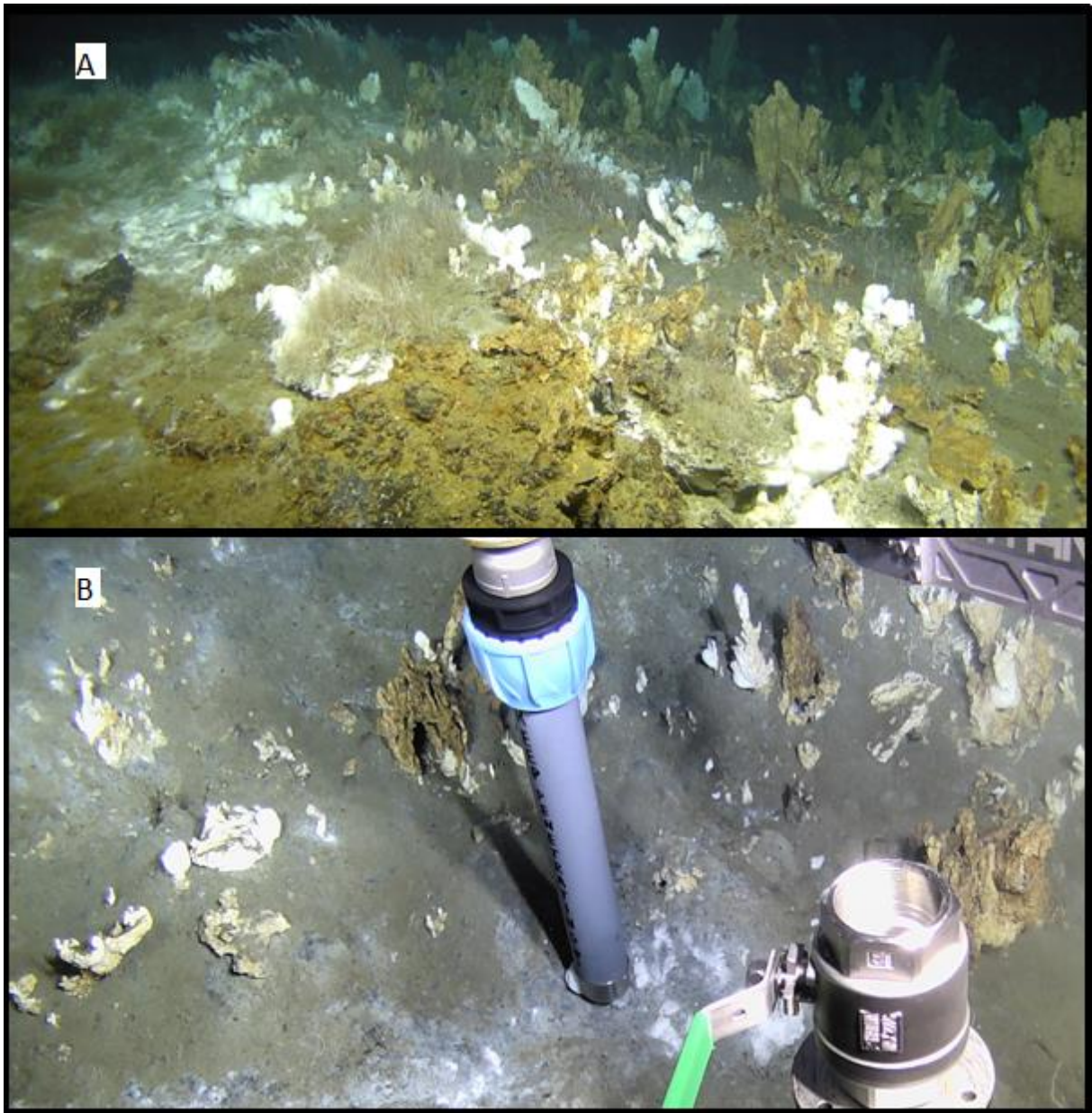


Figure 8. Overview barite field (A). The barite chimneys seems to align along fractures where the fluids are more focused. The sampling site (B) for GS15-AGR09-PC2 display slower flow rate and precipitated barite crust in the sediments.

4. Materials and methods

4.1. Sample locations

Bear island fan, 73° 34.533 N 08° 30.5265 E, 2562 mbsl: Gravity core (GS15-GC1) was sampled as a background from the distal parts of the Bear island fan. The gravity core was 410 cm long and contained light brown silt/clay in the upper part, and greyish sediments towards the bottom of the core.

Sulfide mound, 73°34.019 N, 8°09.535 E, 2350 mbsl: Push core 1 (GS15-AGR08-PC1) was 31 cm long and contained reduced, coarse porous sediments with a rusty layer on top.

Barite field, 73°33. 981 N, 08°09. 740 E, ~2340 mbsl: Push core 2 (GS15-AGR09-PC2) was sampled from the surface sediments in the barite field, and contained coarse-grained sediments mixed with precipitated barite with a distinct sulfidic smell. Fluid effluent from a barite chimney was obtained by a biosyringe (GS15-AGR09-BS), in addition to the Barite chimney (GS15-AGR09-R1) that was collected with Ægir 6000 from one of the diffuse venting chimneys. The chimney was characterized by a white brownish color with a strong sulfidic smell. In addition, a 2.07 m long gravity core (GS14-GC14) was sampled from the center of the barite field in 2014, which contained a mixture of fine-grained marine sediments and coarse-grained barite and sulfidic sediments. Temperature of the vent fluid was measured to be ~20 °C while the sediments were measured to be 7.8 °C.

4.2. Pore fluid sampling and analysis

Pore fluids were extracted from the sediments using 0.2 µm Rhizon filters. For the barite chimney, fluids were sampled with the ROV using the biosyringe sampler. All fluid samples were analyzed for pH, alkalinity and nutrients (NO_3^- , NO_2^- , NH_4^+ , PO_4^{3-} , DIC and H_2S) on board. Aliquots for later ICP-OES analysis of cations were acidified to 2% HNO_3 using concentrated nitric acid, and stored in acid-cleaned bottles at 4°C. A small amount of zinc acetate was added to the aliquots for IC analyses (SO_4^{2-} , Br^- , Cl^-) to avoid oxidation of dissolved sulfide, and samples were stored at 4°C. Fluids were analyzed for anions using a Metrohm ion chromatograph and Thermo iCap™ 7000 inductively-coupled plasma optical emission spectrometer at the University of Bergen.

4.3. Sulfate reduction rates measurement

4.3.1. Sample preparation

Two duplicates with 4 cm³ of sediments each, were sampled from ten horizons in the GS15-GC1, at 50, 100, 150, 200, 250, 300, 340, 360, 380 and 390 cm, respectively, with a 5 mL syringe. Additional two controls (A and B) were sampled at 250 and 390 cm for subtracting natural background noise and radioactivity transferred during the distillation. Same procedure was conducted on the GS15-AGR08-PC1, where two duplicates with 2 cm³ each of sediments for SRR measurement were sampled from 5, 10, 15 and 20 cm with a 5 ml syringe, in addition to control A and B at 5 cm. Two sub-samples (A and

B) were samples from GS15-AGR09-PC2, in addition to one control (control B) and 1 cm³ for porosity measurement. The barite was crushed in a sterilized mortar before the slurry was transferred to a clean 50 mL Falcon tube by a spoon sterilized by a gas burner. A 2 ml syringe were used to sample 1 cm³ of sediments for porosity measurement in GS15-GC1 and GS15-AGR09-PC2, while 0.5 cm³ of sediments were sampled for GS15-AGR09-PC1. For porosity measurement of the barite chimney, 2 x 1 cm³ of slurry was transferred to two centrifuge vials and frozen at -20 °C.

4.3.2. Onboard incubation

The samples were brought to the onboard lab for incubation short after sampling. The carrier-free ³⁵SO₄²⁻- tracer was diluted 1:1 with ultrapure sterile anaerobic water before incubation. The sediments were then injected with 10 µL of diluted ³⁵SO₄²⁻-solution (~185 kBq pr. sample) by a Hamilton syringe, before they were placed in a N₂ containing plastic bag. Sub-samples from GS15-AGR08-PC1 and GS15-GC1 were incubated at 4 °C for 24 hours, while AGR09-PC2 was incubated at 4 °C for 20 hours (*see table 1*). Control A for all samples were transferred to a 50 mL Falcon tube with 5 mL 20% Zinc Acetate without tracer fluid and frozen, while control B was added tracer fluid and 5 mL 20 % Zinc Acetate before it was stored at -20 °C without incubation. For the sample from the barite chimney, 2.5 mL slurry was added to 2 x 8 exetainers, where two exetainers were used as a control, 7 duplicates for incubation at 4 °C and 7 duplicates for incubation at ~20 °C. To add fluid that was lost during preparation of the slurry, 1 ml of fluid collected and filtered from each push core in the barite field was added to the samples together with 10 µl ³⁵S-tracer. Each exetainer was flushed with N₂ gas for 4 minutes before they were overpressured by filling for 10 s. and 30 hours incubation. After incubation, the samples were transferred to a 50 mL Falcon tube containing 5 mL 20% ZnAc and stored at -20 °C.

Table 2. Sample overview, incubation time and incubation temperature.

Overview SRR samples GS15

#	Core / Dive	Sample ID	Location	Inc. Time	Inc. Temp
1	GS15-GC1	50 cm A	Bear Island Fan	24hrs	4.0
2	GS15-GC1	50 cm B	Bear Island Fan	24hrs	4.0
3	GS15-GC1	100 cm A	Bear Island Fan	24hrs	4.0
4	GS15-GC1	100 cm B	Bear Island Fan	24hrs	4.0
5	GS15-GC1	150 cm A	Bear Island Fan	24hrs	4.0
6	GS15-GC1	150 cm B	Bear Island Fan	24hrs	4.0
7	GS15-GC1	200 cm A	Bear Island Fan	24hrs	4.0
8	GS15-GC1	200 cm B	Bear Island Fan	24hrs	4.0
9	GS15-GC1	250 cm A	Bear Island Fan	24hrs	4.0
10	GS15-GC1	250 cm B	Bear Island Fan	24hrs	4.0
11	GS15-GC1	250 cm CONTROL A	Bear Island Fan	24hrs	4.0
12	GS15-GC1	250 cm CONTROL B	Bear Island Fan	24hrs	4.0
13	GS15-GC1	300 cm A	Bear Island Fan	24hrs	4.0
14	GS15-GC1	300 cm B	Bear Island Fan	24hrs	4.0
15	GS15-GC1	340 cm A	Bear Island Fan	24hrs	4.0
16	GS15-GC1	340 cm B	Bear Island Fan	24hrs	4.0
17	GS15-GC1	360 cm A	Bear Island Fan	24hrs	4.0
18	GS15-GC1	360 cm B	Bear Island Fan	24hrs	4.0
19	GS15-GC1	380 cm A	Bear Island Fan	24hrs	4.0
20	GS15-GC1	380 cm B	Bear Island Fan	24hrs	4.0
21	GS15-GC1	390 cm A	Bear Island Fan	24hrs	4.0
22	GS15-GC1	390 cm B	Bear Island Fan	24hrs	4.0
23	GS15-GC1	390 cm CONTROL A	Bear Island Fan	24hrs	4.0
24	GS15-GC1	390 cm CONTROL B	Bear Island Fan	24hrs	4.0
25	GS15-AGR8-PC1	5 cm A	Sulfide mound LCVF	24hrs	4.0
26	GS15-AGR8-PC1	5 cm B	Sulfide mound LCVF	24hrs	4.0
27	GS15-AGR8-PC1	10 cm A	Sulfide mound LCVF	24hrs	4.0
28	GS15-AGR8-PC1	10 cm B	Sulfide mound LCVF	24hrs	4.0
29	GS15-AGR8-PC1	15 cm A	Sulfide mound LCVF	24hrs	4.0
30	GS15-AGR8-PC1	15 cm B	Sulfide mound LCVF	24hrs	4.0
31	GS15-AGR8-PC1	20 cm A	Sulfide mound LCVF	24hrs	4.0
32	GS15-AGR8-PC1	20 cm B	Sulfide mound LCVF	24hrs	4.0
33	GS15-AGR8-PC1	5 cm CONTROL A	Sulfide mound LCVF	24hrs	4.0
34	GS15-AGR8-PC1	5 cm CONTROL B	Sulfide mound LCVF	24hrs	4.0
35	GS15-AGR9-PC2	Sample A	Barite field LCVF	20hrs	4.0
36	GS15-AGR9-PC2	Sample B	Barite field LCVF	20hrs	4.0

37	GS15-AGR9-R1	Sample A (4°C)	Barite chimney LCVF	30hrs	4.0
38	GS15-AGR9-R1	Sample B (4°C)	Barite chimney LCVF	30hrs	4.0
39	GS15-AGR9-R1	Sample C (4°C)	Barite chimney LCVF	30hrs	4.0
40	GS15-AGR9-R1	Sample D (4°C)	Barite chimney LCVF	30hrs	4.0
41	GS15-AGR9-R1	Sample E (4°C)	Barite chimney LCVF	30hrs	4.0
42	GS15-AGR9-R1	Sample F (4°C)	Barite chimney LCVF	30hrs	4.0
43	GS15-AGR9-R1	Sample G (4°C)	Barite chimney LCVF	30hrs	4.0
44	GS15-AGR9-R1	CONTROL A	Barite chimney LCVF	30hrs	4.0
45	GS15-AGR9-R1	CONTROL B	Barite chimney LCVF	30hrs	4.0
46	GS15-AGR9-R1	Sample A (20°C)	Barite chimney LCVF	30hrs	20.0
47	GS15-AGR9-R1	Sample B (20°C)	Barite chimney LCVF	30hrs	20.0
48	GS15-AGR9-R1	Sample C (20°C)	Barite chimney LCVF	30hrs	20.0
49	GS15-AGR9-R1	Sample D (20°C)	Barite chimney LCVF	30hrs	20.0
50	GS15-AGR9-R1	Sample E (20°C)	Barite chimney LCVF	30hrs	20.0
51	GS15-AGR9-R1	Sample F (20°C)	Barite chimney LCVF	30hrs	20.0
52	GS15-AGR9-R1	Sample G (20°C)	Barite chimney LCVF	30hrs	20.0

4.3.3. Lab-based analyses

4.3.3.1. Reagents preparation

On land, the single step cold chromium distillation method, as described in Kallmeyer et al. (2004), was used to retrieve the radioactive reduced sulfur species from the sediments. Before the distillation, oxidized chromium had to be reduced by reactions with reduced zinc. Before the chromium reduction, the zinc pellets were flushed in a reaction flask with 2N HCl under a N₂ atmosphere for 10 minutes. The acid was then disposed of with a 50 mL syringe while maintaining anoxic condition. The oxidized chromium solution was added to the reaction flask where chromium was reduced by the zinc pellets and changed color from dark green to clear blue, before stored in the fridge at 4 °C. The redox reaction can be written as:



4.3.3.2. Distillation process

The sediment samples were then thawed before being centrifuged at 2500 rpm for 5 min. 100 μ L supernatant was then pipetted into a counting vial with 5 mL ZnAc. Residual supernatant was disposed of. 15 mL dimethyl sulfoxide (DMSO) and two drops of anti-foam was added to the sediments in the falcon tube before poured into 3-neck round-bottom glass flasks containing a magnetic stirrer. Citrate buffer was prepared in a citrate trap before it was mounted to the distillation setup. 5 mL 20% Zinc acetate along with one drop of anti-foam was added to a tube and connected to the citrate trap (*fig. 9*). The reaction flasks were then connected to the distillation setup and degassed with nitrogen for 10 minutes before adding 8 mL 6N HCl with a 50 mL syringe through the one-way valve. The magnetic stirrers were set to 750 rpm before adding 16 mL chromium solution. Distillation lasted for 2 hours for every samples. After the distillation, scintillation fluid was poured into the Zn-trap two times and poured into a counting vial. Scintillation fluid was also added to the counting vials containing the supernatant. The radioactivity was counted with PerkinElmer TriCarb[®] Liquid Scintillation Counter and the reduction rates were calculated with the following equation from Kallmeyer et al (2004):

(Eq. 1)

$$\text{SRR} = ([\text{SO}_4^{2-}]_{\text{pf}} \times \Phi_{\text{sed}} \times 1.06 \times (\text{aTRIS}/\text{aTOT})) \times (1/t)$$

Moreover, SRR for the barite slurry was calculated by a modified equation:

(Eq. 2)

$$\text{SRR} = (1.06 \times ([\text{SO}_4^{2-}]_{\text{pf}} \times \Phi_{\text{slurry}} \times V_{\text{slurry}} + [\text{SO}_4^{2-}]_{\text{vf}} \times V_{\text{vf}}) \times (\text{aTRIS}/\text{aTOT})) \times (1/t_{\text{inc}} \times V_{\text{slurry}})$$

Where $[\text{SO}_4^{2-}]_{\text{pf}}$ and $[\text{SO}_4^{2-}]_{\text{vf}}$ is the amount of sulfate in the pore fluid and vent fluid in nmol/cm^3 . A is the activity (cpm-counts per minute) of the total reduced inorganic sulfur (TRIS) and of the supernatant + TRIS (TOT) after the incubation is ceased. Φ is the porosity of slurry and sediments. V_{slurry} and V_{vf} is the volume of slurry and vent fluid. t is incubation time in days and 1.06 is the fractionation factor between ^{35}S and ^{32}S . The units for this calculation is $\text{nmol}/\text{cm}^3 \cdot \text{d}$

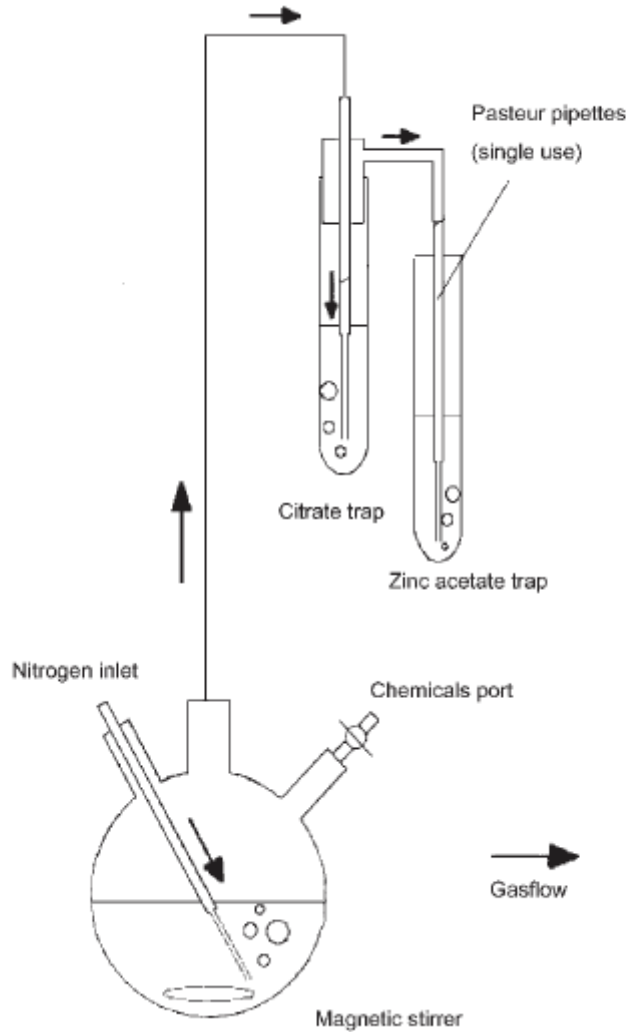


Figure 9. Schematic overview of the distillation setup (Kallmeyer et al. 2004)

4.4. TIC/TOC

30-50 mg sediments were obtained with a spoon from the same horizons as the the SRR samples, in addition to sampling from every 10 cm in GS15-GC1 and GS14-GC1. The sediments were transferred to glass vials prior to drying at 105 °C for 3 days. The dried samples were crushed before placed in the furnace for additional drying. The sediments were transferred to ceramic boats that was fed into the analyzer, where total inorganic carbon and total carbon of the sample was measured. The organic carbon content was measured by subtracting the measured amount of inorganic carbon from the amount of total carbon in g/kg by multi EA[®] software. Samples was measured in the the Analytikjena multi EA[®] 4000.

4.5. DNA extraction and PCR

Total genomic DNA was extracted from sediment with FastDNA[™] SPINKit for Soil according to the protocol supplied with the kit. Samples were thawed before 500 mg of sediments were added to two lysing matrix E tube duplicates along with 978 µL sodium phosphate buffer and vortexed for 15 sec. Additional 122 µL MT buffer was added before vortexing for 15 s. Both duplicates were then

centrifuged at 14000x g for 5 min. to separate the DNA-containing supernatant from the sediments. The supernatant was transferred to a clean 2 mL micro centrifuge tube and added 250 µL protein precipitation solution before the solution was shaken 10 times and incubated at room temperature for 10 minutes. After incubation, the solution was centrifuged at 14000x g for 5 minutes before 800 µL supernatant and binding matrix were mixed in a 15 mL falcon. The solution was shaken gently before placed on a rocker for 5 minutes, allowing the DNA to bind with the matrix. The solution was mixed by pipetting up and down a few times before transferring 800 µL solution to SPIN™ FILTER tube and centrifuged at 14000 x g for 2 minutes before emptying the catch tube. This was repeated until the 15 mL falcon tube was empty. The filter was discarded and 500 µL SEWS-M (ethanol) were supplied to the SPIN™ FILTER tube and shaken gently before centrifuged at 14000 x g for 5 minutes. The catch tube was emptied and centrifuged again at 14000x g for 5 minutes until the residual ethanol was removed. The SPIN™ FILTER was transferred to a clean 2 mL catch tube and air-dried for 5 minutes in room temperature with the lid open. At the end, 100 µL DES was added to the SPIN™ FILTER tube and shaken gently by finger flicking before centrifuged at 14000x g for 2 minutes.

Total genomic DNA was applied in a two-step PCR for amplification of the 16s rRNA gene. The gene was amplified with the 805R (GACTACHVGGGTATCTAATCC) reverse primer and 519F (CAGCMGCCGCGGTAA) forward primer. DNA from each horizon was PCR amplified in triplicate using the above mentioned primer combination. A master mix was made of The HotStar plus that contained polymerase, buffer and nucleotides together with 0.125 µL forward primer and 0.125 µL reverse primer. The PCR cycles was melting for 5 min at 95 °C, 30 rounds x 94 °C at 30 sec, 56 °C for 30 sec, 72 °C for 90 sec and 72 °C for 7 min until it cooled to 4 °C. Before purification of the amplicons, the AMPure® XP bead well and the amplicons was vortexed before mixing 50 µL of AMPure® XP magnetic beads with 75 µL PCR products (beads:DNA ratio = 0.7:1). The mixture was vortexed for 10 s. followed by 5 min incubation before the bead mix was placed on a plate of magnets for 5 min to separate the double-helix from the solution. The remaining clear solution was discarded before 500 µL of 70% ethanol was dispensed into the micro tube that was still on the magnets. The ethanol was removed after 1 minute of incubation, which was repeated on time before the micro tubes was removed from the magnet plate. After 5 min. of air drying, 25 µL of elution buffer was added to the micro tube for 25 s. of vortexing before the bead mix was placed on the magnet plate for 5 minutes. The cleared solution was transferred from the micro tubes to a clean tube without disturbing the beads. The purified DNA concentration was measured in Quantus™ fluorometer and evaluated in gel electrophoresis to ensure the correct amplicon length

For the second amplification, a maximum amount of 10 ng/µl of PCR products

from the first PCR were used as template and a specific primer containing a MID sequence of 44 bp was used for each reaction to label each isolated DNA. This was performed according to the first round, using seven cycles. The purification of the PCR products from the second amplification were performed as described above before the concentration was measured by Quantus™ fluorometer. The sample were then stored at -20 deg. Before sequencing by IonTorrent, the samples were additionally diluted to 40 pM.

5. Results

5.1. Background sediments

5.1.1. Pore fluid geochemistry

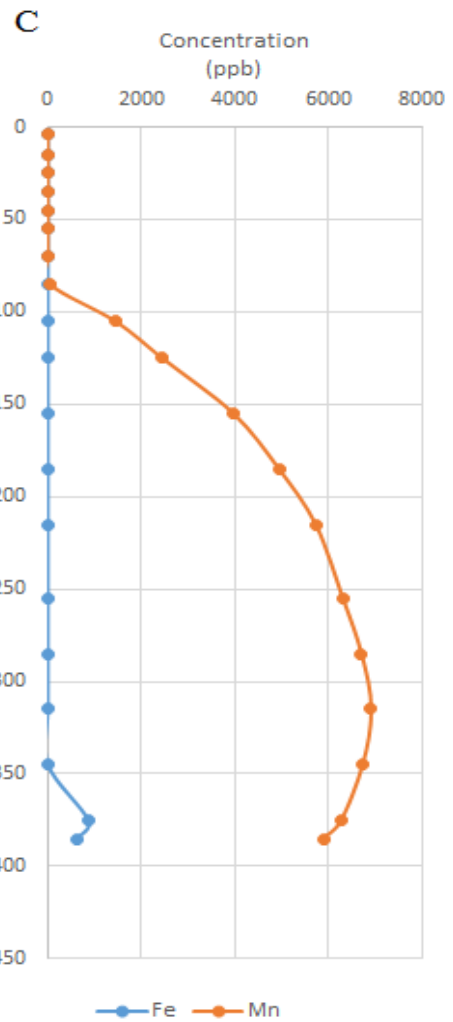
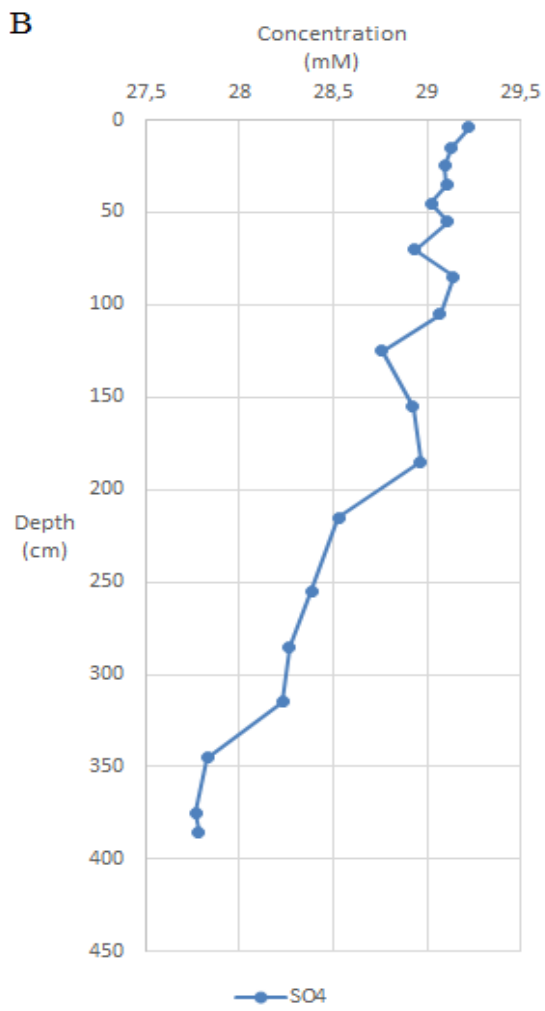
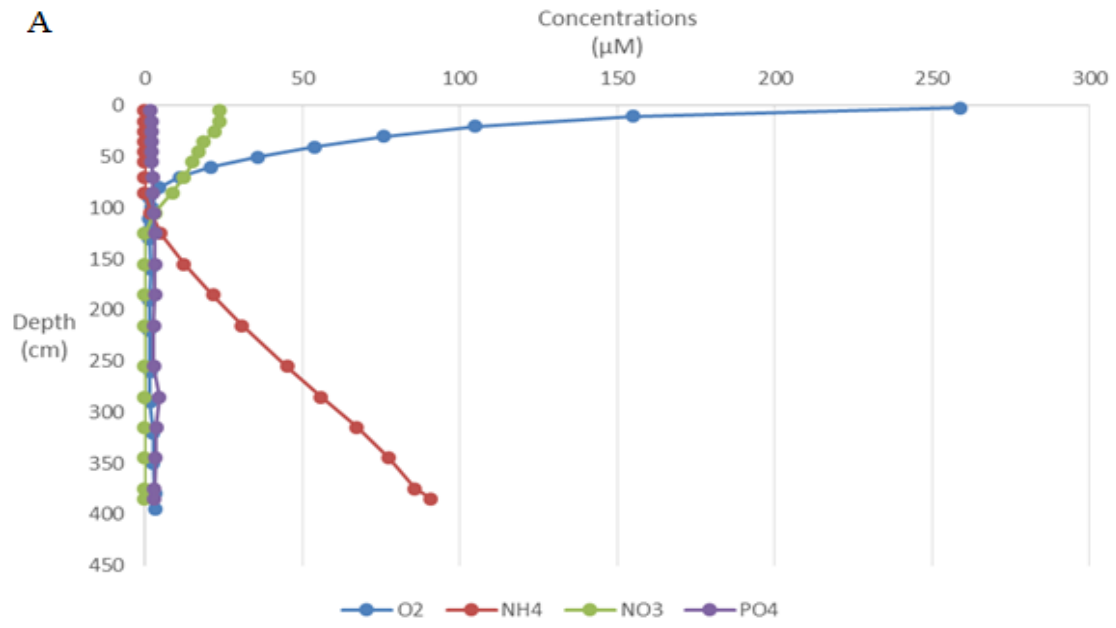
All the data from GS15-GC1 are listed in table 1 in appendix 1. The concentration of O₂, NO₃⁻, PO₄³⁻ and NH₄⁺ are shown in figure 10A, while the sulfate and dissolved metals, Mn and Fe, are shown in figure 10B and 10C, respectively. Oxygen and nitrate display highest concentration in the upper section of the core, where the concentration of oxygen range from 259 μM at the sediment-water interface to 1.5 μM at 90 cm. The decline in nitrate concentration follow the oxygen depletion and is depleted at 105 cm. This part of the core (85-105 cm) marks the shift from the domination of oxidized compounds to anoxic condition with an increase of reduced compounds. NH₄⁺ also appear at 105 cm and increase constantly towards the bottom of the core, while PO₄³⁻ display stable concentrations all the way towards the bottom of the core. Dissolved Mn starts to appear at 85 cm and increase down-core to 315 cm, where the concentration peaks out at 6918 ppb. This concentration is high compare to other metal rich deep-sea sediments (*e.g. Løvemark et al, 2013; Sørensen et al, 2004*), but consistent with concentrations reported from other sediment cores that were obtained from this area (*e.g. Jørgensen et al, 2012*). Iron enrichment occurs first at 375 cm with 865 ppb, but starts to drop immediately to 631 ppb in the last sediment horizon at 385 cm. The core display high sulfate levels throughout the core, with concentrations comparable to seawater values in the upper 185 cm. The concentration declines somewhat in the lower section where it end up at 27.8 mM.

5.1.2. Sulfate reduction rates

No measurable levels of sulfate reduction rates were detected in GS15-GC1

5.1.3. Organic and inorganic carbon

The TOC measurement shows two distinct spikes with an organic carbon load of 8.9 g/Kg at 40 cm and 390 cm (*fig.11*). Between these concentration peaks, the values drop to 0.2 g/Kg before it stabilizes at 0.9 g/Kg between 100 and 340 cm. This section also seems to have an inverse correlation with the dissolved manganese concentration. The DIC and alkalinity data coincides with the geochemical zones, where DIC (2-3.5 mM), alkalinity and NH₄⁺ increase concomitantly after NO₃⁻ and O₂ depletion (*fig.10D*). pH is stable during the whole core and lies close to seawater values.



D

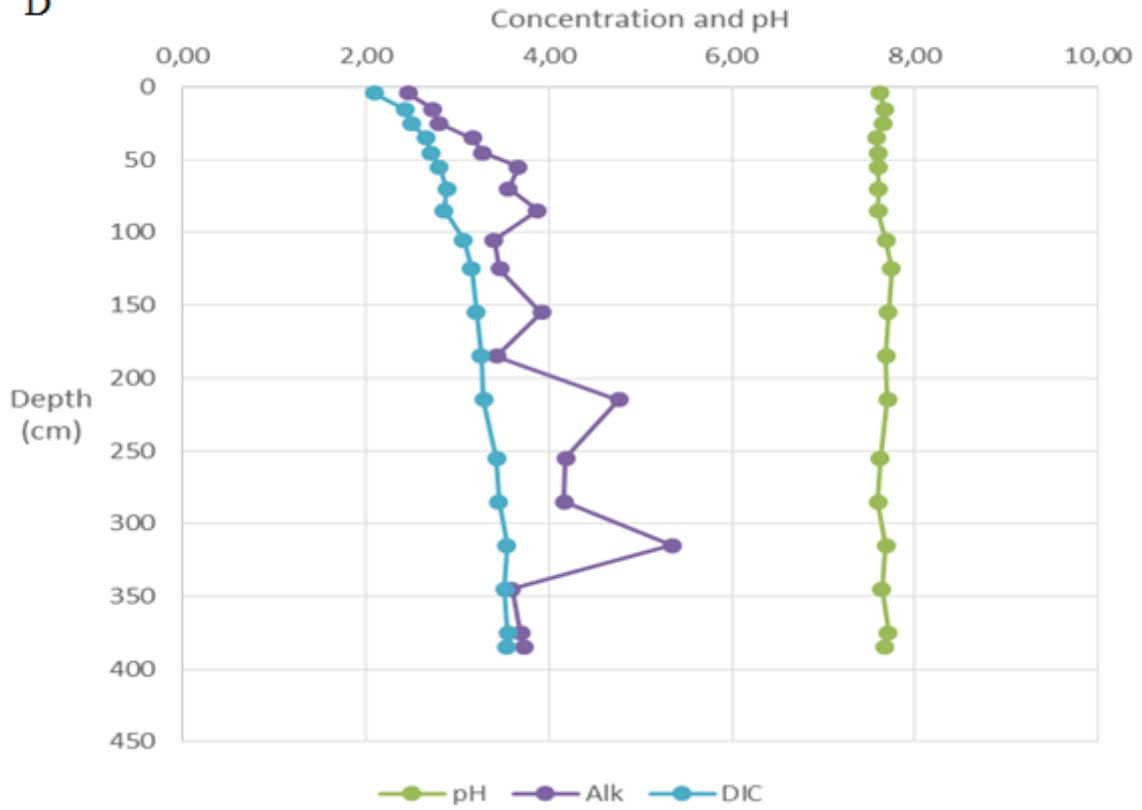


Figure 10. The geochemical analyse of the pore fluid in GS15-GC1 show stable concentration of PO_4^{3-} throughout the core, while O_2 and NO_3^- are depleted in the upper 105 cm. The depletion of NO_3^- is followed by a constant increase of NH_4^+ towards the bottom of the core (A). The sulfate concentration fluctuate through most of the core, but display a net decrease towards the bottom (B). Mn is the dominant metal in GS15-GC1, while Fe is displace to the lower section of the core (C). Alkalinity and DIC (mM) showed an increase in concentration in the upper section of the core before is flattens out. pH seems to be stable through the core (D).

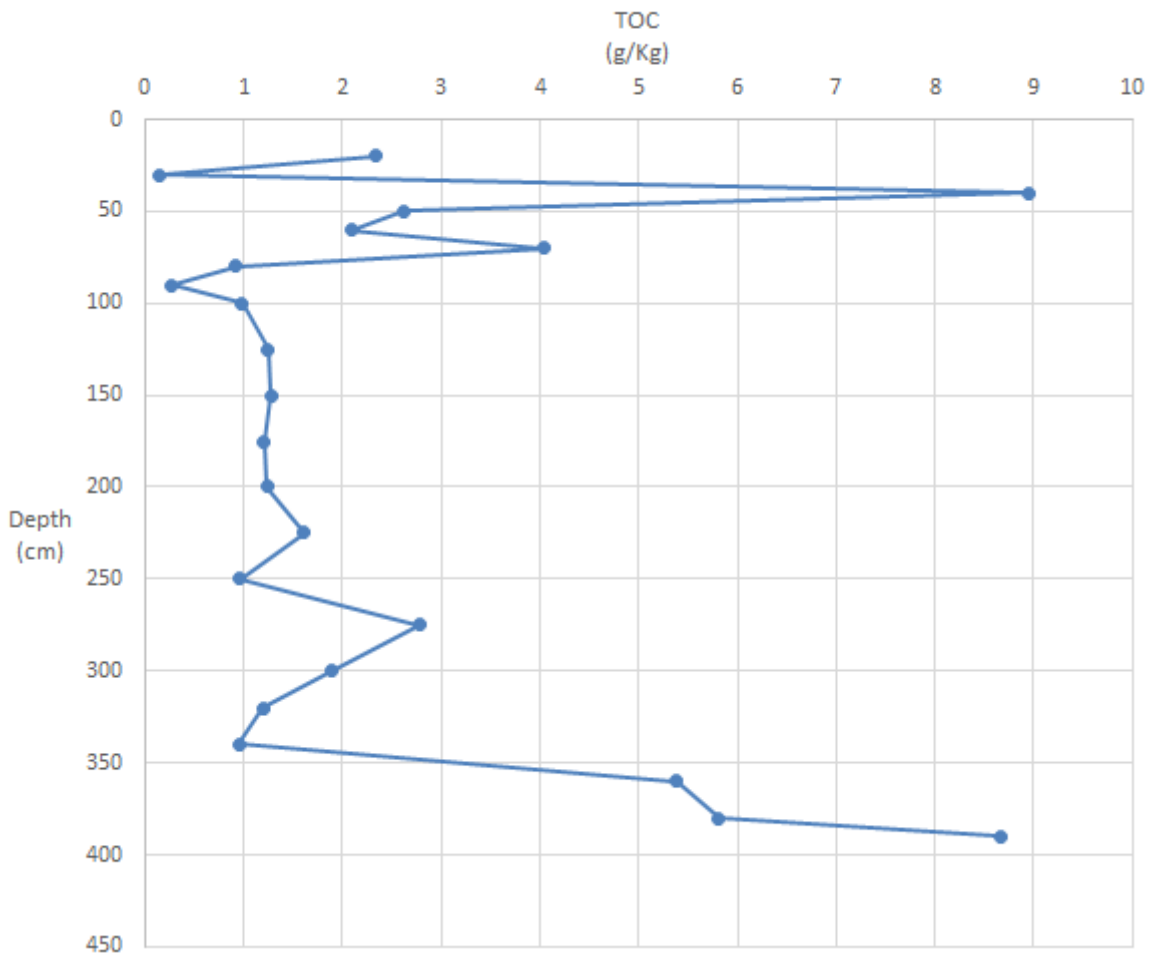


Figure 11. TOC concentration in gram per kilogram sediments in GS15-GC1. The concentrations range between 8.9 g/Kg at 40 cm to 0.27 g/Kg at 90 cm.

5.1.4. Composition of the microbial community

55 phylum, 103 class, 196 orders, 249 family, 364 genera and 21 species was sequenced, where the bacteria domain dominated the microbial community in all horizons, except at 350 cm where archaea represented 58% of the community. Proteobacteria and Chloroflexi was the dominant phylum throughout the whole core, while the dominant class was Alphaproteobacteria followed by Gammaproteobacteria and Deltaproteobacteria. Sulfate reducers were detected at in GS15-GC1, where the majority were clustered at 190-250 cm, ranging from ~0.5% at 190 cm to 1.2 % at 220 cm and 0.6 % of all OTU's at 250 cm. The highest relative abundance of sulfate reducers were found at the bottom of the core with 1.6 %. All sulfate reducers were from the Deltaproteobacteria class that was affiliated with Desulfobacterales order. The only sulfate reducing genus that was detected was SEEP-

SRB1, which belong to Desulfobacteraceae and ranged from 0.4% at 190 cm to 1.25% at 220 cm and 0.4 to 1.5 % at 380 and 390 cm.

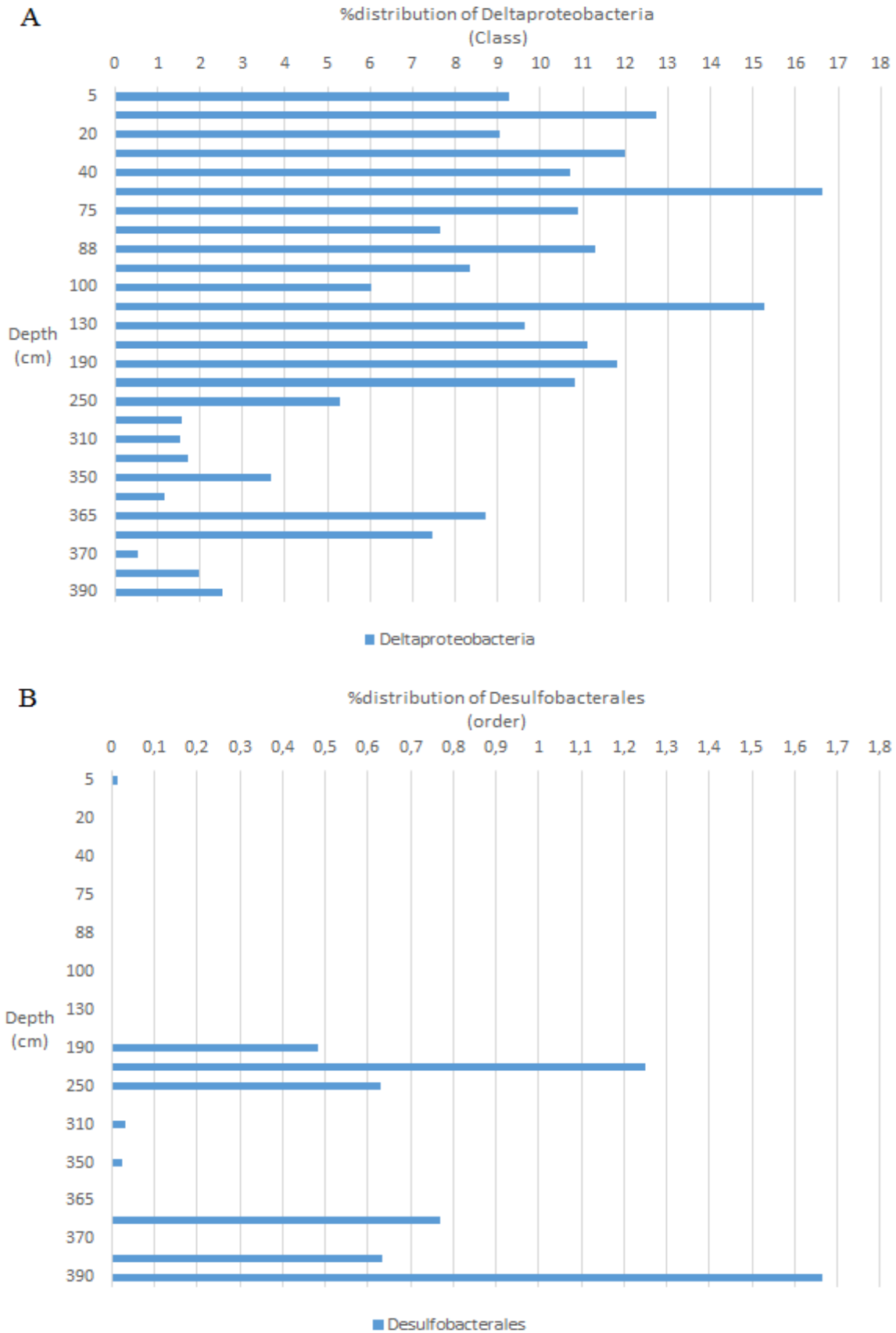


Figure 12. Relative abundance of Deltaproteobacteria (A) and Desulfobacterales (B) in GS15-GC1, which was the only identified prokaryote known to reduce sulfate.

5.2. The inactive sulfide mound

5.2.1. Pore fluid geochemistry

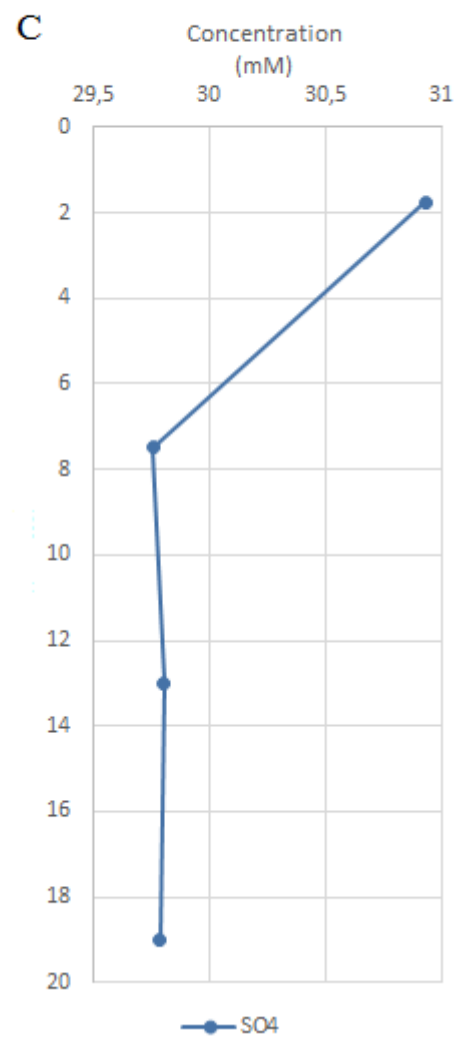
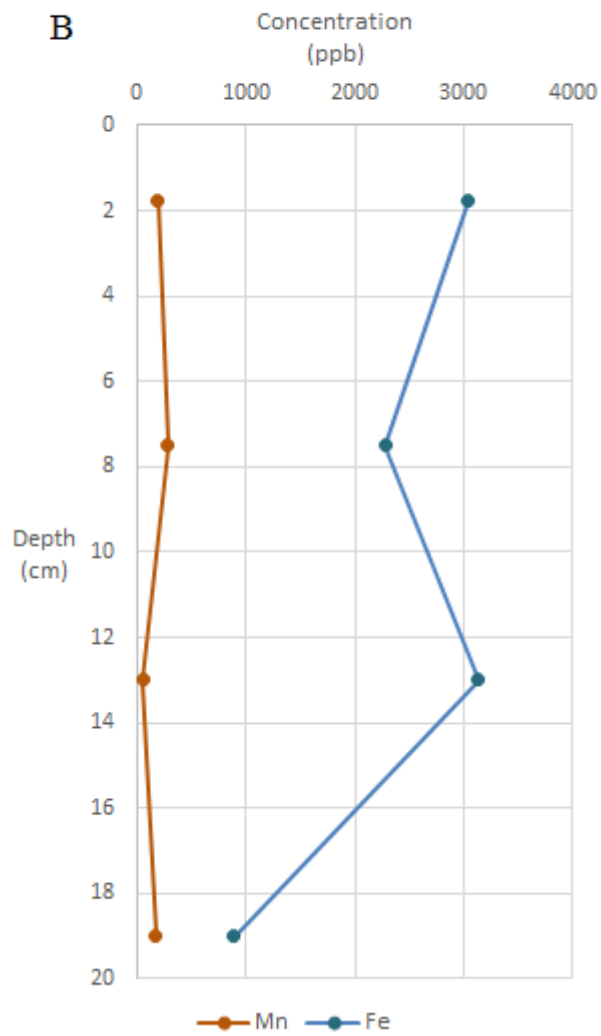
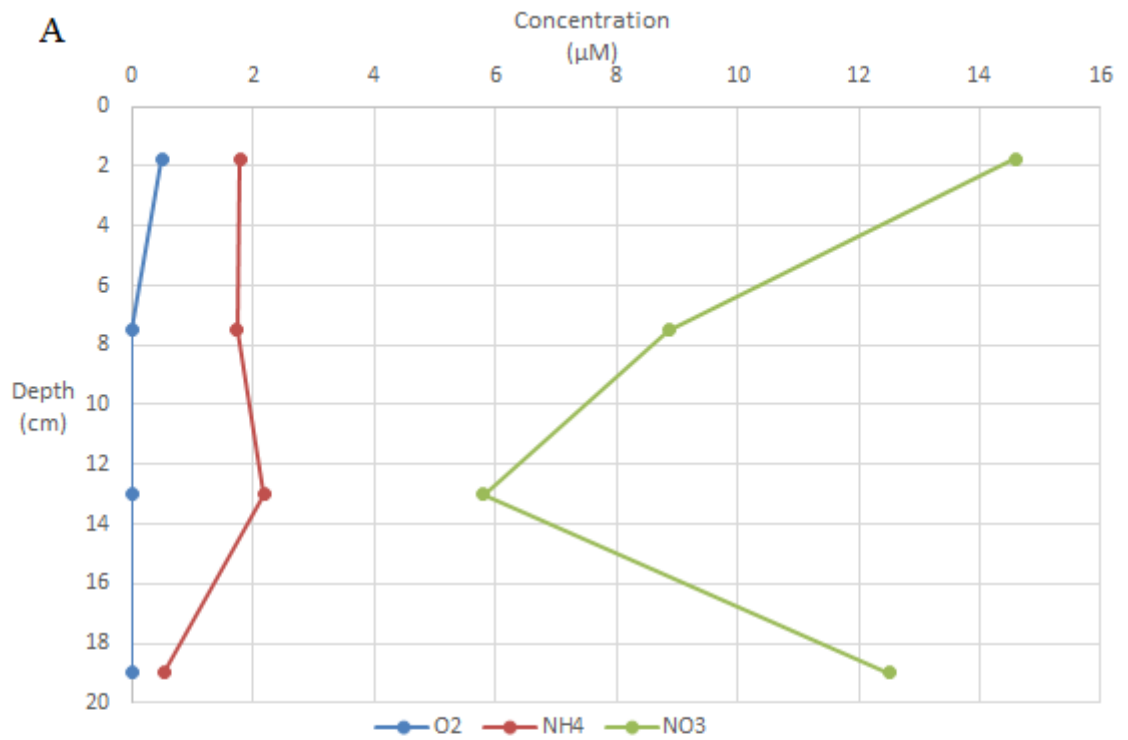
In push core GS15-AGR08-PC1, oxygen levels declined sharply the first 1 cm of the core, leaving only 0.5 μM of oxygen in the upper horizon. Anoxic conditions and elevated levels of dissolved iron and nitrate characterized the rest of the core (*fig.13A*). The Mn concentration is low throughout the entire core, with 188 ppb Mn in the top layer, decreasing to 56 ppb at 13 cm before increasing again to 175 ppb at the bottom of the core (19 cm). Iron is the dominating dissolved metal in the pore fluid, as opposed to the background core where Mn dominates (*fig.13B*). The Fe values range from 3044 ppb at the top and 888 ppb at the bottom, and displays generally more fluctuations than Mn. Nitrate decreases within the first centimetre of the core, with a starting concentration of 14.59 μM in the top horizon. The concentration decreases to 5.81 μM at 13 cm depth before it rises again to 12.51 μM towards the bottom at 19 cm. The nitrate concentration seems to have a weak inverse correlation with Fe in the lower half of the core, where Fe decreases and nitrate increases. NH_4^+ levels, however, are quite constant over the first 12 cm (1.78 to 2.18 μM). Below 13 cm depth, ammonia concentrations decrease to 0.53 μM at the bottom. NH_4^+ concentrations show a weak inverse correlation with both nitrate and dissolved Mn. Sulfate concentration decrease the upper 7 cm of the core, from 30.9 mM to 29.7 mM, which is similar to seawater concentrations (*fig.13C*).

5.2.2. Sulfate reduction rates

The push core from the inactive sulfide mound, GS15-AGR08-PC1, showed no detectable sulfate reduction rates, even though the core was anoxic.

5.2.3. Organic and inorganic carbon

TOC concentrations in the push core display a sharp decrease in the upper 10 cm, where it range from 4.5 g/Kg at 1.5 cm to 1.2 g/Kg at 10 cm, until TOC concentration falls below measurable quantities in the lower half of the core. This sharp decline in organic carbon does not covary with the DIC and alkalinity concentrations, which exhibit generally constant and low values (below 2 mM) throughout the core. Nevertheless, both DIC and alkalinity levels seem to increase after 13 cm, which correspond with the trend shown in both ferrous iron and nitrate levels.



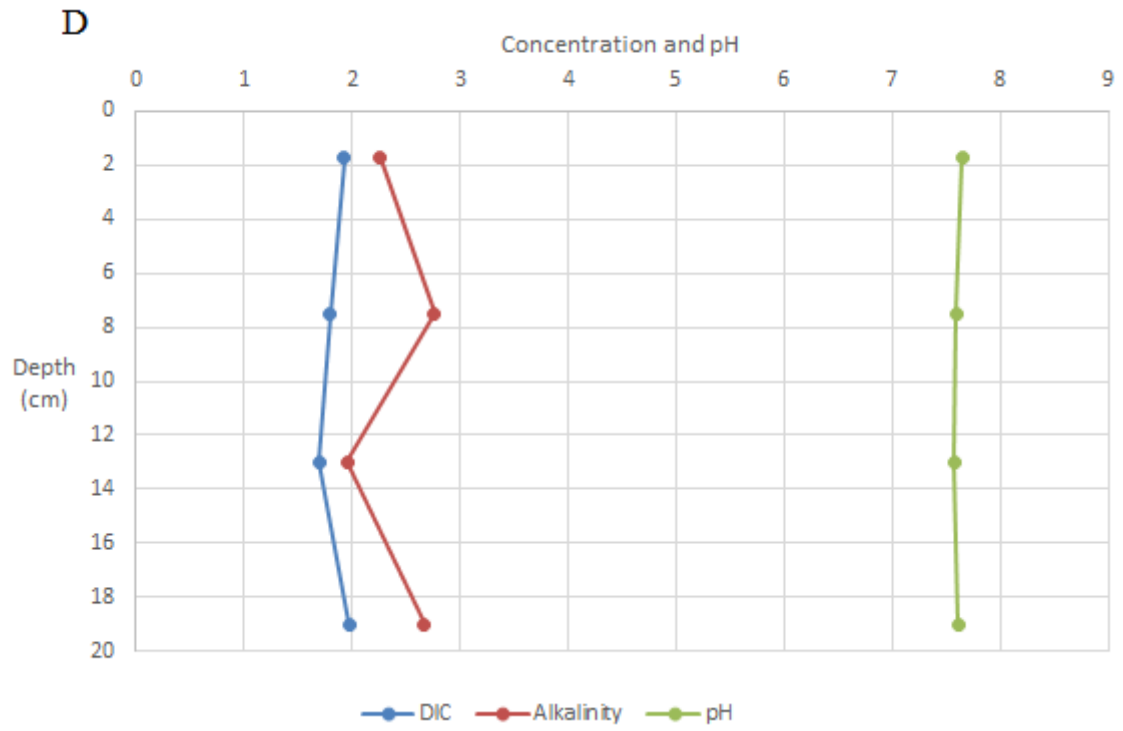


Figure 13. The measurement of pore water chemistry shows anoxic conditions throughout the whole core with nitrate as the dominant species (A). Fe is the most abundant metal in the core, which contrasts the background sediments where Mn dominated (B).

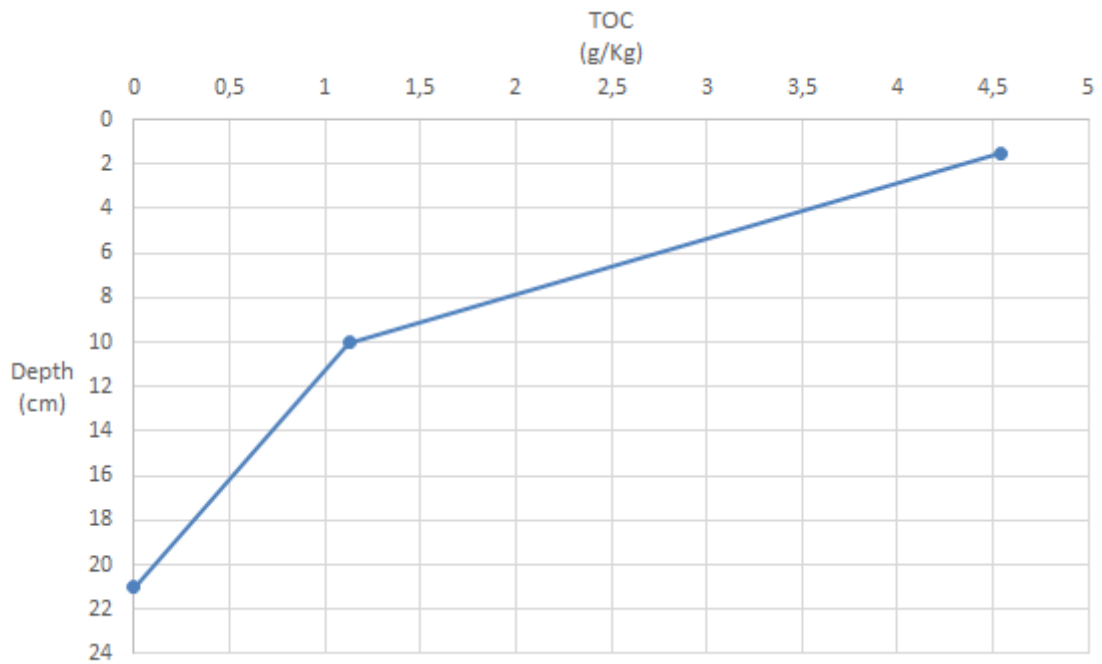


Figure 14. Results from TOC calculations in GS15-AGR09-PC1. TOC values decline sharply from 4.5 to 0 g/Kg at 20 cm.

5.2.4. Microbial community

GS15-AGR09-PC1 also contained sulfate reducing bacteria, where all belong to Deltaproteobacteria class (*fig. 15A*). The sulfate reducers were affiliated with Desulfarculales and Desulfobacterales order. The relative abundance ranged from 0.3 to 3.6 % at 25 cm for the Desulfarculales and 0.6 % at 0 cm to 4.3 % of all OTU`s at 18 cm for Desulfobacterales (*fig.15B*). There were only a few hits at higher level, were two sulfate reducers were identified at family level. Both belonged to the Desulfobacterales order, where Desulfobacteraceae was the most prevalent with 0.4 to 2.7% of all OTU`s. No sulfate reducers at genus level or species level were identified.

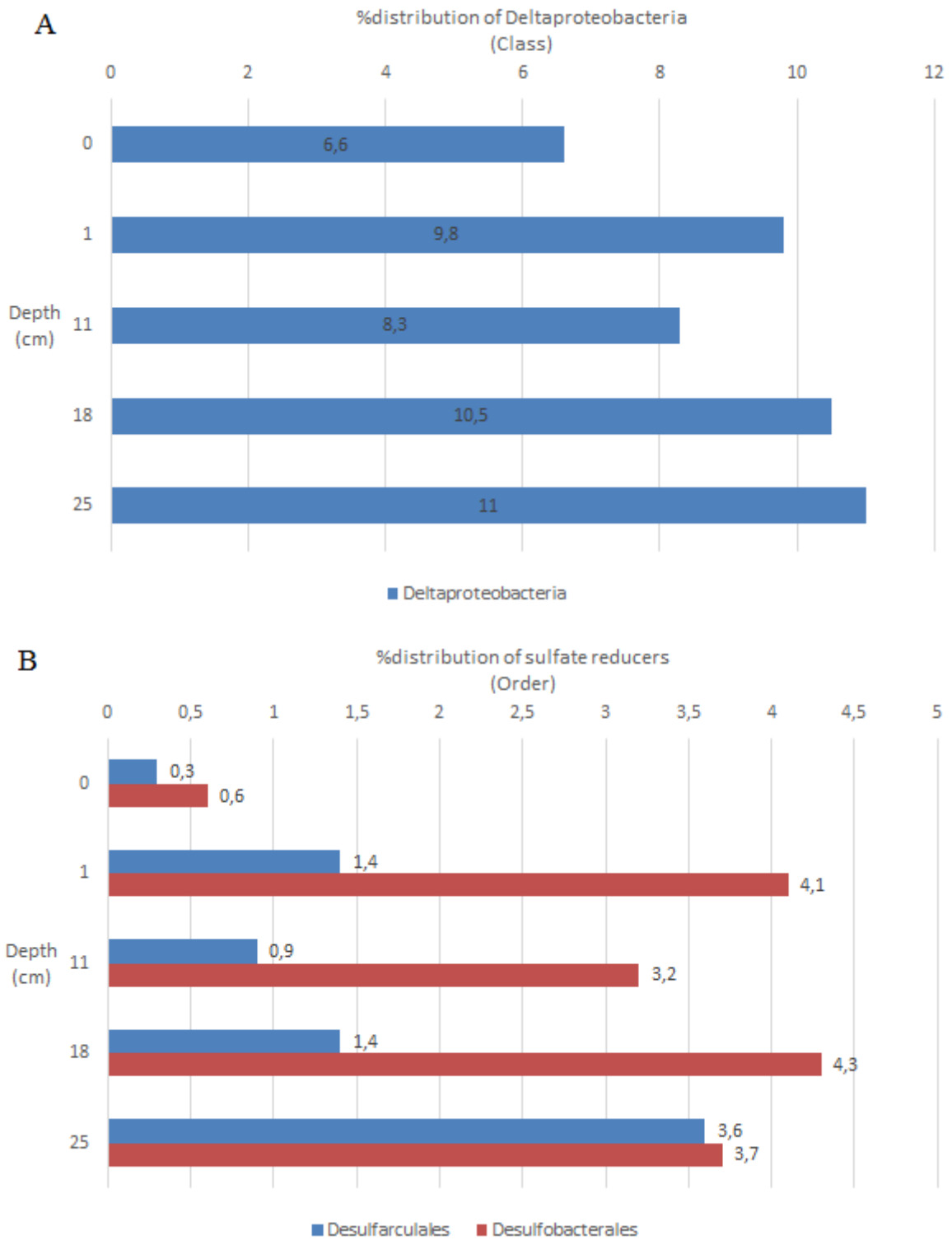


Figure 15. All sulfate reducers belonged to Deltaproteobacteria class. Desulfobacterales and Desulfarculales was the only sulfate reducers identified at order level.

5.3. Surface sediments from the barite field

5.3.1. Pore fluid geochemistry

The GS15-AGR09-PC2 was sampled in an area of diffuse venting from a fracture covered with barite crust that was associated with bacterial mats. The sample contained coarse hydrothermal sediments mixed with precipitated barite and abundant tubeworms. The core displayed an anoxic character with depletion of both NO_3^- and O_2 and high concentrations of sulfide and NH_4^+ , with 2555 μM and 1255 μM , respectively. Moreover, the methane concentration was the second highest measured (0.185 μM) of all samples (*Table 3*), while Sulfate levels were the lowest measured from the barite field with 21.5 mM. Fe was absent, but relative high concentrations of Mn was detected with 1002 ppb.

5.3.2. Sulfate reduction rates

The anoxic character is further supported by detection of microbial sulfate reduction (*fig. 17A*). Rates were measured from two duplicates (A and B), where average rate was calculated. Rates in A was 89.95 $\text{nmol}/\text{cm}^3 \text{ d}$ and 130 $\text{nmol}/\text{cm}^3 \text{ d}$ in duplicate B. the average rate from the two duplicates (A and B) yielded 110 (± 20.46) $\text{nmol}/\text{cm}^3 \text{ day}$, which was the highest rate measured from the barite field .

5.3.3. Organic and inorganic carbon

The push core also exhibits the highest concentration of DIC and TOC (*fig. 17B and D, respectively*) with 4.94 mM and 6 g/Kg, respectively. TOC was still lower than the highest value from the background core (9 g/Kg) (*fig. 17C*). The pH was close to seawater levels with 7.78.

5.3.4. Composition of the microbial community

The sequencing of the 16S rRNA PCR amplicons were used to study the distribution of taxa within four depths in GS15-AGR09-PC2. All horizons were dominated by Bacteria, which varied from 81.7 to 95.5% of the detected domain. Proteobacteria was the dominant phylum in all horizon and mostly represented by Gammaproteobacteria (28.8-31.6%) and Epsilonproteobacteria (20.8- 32.4%). Deltaproteobacteria was of minor importance in all horizon. Both phylum from the archaean domain were found in the subsamples, but at lower density than the bacteria domain. The deepest horizon, however, display an increase in archaean community, which contained groups affiliated the Crenarchaeota phylum, which represented all of the archaean taxa with 18.2 % of detected OTU`s. Archaeans that was affiliated to ANME-1 represented 0.1% at 8 cm and 0.3% at 10 cm. No sulfate reducing archaean was found. Desulfobacterales order was the most prevalent bacteria among the sulfate reducing community (*fig. 16B*). The group belong to the Deltaproteobacteria class, and ranged from 2.7% at the top section to 9.3% at the lowest section, where it was the only detectable SRB (*fig. 16B*). Members of the Desulfarculales and Desulfuromonadales order was also present, but at low

density (fig. 16B). *Desulfocapsa* and *Desulfococcus* was the most prevalent genus in all of the horizons, with highest relative abundance at the lowest horizon with 4.5 % of the detected OTU's

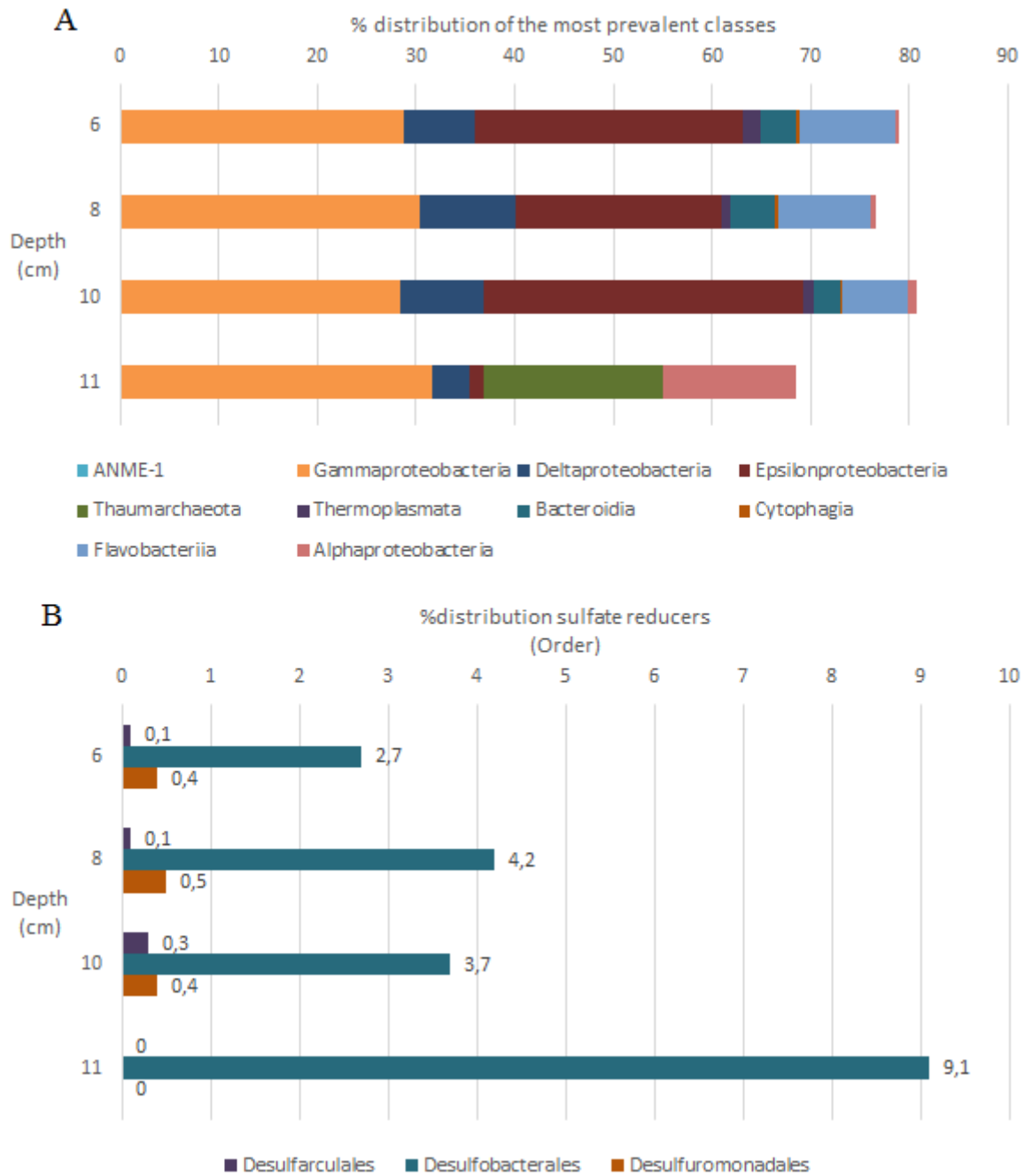


Figure 16. The results from the DNA sequencing in GS15-AGR09-PC2 show that *Desulfobacterales* was the most prevalent order in all sampled horizon.

5.4. Active barite chimney from the barite field

5.4.1. Pore fluid geochemistry

Although pore fluids could not be directly extracted from the barite chimney, a biosyringe (GS15-AGR09-BS) was sample taken from a microbial mat on a nearby barite chimney is assumed to be representative of the chimney fluids (*table 3*). The fluid contained H₂ (16 nM), and elevated concentrations of CH₄ (105.4 μM). This was the only sample in which H₂ was detected, and was the sample that contained the highest concentration of methane relative to the other samples from the barite field. Both Mg and sulfate concentrations are similar to seawater levels with 1217 ppm and 29 mM, respectively. Furthermore, H₂S was absent from the barite effluent, which was also characterized by lower levels of NH₄⁺ (150.45 μM) compare to GS15-AGR09-PC2.

5.4.2. Sulfate reduction rates

The slurry from the barite chimney, GS15-AGR09-R1, was incubated in 7 duplicates at 4 and 20 °C, from which an average sulfate reduction rate was calculated (*fig. 17A*). The resulting reduction rates showed a higher rate for the duplicates incubated at 20 °C than 4 °C, with an average value of 50 and 32 nmol/cm³ d, respectively.

5.4.3. Organic and inorganic carbon

TOC values falls below that of GS15-AGR09-PC2 at 1.4 g/Kg, but show DIC concentrations and pH at 2.22 μM and 7.48, respectively, which is close to seawater values (*fig. 17C*).

5.4.4. Composition of the microbial community

The microbial community structure of GS15-AGR09-R1 are dominated by bacteria with 80.3% of the OUT`s, while archaea represents 9.5 % of the domain. The prokaryotic composition differ somewhat from GS15-AGR09-PC2 by higher relative density of Euryarchaeota (8.9%) and generally higher density of Bacteroidetes (18.3%). Proteobacteria was still the most prevalent Phylum, in which Deltaproteobacteria was the dominating class in the chimney (16.2 %). The highest relative abundance of ANME-1 (8.7 %) compared to GS15-AGR09-PC2 also characterized this sample. The sulfate reducing community was represented by Desulfobacterales, Desulfarculales and Desulfuromonadales. Desulfobacterales was also the dominant sulfate reducer (4.6%), followed by Desulfarculales and desulfuromonadales (0.5 and 0.4 %, respectively) (*fig. 18A and B*).

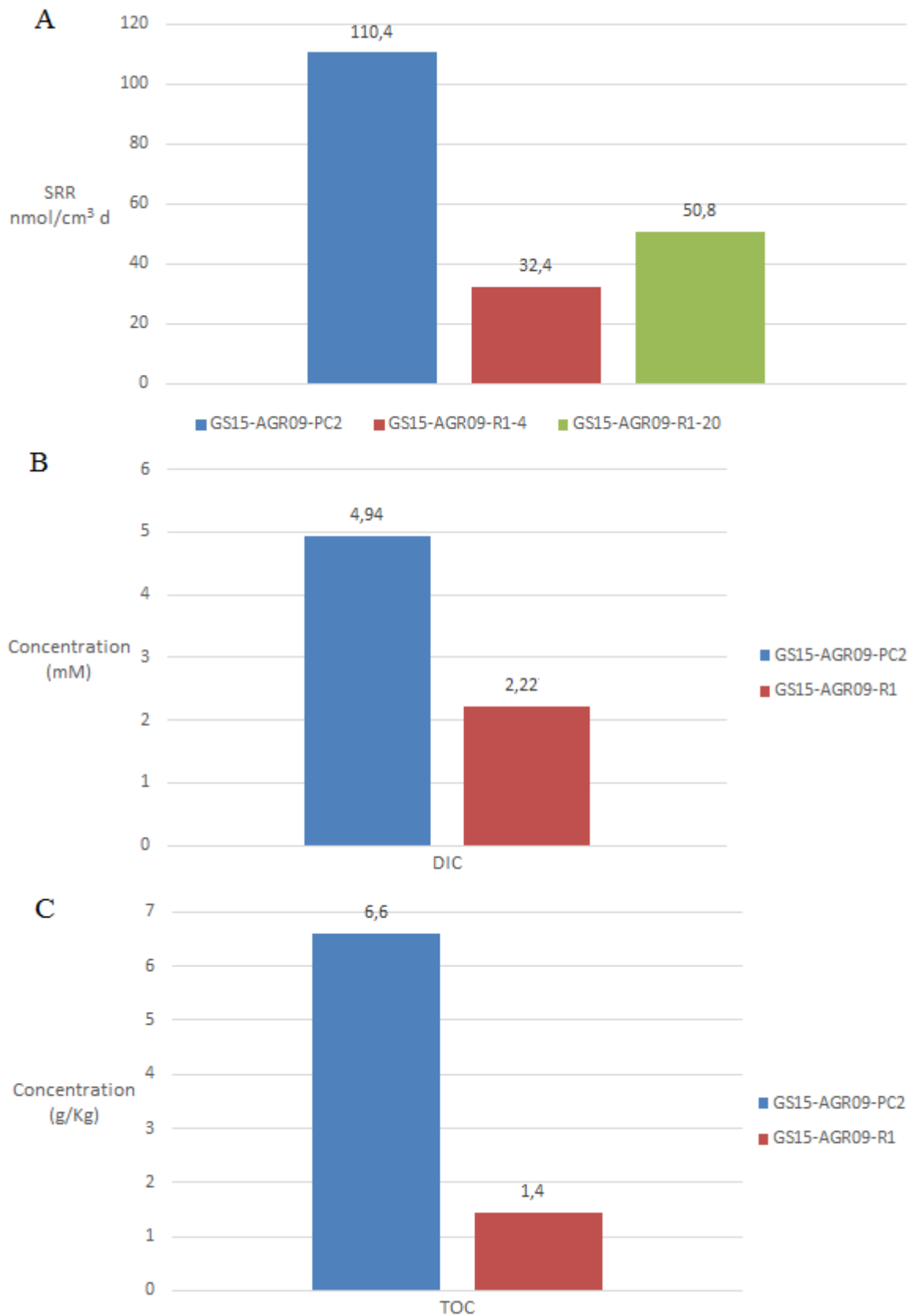
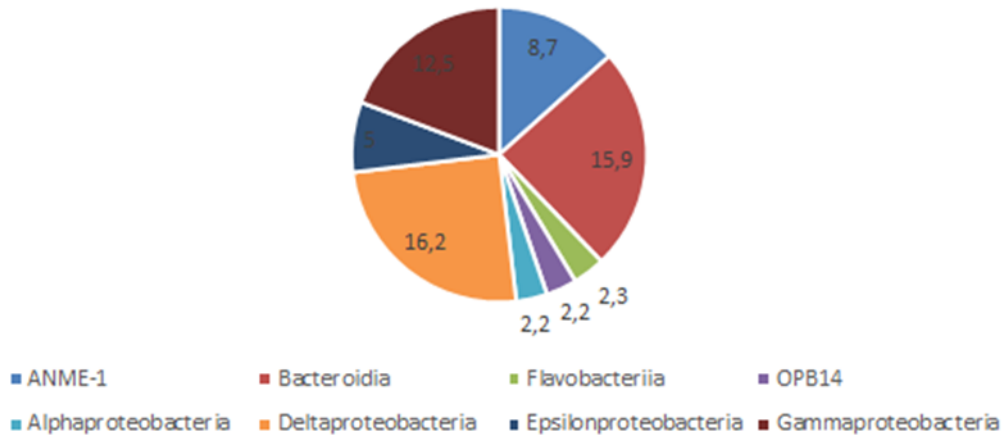


Figure 17. Sulfate reduction rates measurements for GS15-AGR09-PC2 and GS15-AGR09-R1 (A). TOC concentration from the barite chimney was sampled from the barite slurry, while DIC was obtained from the biosyringe sample.

Table 3. Fluid composition in the surface sediments (GS15-AGR09-PC2) and in the biosyringe (GS15-AGR09-BS). All samples were obtained from the barite field. ^aFluid used for ³⁵SO₄²⁻ incubation of the barite slurry. The fluid was obtained from the top water from GS15-AGR09-PC2.

Sample	H₂ (nM)	CH₄ (μM)	pH	SO₄²⁻ (mM)	H₂S (μM)	NH₄⁺ (μM)
GS15-AGR09-PC2	nd	0.185	7.78	21.5	2555	1255
GS15-AGR09-BS	16 nM	105,4	7.48	29	nd	150.45
Incubation medium ^a	nd	nd	nd	27.7	nd	nd
Sample	Mg (ppm)	Mn (ppb)	Fe (ppb)	DIC (mM)	Ba (ppb)	NO₃⁻ (μM)
GS15-AGR09-PC2	1032	1002	0	4.94	68	0
GS15-AGR09-BS	1217	22	0	2.22	36	12.87

A %distribution of the most prevalent classes



B %distribution of sulfate reducers (order)

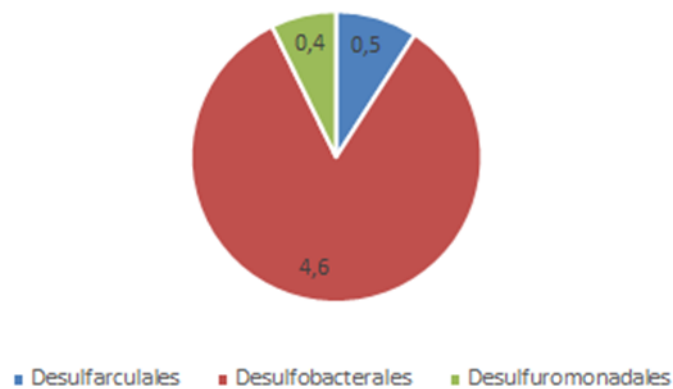


Figure 18. ANME-1 represented 8.7 % of the microbial community in the barite chimney (A), while *Desulfobacterales* was also the most prevalent sulfate reducer in GS15-AGR09-R1.

5.5. Sediments from barite field

5.5.1. Pore fluid geochemistry

The gravity core, GS14-GC14, was also characterized by highly fluctuating concentrations of sulfide and methane (*fig. 21B and C*). The sulfide concentration is highest at the lower section of the core with 55.40 μM at 198 cm, and show a net decrease towards the surface until the sulfide is depleted at 35 cm. The methane was measured at only seven horizons and show therefore a lower resolution than the sulfide measurement. However, the methane concentrations show the same trend, with values ranging

from 1.29 nM at 90 cm to 13.09 nM at 200 cm. These values are significantly lower than in GS15-AGR09-R1 and GS15-AGR09-PC2, but it seems that there is a net increase towards the lower section as with the sulfide. The core also contained seawater levels of sulfate through the whole core, with concentrations that lies between 28.02 to 28.52 mM, but show some tendencies to decline the last 15 cm of the core (*fig. 21A*).

Iron was depleted through most of the core except for a small enrichment 0.12 ppb at 50 cm. The manganese, however, was more abundant through the core and varied between 0.7 and 0.20 ppb, with a nett increase toward the bottom of the core (*fig. 20B*). Nitrate was only measured in the top 5 cm of the core, with 2.16 μM (*fig. 20A*). The depletion of nitrate occur concomitantly with a slight increase in ammonia concentration from 29.46 μM at 5 cm to 77.22 μM at 40 cm (*fig. 22*). The concentration is generally low throughout the core with stable values below 80 μM . PO_4^{3-} concentration also seems to display low variation in the sediments, with values that stays around 0.3 to 0.7 μM before a sudden increase at 102 cm to 1.16 μM (*fig. 20A*).

5.5.2. Sulfate reduction rates

Microbial sulfate reduction was also observed in the gravity core GS14-GC14 (*fig. 19A*), but at lower rates than in GS15-AGR09-R1 and GS15-AGR09-PC2 (*fig. 14A*). The activity was detected in the upper 120 cm, with highest rates at 90 and 30 cm (132 $\text{pmol}/\text{cm}^3 \text{ d}$ and 123 $\text{pmol}/\text{cm}^3 \text{ d}$, respectively). The microbial sulfate reduction disappear after 120 cm.

5.5.3. Organic and inorganic carbon

TOC concentrations are generally lower than measured in GS15-AGR09-PC2 and GS15-AGR08-PC1, but are comparable to the TOC concentration in GS15-AGR09-R1. The TOC concentration decrease from 2.3 g/Kg in the upper horizon until it stabilizes at 30 cm. The values stays above 1 g/Kg down to 80 cm, before it is depleted below detectable concentrations from 130 cm. The same pattern can be seen in the DIC concentration, alkalinity and pH, with stable concentrations and no nett increase. The DIC levels never exceed 2 mM, which is below seawater concentration that normally lies around 2 mM. The pH varies between 7.45 and 7.68, but display no nett change through the core.

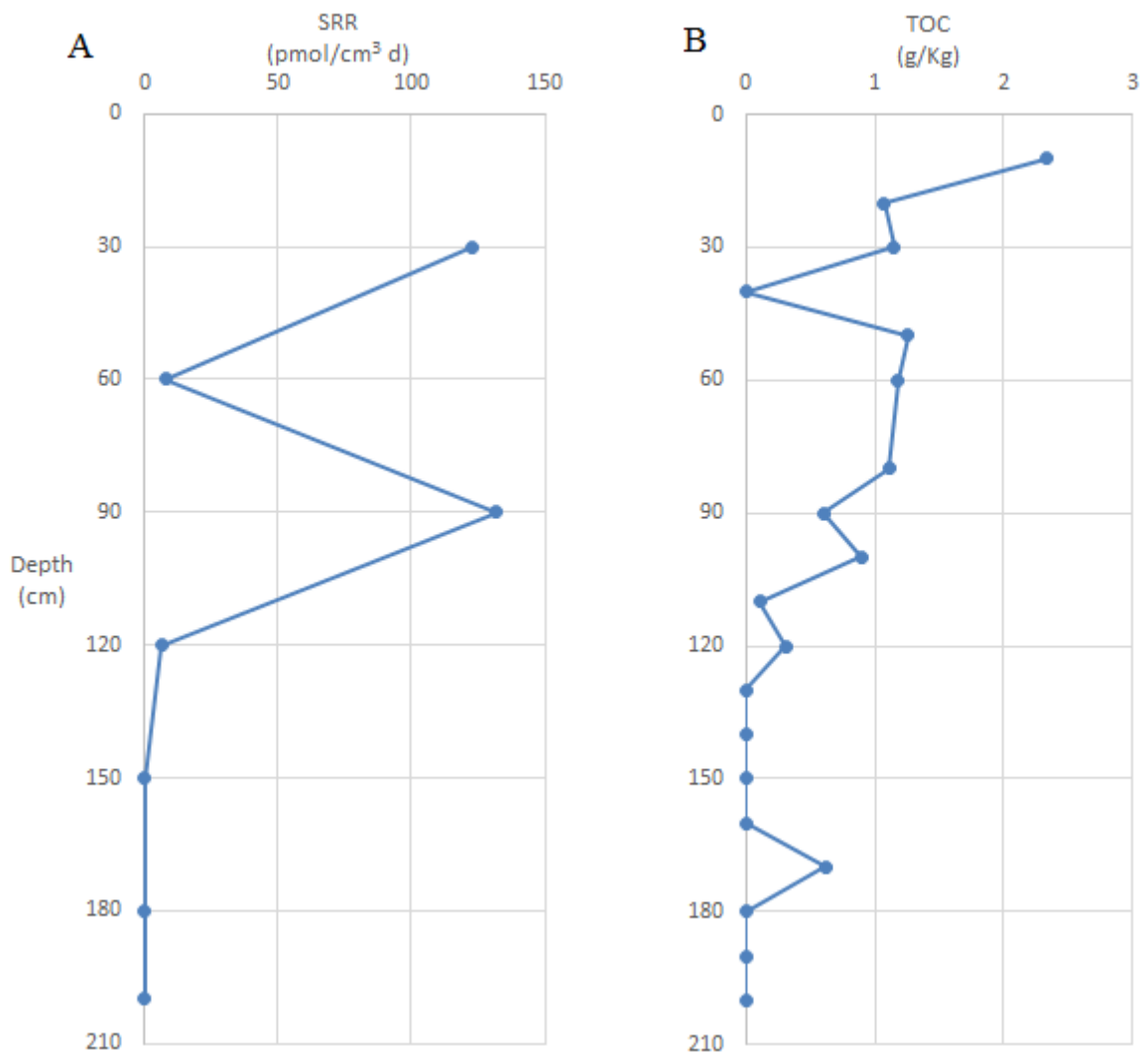


Figure 19. Sulfate reduction rates (A) and TOC concentrations (B) in GS14-GC14.

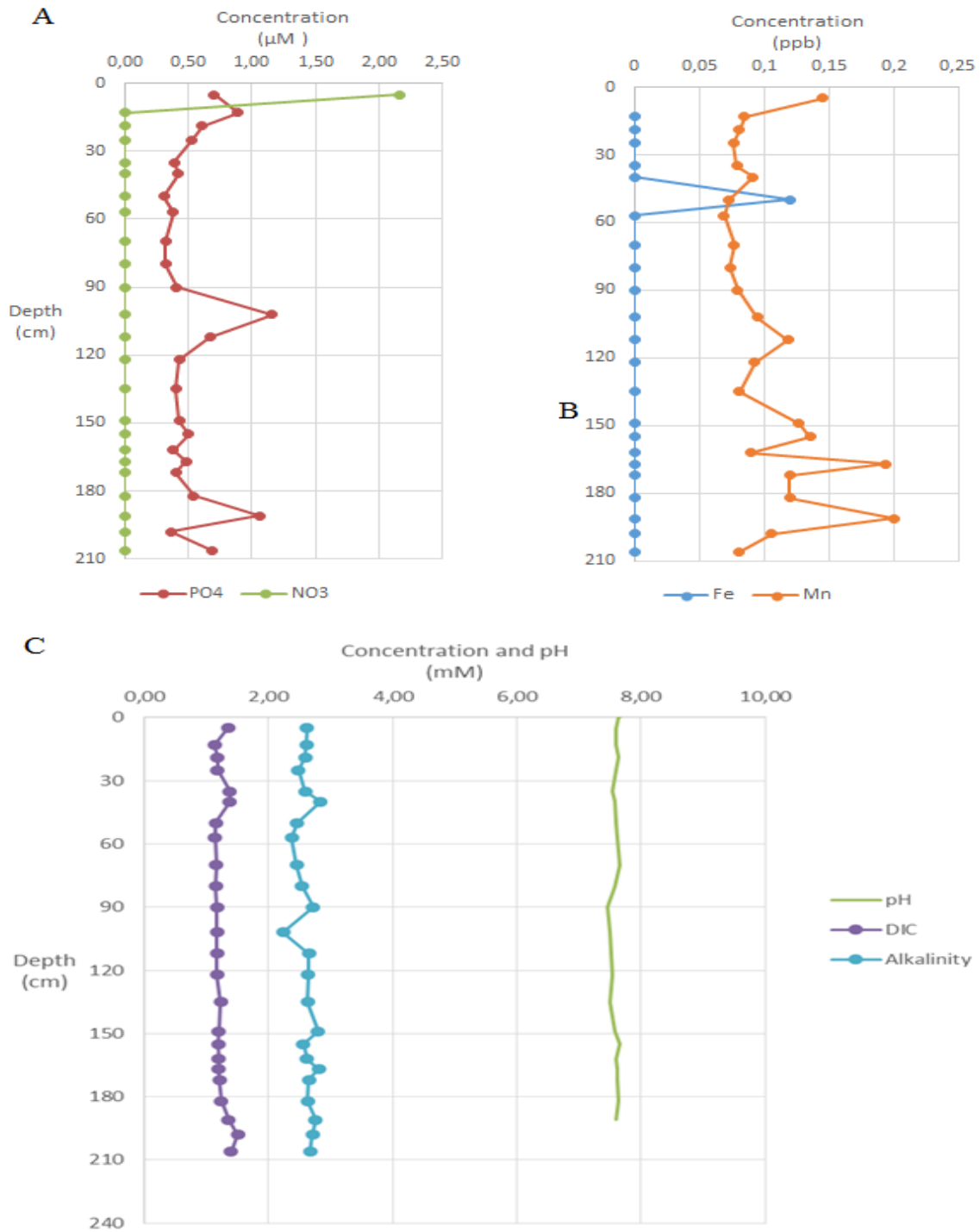


Figure 20. Nitrate was quickly consumed in the upper 5-6 cm of the core (A), while PO_4^{3-} levels were relative stable throughout the whole core. The concentrations are slightly elevated at 100 cm but decrease again down to 180 cm (B). Fe was more or less depleted in GS14-GC14, while Mn was present at relatively low concentrations (B). DIC, alkalinity and PH showed stable levels through the whole core (C).

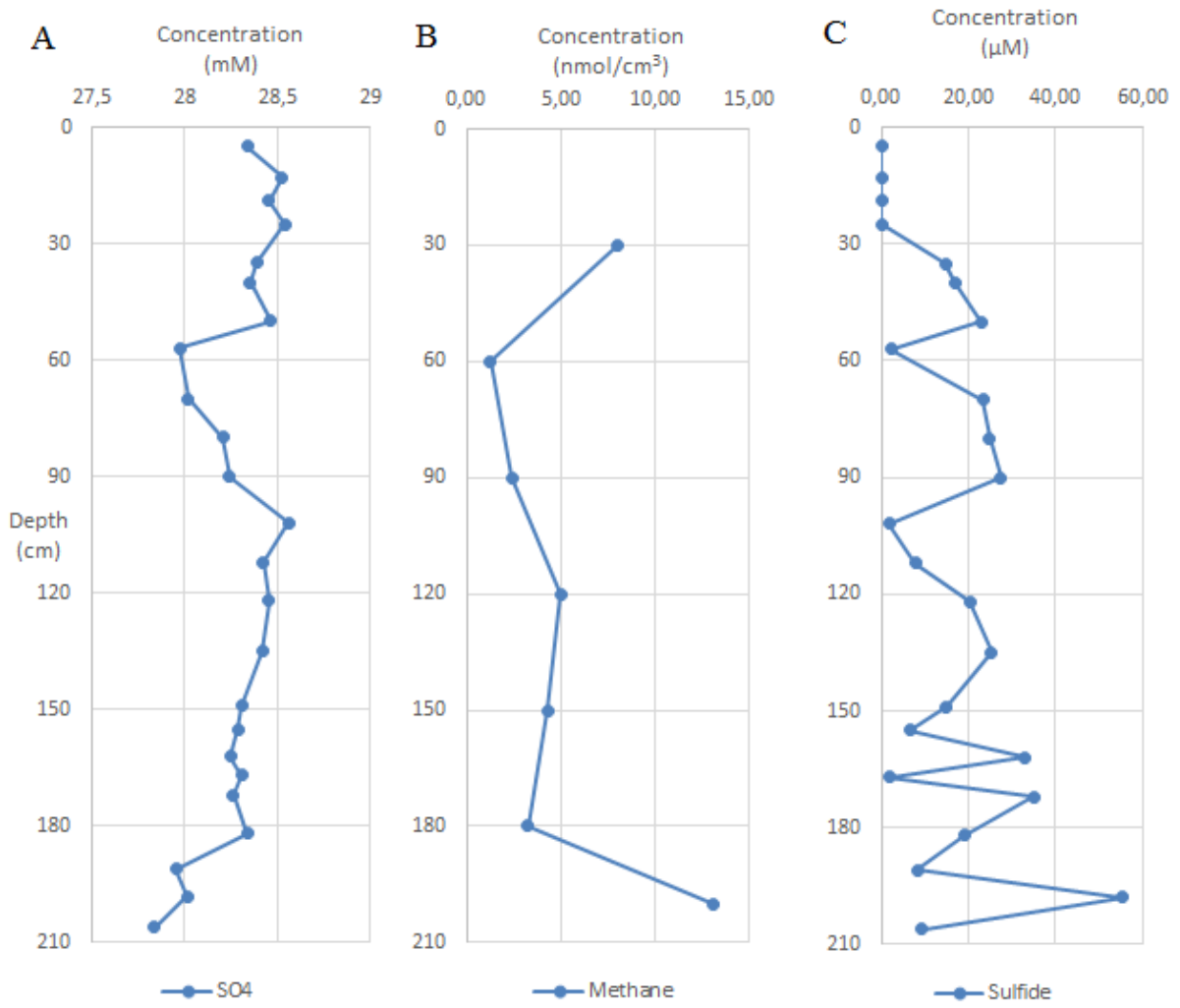


Figure 21. Sulfate concentrations were comparable to seawater concentrations through most of the core (A), while methane (B) and sulfide concentrations (C) fluctuated. Methane concentration was the lowest that were measured amongst the samples from the barite field.

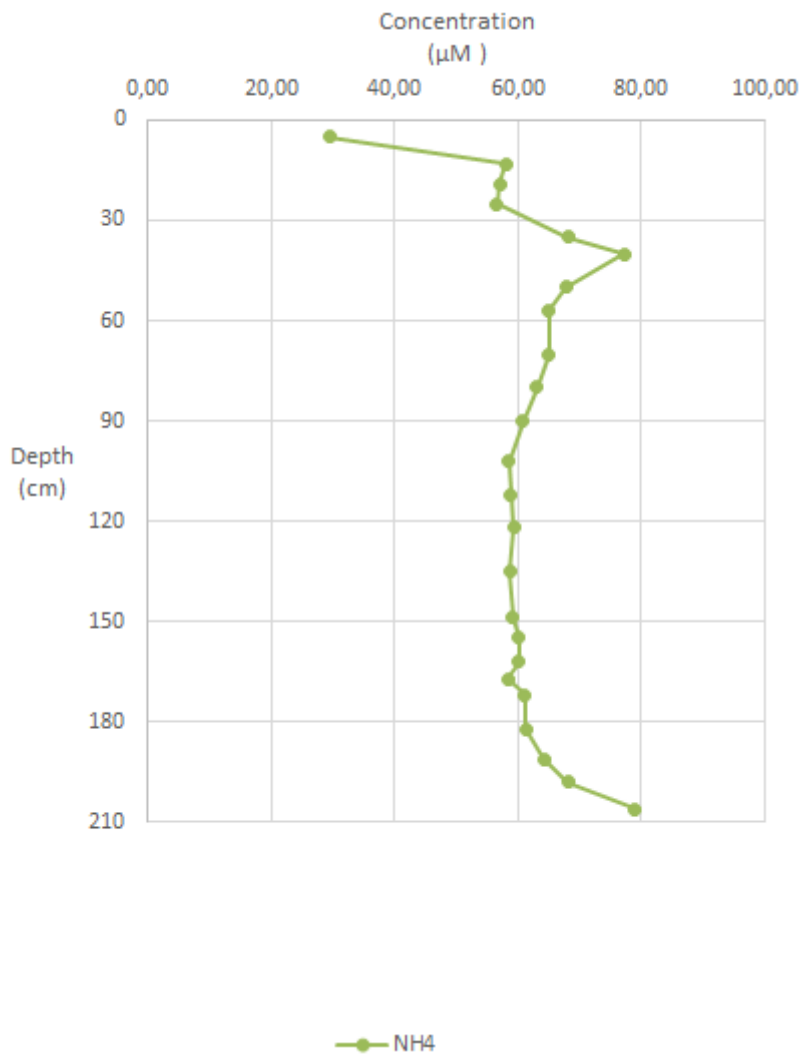


Figure 22. NH_4^+ concentration in GS14-GC14 was also quite stable through most of the core.

5.5.4. Composition of the microbial community

Bacteria was the dominant domain with the highest relative distribution at 90 cm with 96% of the detected OTU`s. All horizons were dominated by Proteobacteria, which was affiliated to Gammaproteobacteria, Deltaproteobacteria, betaproteobacteria and Epsilonproteobacteria (*fig. 23A*). The distribution of the Deltaproteobacteria range between 7.5 % at 60 cm to 13.5 % at 90 cm. Two orders that contain sulfate reducers were detected, where Desulfobacterales was the most prevalent with 8.6% at 90 cm. There were no hits for sulfate reducers at 30 cm despite the observed microbial sulfate reduction. Desulfobacterales was also found at 60 cm with 0.07% of the OTU`s. Desulfuromonadales was the dominant sulfate reducer in the lower section at 200 cm with 0.6 % of the OTU`s (*fig. 23B*). Only one sulfate reducer was detected at species level and one at genus level. The psychrophilic *Desulfofaba gelida* is affiliated with the Desulfobacterales order and represented 0.003% of all OTU`s, while SEEP-SRB1 was the most prevalent sulfate reducers at the 90 cm horizon with 0.08% of all OTU`s in that sample.

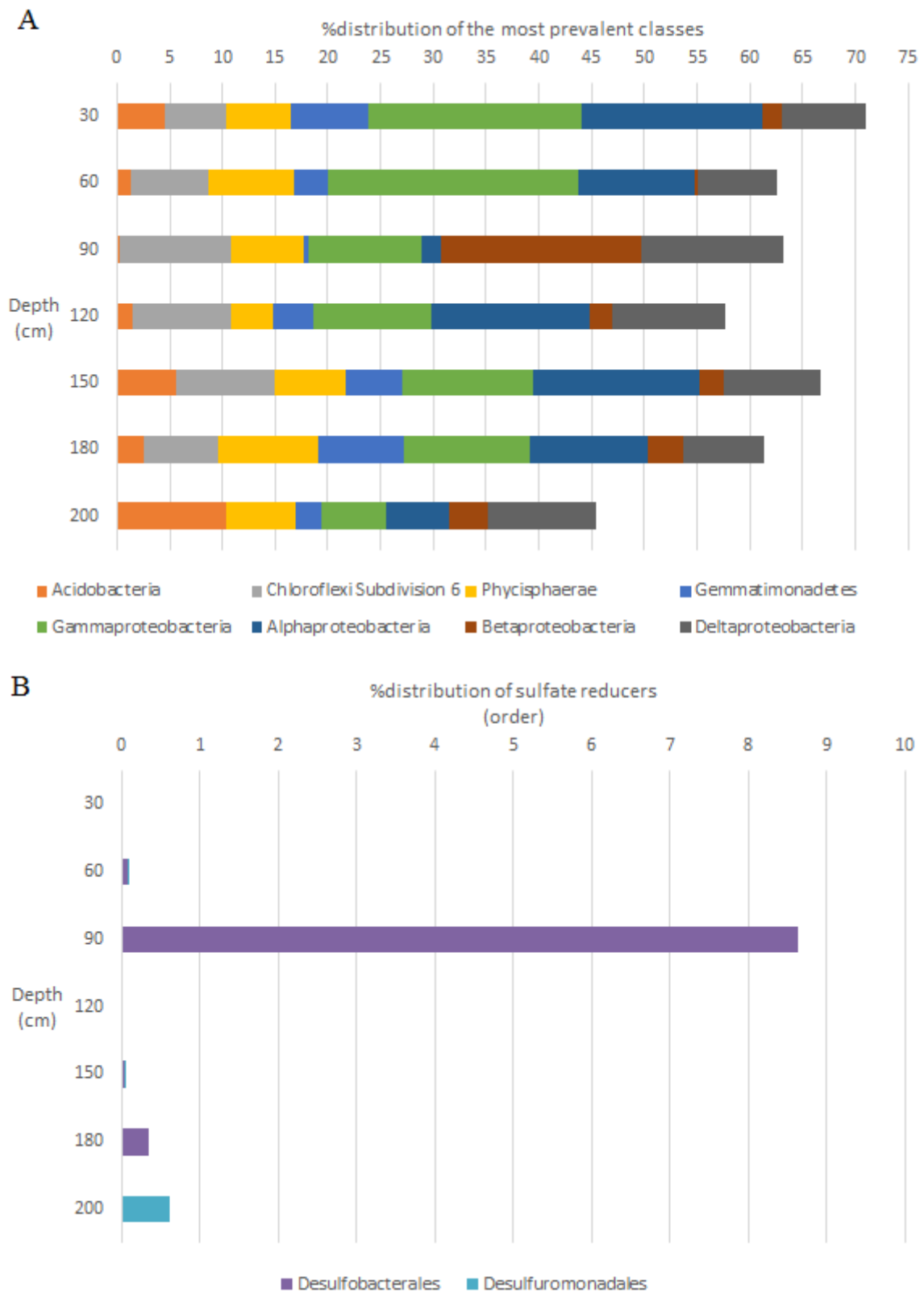


Figure 23. The distribution of the most prevalent classes (A) in the GS14-GC14, where Gemmatimonadetes and Gammaproteobacteria are the most abundant. Desulfobacterales are the most dominating sulfate reducer in the gravity core.

6. Discussion

6.1. Geochemistry of hydrothermal and non-hydrothermal sediments

6.1.1. Geochemistry of the background sediments

The background sediments that are associated with the LCVF, represented here by GS15-GC1, display geochemical features common for deep marine sediments. A deep-marine zonation signature with increased vertical distribution of the different geochemical zones characterizes the background sediments, which is in agreement with the general trend in low productivity areas (*e.g. Canfield, 1991; Jørgensen, 2006; Bowles et al, 2014*). Four geochemical redox zones can be recognized based on the classification criteria defined by Canfield and Thamdrup (2009), which include an oxic, nitrogenous, manganous and ferruginous zone. The oxic boundary is marked by the enrichment of dissolved Mn at 85 cm that co-occurs with the production of NH_4^+ (*fig. 10*). A characteristic feature of this core is the vertical distribution of the manganous zone that spans from 85 cm to the bottom of the core at 390 cm. The maximum concentration reaches 125 μM at 315 cm, which is equivalent to values reported from other metal rich deep-sea sediments (*e.g. Sørensen et al, 2004*), but slightly lower than observed in gravity cores closer to the vent field (*Jørgensen et al, 2012*). This deviates from the push core, GS15-AGR08-PC1, where iron is the dominant metal (*fig. 13B*). The primary source of Mn in arctic deep-marine sediments are continental weathering and/or riverine inputs (*Løwemark et al, 2013*). On the shelves, manganese undergoes repeated cycles of re-oxidation and reduction caused by the high organic carbon content in the sediments before it is exported to the deep-sea basins by scavenging processes in the water column and subsequent deposition as Mn-(oxyhydr)oxides (*see Løwemark et al, 2013*). However, ~90% of the Mn introduced to the global oceans has a hydrothermal origin (*Elderfield and Schultz, 1996; Glasby, 2006*), which point to the possible influence of LCVF on the geochemistry in the background sediments, considering that The black smoker fluid from LCVF is characterized by the enrichment Mn relative to Fe. Additionally, Mn-oxides can also act as a sink for reduced iron as a result of the higher electron affinity of Mn and the relative stability of some of the iron oxides Mn can therefore hamper the enrichment of reduced Fe in sediments with high concentrations of Mn-oxides (*Burdige, 1993; Haese, 2006*). This can potentially contribute to the low concentration of Fe in the upper 400 cm of the background sediments. However, the key determining factor of the iron depletion can probably be attributed to the distance from potential sources. Coastal areas are usually the main sink for iron, which render the deep-marine sediments depleted in iron (*Canfield et al, 1993; Haese, 2006*).

The sediments in the sampling site are a part of the Bear Island Fan that consists of transported and reworked sediments from the Barents shelf, that were supplied through melting plumes and debris flows during glacial activity. Sediments with higher organic carbon content were transiently supplied

to the fan (*Laberg and Vorren, 1995; 1996*) which explains the variable TOC values that range from 2 to 9 g/kg (*fig. 11*). These values are considered high compared to other deep-sea sediments, but are still lower than more productive areas along the coast (*Jørgensen et al, 2012*). Similar values have also been observed in the gravity cores that were obtained by *Jørgensen et al (2012)*. Arctic oceans are generally characterized by relative high organic matter input of terrestrial carbon (*Vogt and Knies, 2008*), which is less reactive than organic matter derived from marine primary production (*e.g. Hedges, 1992*) and can cause a higher degree of accumulation in arctic marine sediments. The recalcitrant nature of the carbon leads to a decrease in microbial activity, which causes the increase in vertical distribution of the geochemical zones in deep-marine sediments.

6.1.2. Geochemistry of the barite field

The chemical signature of hydrothermal fluids originates from the physical and chemical processes occurring during the fluids residence time in the reaction zone and discharge zone (*e.g. Alt, 1995; Baumberger, 2011*), where phase separation (i.e. boiling of fluids) and water-rock interaction with host-rocks and sediments are the most important processes. Sediments from the Bear Island Fan that underlie the axial volcanic ridge that hosts LCVF, also contribute to enrichment of organic and inorganic carbon in the vent fluid (*Welhan, 1988*). The modified fluids display increased concentrations of CH₄ and NH₄⁺ (*Baumberger, 2011*), which generates a larger diversity of catabolic energy sources. The supply of dissolved carbonate and NH₄⁺ to the hydrothermal fluids buffers the solution and causes the pH to increase (*Baumberger, 2011*). The pH in the end-member fluid (EM) at LCVF is around 5.6-5.8, which is similar to other sediment-influenced systems (*e.g. Von Damm, 1995; Tivey et al, 2007; Frank et al, 2011, Baumberger, 2011*). Increased pH also affects the metal composition in the solution by decreasing the solubility of sulfides, because at high pH most sulfide is present as S²⁻ that can combine with metal ions to form insoluble sulfides. Furthermore, both Mn and Fe are scavenged from the solution and precipitated as metal sulfides (*Baumberger 2011; Tivey et al, 2007; Hannington et al, 1995*), but since dissolved Mn is more stable than Fe, the original Fe/Mn ratio changes in favour of Mn when introduced to more alkaline solutions (*Burdige, 1993; Elderfield and Schultz; 1996; Jørgensen, 2006; Glasby, 2006*). Hence, the Mn and Fe EM concentrations range from 62.2-65 and 8.7-19.6 μM, respectively (*Baumberger et al, 2011*). Consequently, the estimated Fe/Mn ratio of ~ 0.6 is lower than reported from other sites, which often ranges between 1 and 5 (*Von Damm, 1995*). Mn and Fe are totally absent in GS15-AGR09-BS, while small concentrations of dissolved Mn are detected in GS15-AGR09-PC2 and GS14-GC14 (*Table 3, fig. 20B*). The consumption can be further enhanced by the production of sulfide by sulfate reduction that increases the H₂S/Fe ratio, causing further precipitation of manganese and specially iron sulfides. Thus, Mn is often enriched relative to Fe in sediment influenced vent fields (*Tivey et al, 2007*).

The hydrothermal fluid is further modified when mixed with seawater in the active barite field. The percolating fluids undergo complex subsurface processes that include both biotic and abiotic reactions

in sediments with divergent permeability that causes a heterogeneous distribution of fluid composition and flow pattern (Weber and Jørgensen, 2002; Proskurowski et al, 2008; Eickmann et al, 2014; Nakamura and Takai, 2014; Steen et al, 2016). The modification of the fluid is featured in all samples obtained from the barite field. The variable chemical composition of GS15-AGR09-PC2, GS15-AGR09-BS (bio syringe), GS14-GC14 and GS15-AGR09-R1 (Barite chimney) reflects the subsurface consumption and production of the different chemical constituents. The fluids show a seawater (SW) to hydrothermal fluid (HF) ratio (SW:HF) of 9:1 relative to the EM. This mixing ratio is calculated by comparing the Mg concentration in the diffuse fluid with that of seawater. EM fluid is usually depleted in Mg by reactions in the recharge zone (see introduction), which means that any enrichment of Mg is supplied by seawater entrainment. The near-seawater concentration of Mg in the diffusing effluent can thus only be explained by the mixture of seawater in the mound, in which case the ratio between the fluid and seawater is equal to the Mg ratio between the diffuse fluid and seawater. The mixing ratio explains the Mg content (see table 4), but fails to explain the sulfide, sulfate and the variable Ca concentrations (e.g. Eickmann et al, 2014). The sulfate and sulfide are explained by subsurface microbial sulfate reduction (see next section), while the Ca concentration can be explained by the influence of other modifying processes. The EM fluid at LCVF is enriched in Ca compared to seawater values (table 4), which can be caused by dissolution of carbonates in the underlain sediments,. The Ca in GS15-AGR09-BS is probably affected by seawater during sampling and displays seawater values of both Ca and Mg in an otherwise evolved fluid. However, the depletion of Ca relative to seawater in GS14-GC14 suggest that there is reactions consuming Ca in the mound. Bicarbonate or metals are potential candidates. Additionally, crust are formed by the precipitation of metal sulfides and different types of carbonates, which will inflict further changes in the permeability and heterogeneity of the sediment structure. This can be one probable cause of the difference in geochemistry of the pore fluid between the samples.

Despite the high seawater influence, the sediments show reducing conditions with anoxic conditions close to the surface. The most probable cause is oxygen consumption by abiotic reactions with reduced compounds or microbial activity close to the surface. These processes have been shown to consume O₂ in diffuse fluids above 8-12 ° C in hydrothermal sediments (Corliss et al, 1979; Johnson et al., 1988; Proskurowski et al, 2008), and explain why hydrothermal mounds with high seawater influence are anoxic. The detection of a nitrogenous zone in the upper 5-6 cm of the GS14-GC14, a steep TOC gradient in the top section and a shallow anoxic zone in GS15-AGR09-PC2 bolster the assumption of heterotrophic contribution to the consumption of oxygen in the surface. The TOC concentration in the active hydrothermal sediments shows concentrations equivalent to the background sediments, but the occurrence of DSR close to the surface suggests that the organic matter associated with the surface hydrothermal sediments (e.g. GS15-AGR09-PC2) probably consists of carbon that is more liable and thus promote faster consumption of oxygen. Nevertheless, these values are low compared to other vent

sites and other productive areas and may cause the system to be substrate limited, which hampers the activity of the heterotrophic community (see below).

The distribution of the organic matter seems to correlate with the fluid composition in the barite field. The most evolved fluid contains the highest amount of electron donors for the chemoautotrophic community, which in turn facilitates production of organic matter. This is demonstrated by the relative high concentration of electron donors in GS15-AGR09-BS, which consist of fluids that were sampled from a barite chimney covered in thick layers of microbial mats. The distribution of microbial mats are thus strong indicators of available nutrients and marks the flow pattern of the most evolved fluids (*fig. 8A*). The most evolved fluid is also associated with chimney formation, which is often associated with areas of higher flow rates (*Eickmann et al, 2014*). Combined with the enrichment of ^{34}S and ^{18}O in the inner part of the barite chimneys compared to the outer part, chimney effluent function as a window to the inner part of the mound, and reveals the possibility of subsurface microbial induced fractionation of oxygen and sulfur (*Eickmann et al, 2014*). The chimney effluent (represented by the GS15-AGR09-BS) displayed elevated concentrations of CH_4 (105.4 μM) and H_2 (16 nM) compared to GS15-AGR09-PC2 (0.1853 μM and no H_2) and GS14-GC14 (between 1 and 13 nmol), which suggests that CH_4 and H_2 are consumed subsurface, implying microbial consumption of the reduced fluids. The GS14-GC14 displays seawater levels of sulfate through the whole core, which is a necessary component in anaerobic oxidation of methane (AOM). The seawater signature implies low flow rates of the hydrothermal fluids in that area, which causes longer residence time for the CH_4 and H_2 in the sediments. The difference in residence time and CH_4 and H_2 concentration between high flow rate areas and low flow rate areas underscores the spatial heterogeneity of the processes that affects the chemical composition of the hydrothermal fluid, and show that areas with longer residence time have lower concentrations of CH_4 and H_2 . Hence, the geochemical data gives a strong indication for a subsurface sink of CH_4 and H_2 in the sediments.

Table 4. Chemical composition from the surface samples where A) is obtained from *Eickmann et al (2014)* for comparative purposes, while B) is from this study. The chemical composition from GS14-GC14 fluid are listed in...

A	Na (mM)	K (mM)	Ca (mM)	SO_4^{2-} (mM)	H_2S (mM)	NH_4 (mM)	Mg (mM)	Ba (μM)
EM-fluid	397	34.5	28.1	0.7	3.59	5.4	0.0	40.5
GS09-ROV7-BS	442	11.9	11.5	24.1	0.1	0.6	46.9	5.1
GS09-ROV8-BS	440	11.8	11.4	24.8	0.1	0.6	46.8	1.7
GS09-CTD 7-2	445	9.6	10.1	29.2	0.0	0.0	51.6	0.0
GS09-CTD 8-4	440	9.5	10.2	29.2	0.0	0.0	51.6	0.1
Chemical composition of GS15-AGR09-PC2, GS15-AGR09-BS								

B								
GS15-AGR09-PC2	444.1	14.19	11.90	21.52	2.55	1.255	42.46	0.5
GS15-AGR09-BS	454.8	10.43	10.03	28.97	nd	0.150	50.07	0.2

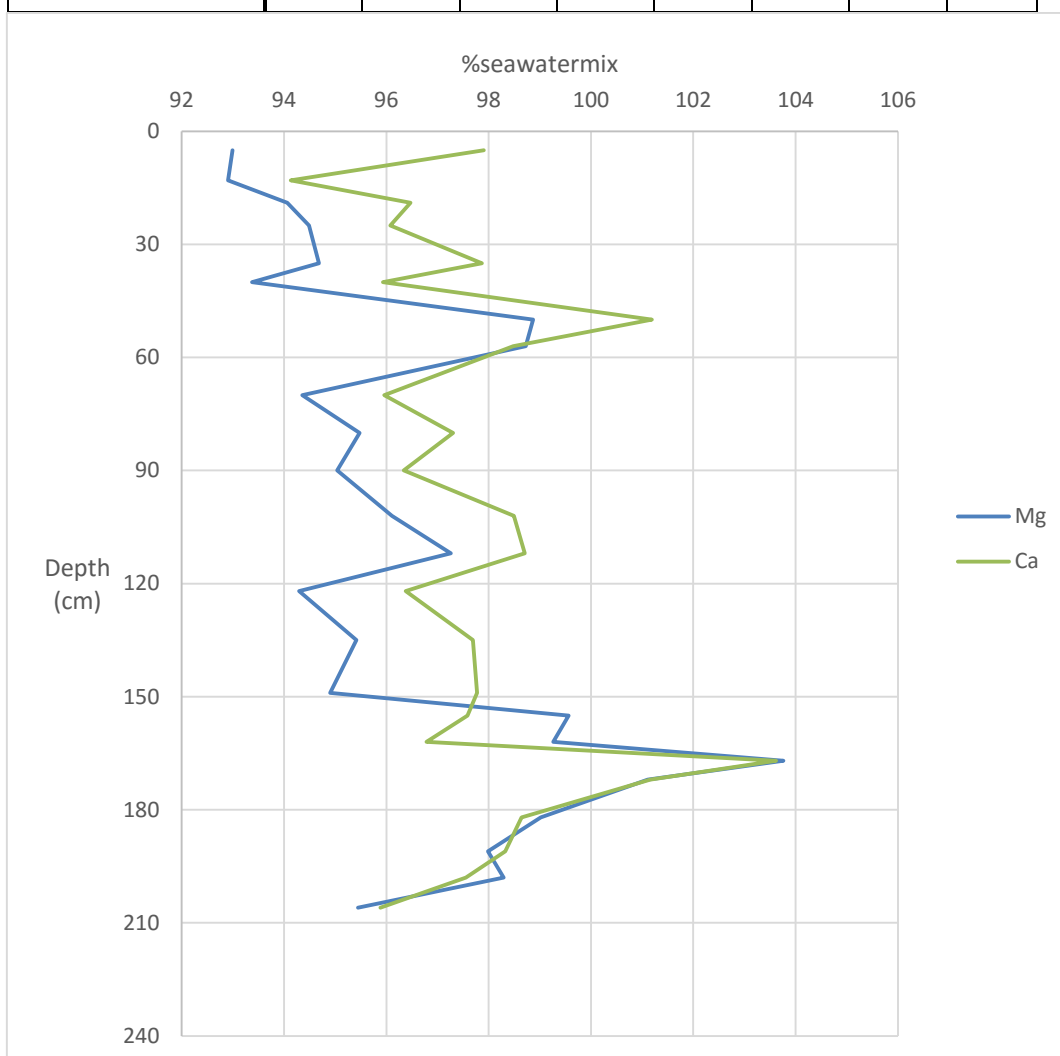


Figure 24. The general mixing ratio between seawater and end-member fluid based on calculations with Mg and Ca concentrations in GS14-GC14 and CTD data obtained from Eickmann et al (2014).

6.2. Distribution of SRB in the barite field

As shown in the last section, the energy availability in the vent area is considerably higher than the surrounding seafloor and is the likely cause of the flourishing primary production in the barite field. The spatial distribution of fluid compositions and flow patterns seems to determine the distribution of the metabolically functional groups in the barite field (fig. 25) (Amend et al, 2011; Dahle et al, 2015; Steen et al, 2016), and functions as a geochemical constraint on the chemoautotrophic primary production. Hence, the divergent fluid pattern and energy supply determines the organic carbon production, which in turn determines the distribution of the heterotrophic community (fig. 26 and 27). Accordingly, the sample which yielded the highest sulfate reduction rates at $\sim 110 (\pm 21.5) \text{ nmol/cm}^3 \text{ d}$,

GS15-AGR09-PC2, was associated with a lower mixing ratio (SW:HF ~ 8:2) and the highest carbon load (fig. 27). This sample contained the highest relative abundance of sulfate reducing bacteria (9.1% of all OTU`s at 11 cm depth), in which Desulfobacterales was the dominant phyla in all 4 horizons. The mesophilic *Desulfocapsa* was the most prevalent genus. This contrasts with the activity of the SRB community in GS14-GC14, which displays slow sulfate reduction rates (between 6 and 132 pmol/cm³ d), low carbon load and low temperatures (7.8 °C 20 cm into the sediment). This was also the only core with positive hits for a psychrophilic sulfate reducer, represented by *Desulfofaba gelida*. Few psychrophilic sulfate reducers are known, but rate measurements from sediments that were sampled in Hornsund, Svalbard, show equivalent rates as the temperate sediments further south, which indicate adaption to the low temperature (*Sageman et al, 1998*). In fact, a psychrophilic sulfate reducer, *Desulfofaba gelida*, was isolated from these sediments (*Knoblauch et al, 1999*). *D. gelida* was detected at 90 cm, which co-occur with the highest rates. However, it got only 84 positive hits out of 22004 (0.003% of the prokaryote community) and has probably no significant effect on the rates. Additionally, the relative abundance of sulfate reducers in GS14-GC14 was the lowest of all samples. Desulfobacterales was the only detectable order with 0.08% of the OTU`s, which is a lower relative abundance of SRB than in GS15-GC1, where Desulfobacterales represented 1.3 % of all OTU`s. The low rates in GS14-GC14 are thus probably not from incubation artefacts but generally poor growth conditions for the sulfate reducers.

The barite slurry also contained low TOC concentrations that were comparable to values in GS14-GC14 (~1.5 g/Kg), but displayed sulfate reduction rates that were 2-3 orders of magnitude higher than in GS14-GC14 (32-50 nmol/cm³ d and 6-132 pmol/cm³ d, respectively). The rates does not correspond to the TOC concentrations, but the activity does reflect an environment ideal for sulfate reducing bacteria. However, the relative abundance of sulfate reducers were much higher than in GS14-GC14, where the sulfate reducing community represented 5.5 % of all the OTU`s. The presence of H₂ in fluids sampled close to the barite chimney (GS15-AGR09-BS) suggest that this pathway could have function as a substrate for autotrophic sulfate reduction in the barite chimney. The addition of CH₄ and H₂ could accordingly support better growth condition in the chimneys and compensate for the lack of availability of organic carbon. This assumption is bolstered by the high relative abundance of ANME-1, 8.7% of the detected OUT`s, which is higher than SRB (fig.18A). This suggests that anaerobic oxidation of methane could occur in the inner part of the chimney (e.g. *Steen et al, 2016*). However, no known sulfate reducing associates were detected in the barite slurry, which can imply that the ANME-1 that was present was free-living. This finding has previously been observed from cold seeps (*Orphan et al, 2002; Roalkvam et al, 2011*) and from previous studies from the barite field (*Steen et al, 2016*). It is also possible that the detected ANME-1 members forms consortia with uncultivated SRB lineages that could be novel syntrophs (*Teske et al, 2002, Pernthaler et al, 2008*), in which case they would not be detected. ANME-1 are usually associated with sulfate reducers affiliated to the

Desulfobacterales order (*Knittel and Boetius, 2009*), which ~83% of the sulfate reducers in the barite slurry (GS15-AGR09-R1). However, SEEP-SRB1 groups, which is known to form consortia with ANME-1 (*Knittel and Boetius, 2009; Roalkvam et al, 2011*), were absent from the Barite. The reduction rates in the three samples correlate well with microbial density, which in turn seems to be controlled by nutrient supply in form of organic matter and the additional supply of H₂ and CH₄ in the barite chimney.

6.3. Comparing LCVF with equivalent sites

6.3.1. Rate differences

Previous rate measurements in hydrothermal systems have been restricted to only a few sites, namely; Guaymas Basin vent field, Gulf of California (*Weber and Jørgensen, 2002; Kallmeyer and Boetius, 2004; Elsgaard et al, 1994a*); Middle Valley vent field, Juan de Fuca Ridge (*Frank et al, 2013*) and Lake Tanganyika, East Africa (*Elsgaard et al, 1994b*). The latter is the only fresh water vent field and is exposed to lower concentrations of sulfate. Nevertheless, the Lake Tanganyika vent field exhibits substrate availability equivalent to that of estuarine environments, which normally experience high supply of organic carbon (*Elsgaard et al, 1994b*). The rate measurements in these sediments showed a rate optimum at lower temperatures than Middle Valley and Guaymas basin vent fields, with 34-45 °C for the mesophilic community, and 56-65 °C for the thermophilic community (*Elsgaard et al, 1994b, Kallmeyer and Boetius, 2004; Frank et al, 2013*). A wide range of sulfate reduction rates were also reported from Middle Valley and Guaymas Basin, where Middle Valley demonstrated SRR from 16 to 2700 nM/cm³ d, while significantly higher rates were measured in Guaymas Basin. The highest rates recorded in marine sediments stem from the Guaymas Basin vent field with 6700 nmol/cm³ d (*Kallmeyer and Boetius, 2004*), which is ~60 times higher than in GS15-AGR09-PC2. Both vent field are covered by sediments, where Guaymas basin is characterized by especially high sedimentation rates (> 1 mm/yr) and 200 times more organic carbon than Middle Valley (*Frank et al, 2013*). Moreover, the sediments that are associated with the Guaymas basin vent field are supplied with additional substrates that are carried by the ascending vent fluid. These fluids supports the thermophilic and hyperthermophilic sulfate reducers with thermogenic decomposed organic carbon from below. The spatial distribution of the mesophilic community, however, close to the surface, is constrained by the distribution of primary production on the surface (*e.g. Beggiatoa* mats), which is mostly controlled by the substrate supply from ascending fluids (*i.e. H₂S and CH₄*) (*Weber and*

Jørgensen, 2002). The samples from Middle Valley were gathered from sulfide deposits where thermophilic and hyperthermophilic SRB dominated. The SRR showed an optimum reduction rate at ca. 90 °C, which deviate from all other sampling sites, which showed optimum between 40 and 70 °C (Frank et al, 2013).

6.3.2. Effect of temperature on sulfate reduction rates

The variation in SRR between these sites and LCVF demonstrates the effect of substrate supply and temperature on the microbial activity. The importance of temperature has been demonstrated with several studies from permanently cold sediments (e.g. Jørgensen et al, 1992; Isaksen and Jørgensen, 1996; Sageman et al, 1998), which show that most SRB display increasing rates at higher temperature than the *in situ* temperature. In fact, the lowest optimum temperature for a sulfate reducer is measured to be 21 °C and is obtained from Antarctic sediments with *in situ* temperatures of ca. -1 °C (Jørgensen et al, 1992; Isaksen and Jørgensen, 1996). Most SRB are thus adapted to higher temperatures than found in deep-marine sediments (Isaksen and Jørgensen, 1996). Thus, hydrothermal sediments with steep temperature gradients creates *in situ* temperature that coincide with the temperature optimum for any given SRB community, which promote higher rates (Isaksen and Jørgensen, 1996). LCVF have less steep temperature gradients and are more influenced by the surrounding seawater conditions, which is one possible reason for the observed rate differences between Guaymas basin, Middle Valley and LCVF. In fact, sulfate reduction rates have been demonstrated to increase 4- to 10-fold from *in situ* temperature to the optimum temperature (Sageman et al, 1998). The incubation temperature at 4 °C for GS14-GC14 and GS15-AGR09-PC2 are therefore way below the optimum temperature for the mesophilic community which usually lies around 30-40 °C (Isaksen and Jørgensen, 1996) and does probably not reflect the *in situ* SRR. Thus, a wider range of incubation temperatures for this project would probably result in higher reduction rates, and more importantly, a better knowledge of the *in situ* temperature would have demonstrated the *in situ* SRR from LCVF. The barite slurry, however, was the only sample incubated at ambient temperature (assuming effluent temperature of 20 °C), which is closer to optimum temperatures for mesophilic SRB. The sulfate reduction rates increased accordingly from 32 nmol/cm³ d to 50 nmol/cm³ d, which highlight the temperature sensitivity of dissimilatory sulfate reduction. However, the slurry was incubated with fluids collected from the top of the GS15-AGR09-PC2 push core (c.f. the artificial vent fluid used by Frank et al, 2013), which is assumed to reflect the approximate seawater composition in the barite field (with elevated H₂S and decrease SO₄²⁻ relative to ambient seawater, Table 3). However, this may not represent the exact *in situ* conditions of the barite chimney environment. How this affects the rates is uncertain, but the chimney effluent carried extra potential substrates that could support higher rates. These substrates were not present in the incubation medium and could therefore result in lower than *in situ* rates.

6.3.3. Effect of substrate availability on sulfate reduction rates

The substrate supply differs greatly between LCVF, Middle Valley and the Guaymas Basin vent field. The measured SRR in non-hydrothermal sediments associated with the Guaymas Basin vent field showed rates up to $11.8 \text{ nmol/cm}^3 \text{ d}$ in sub-samples obtained from near the surface and that were incubated at $3 \text{ }^\circ\text{C}$ (Elsgaard *et al*, 1994a). This is slightly higher than other deep-sea sediments, which exhibit rates around $0.2\text{-}2 \text{ nmol/cm}^3 \text{ d}$ (Elsgaard *et al*, 1994a), and is probably caused by the transport of high amount of organic matter to the seafloor and influence from the primary production in this vent field (Elsgaard *et al*, 1994a). The Guaymas Basin has generally more nutrient supply from the water column than LCVF as shown by the absence of sulfate reduction in GS15-GC1, which receive the same amount of organic carbon supply from the photic zone as LCVF. The precipitation of organic carbon from the euphotic zone is therefore not important in the LCVF. Primary production are the main supplier of organic matter to the mesophilic community in both LCVF and Guaymas Basin, where the highest rates are associated with highly productive areas at both sites (Elsgaard *et al*, 1994a; Weber and Jørgensen, 2002). The rates measured in LCVF are lower than reported from arctic sediments sampled in Hornsund, Svalbard, with an *in situ* temperature of -1.7° (Sageman *et al*, 1996) and SRR at $240 \text{ nmol/cm}^3 \text{ d}$, which is twice as high as measured in GS15-AGR09-PC2, and 3-5 orders of magnitude higher than measured GS14-GC14. However, the Svalbard sampling area was characterized by a higher nutrient supply, which underscores the importance on substrates for SRR. The difference in SRR between these sites are likely caused by a combination of temperature and nutrient supply, where the barite field shows lower carbon load and less steep temperature gradients than in the sediments of these other sites. However, temperature and substrate availability are probably more favourable in the interior of the barite field, where methane and hydrogen are potential candidates as electron donors and less seawater influence cause the temperature to be higher.

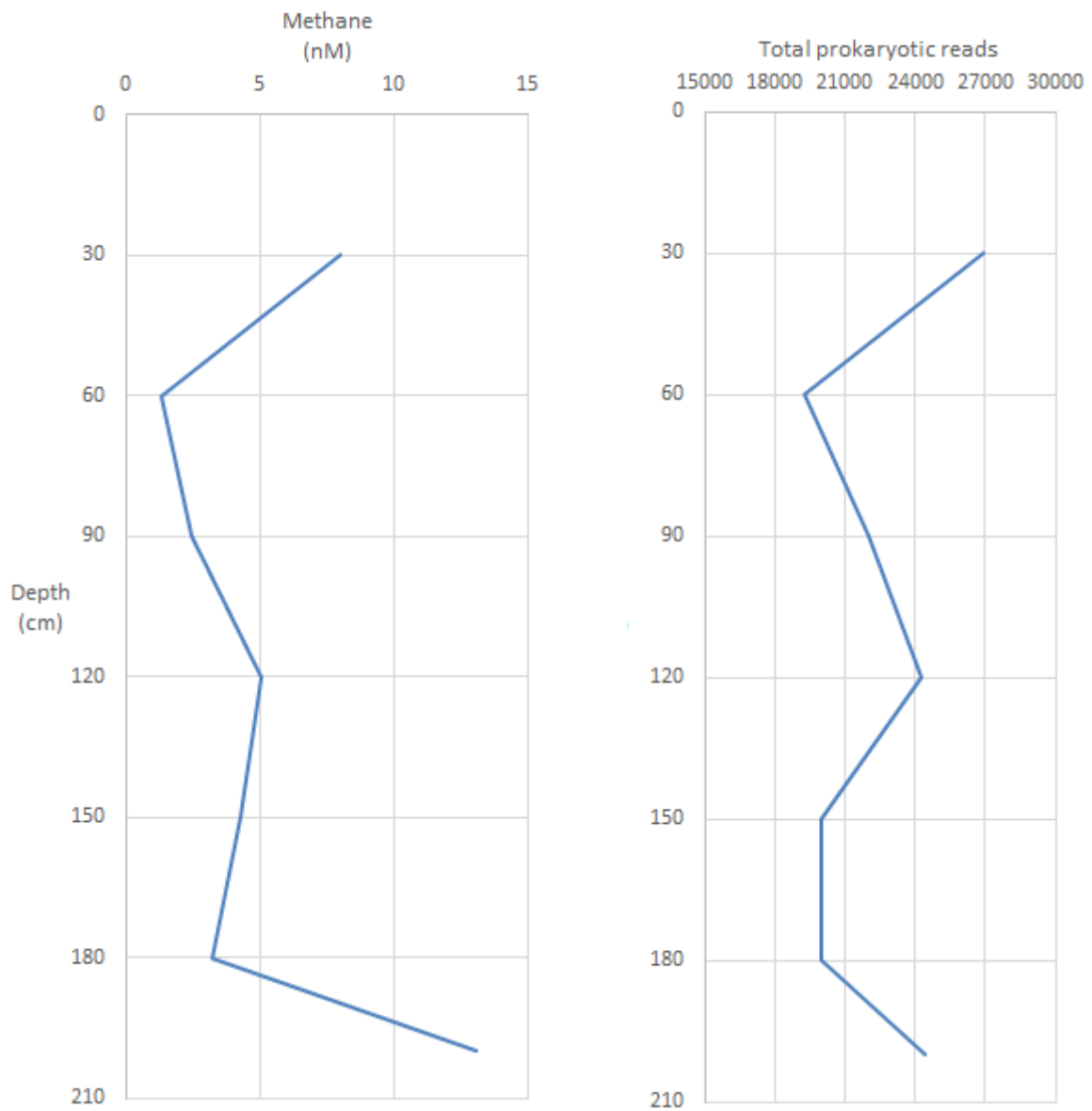


Figure 25. The GS14-GC14 show a strong correlation between prokaryotic density and fluid composition. The resolution of the methane concentration is quite poor due to only seven sampling points. The concentration may be more similar to the sulfide concentrations, which fluctuate more.

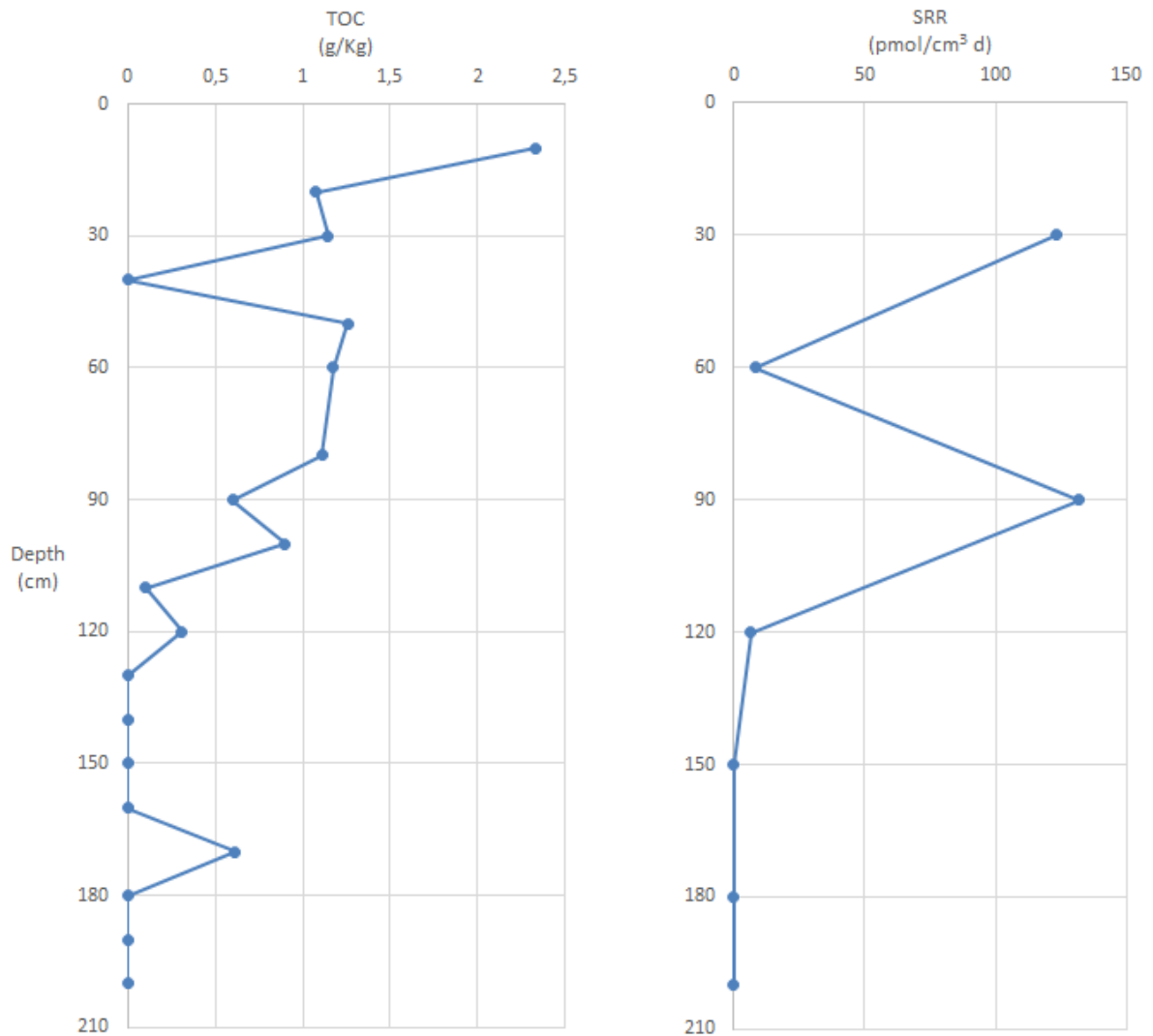


Figure 26. Correlating SRR and TOC in GS14-GC14. It is suggested that the organic carbon in the top sediments are the main substrates for SRB. AOM could occur, but no ANME was detected.

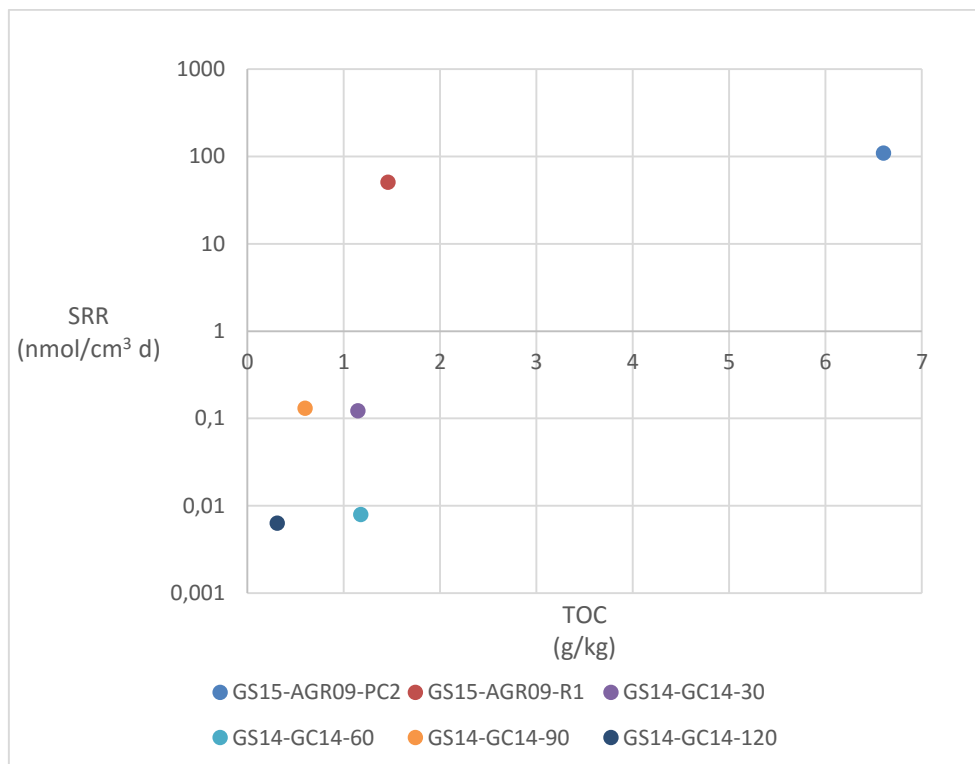


Figure 27. Correlating TOC concentrations and SRR. Reduction rates for GS14-GC14 was significant lower than for the surface sediments and contained lower concentrations of organic carbon.

6.4. The potential for an additional deep sulfate reduction zone

While the distribution of the sulfate reducers at the surface seems to be controlled by the quality and abundance of the organic carbon, isotopic and geochemical measurements of the more evolved fluids emanating through the barite chimney reveals the possibility of an additional sulfate reduction zone occurring at greater depths (*e.g. Eickmann et al, 2014; Steen et al, 2016*). A sulfate reduction zone independent of the primary production at the surface is possible due to the continuous supply of H_2 and CH_4 from below, and can sustain SRB as long as the temperature conditions are within the biological window. As sulfate is always an important constituent of diffuse fluids in mixing zones (*Nakamura and Takai, 2014*), the key determining factor is temperature and substrate availability.

6.4.1. Anaerobic oxidation of methane (AOM)

Despite the the thermodynamic potential for the reaction to proceed, the stability of methane and the sluggish reaction kinetics exclude any abiotic sink in the mound. This makes microbially mediated oxidation of the methane the most plausible cause of the methane depletion (*Reysenbach and Shock, 2002; Kasten and Jørgensen, 2006; Widdel et al, 2006*). As anaerobic oxidation always co-occurs with sulfate reduction (*Orphan et al, 2002; Martin et al, 2008; Brazelton et al, 2006*), the disappearance of methane in the mound is assumed to be associated with sulfate reduction and should therefore function as a sulfate sink. The elevated levels of EM fluid in the chimney effluent (GS15-AGR09-BS)

compared to the sediment samples confirms that the fluid emanating through the barite orifice is less influenced by seawater and represent the more reducing conditions that are found deeper into the mound (Eickmann *et al*, 2014). This fluid also carries sulfate enriched in ^{34}S , in which the fractionation is attributed to microbial fractionation of sulfate. The isotopic signature of the fluid is reflected in the interior of the barite chimney, which shows more positive $\delta^{34}\text{S}$ and $\Delta^{33}\text{S}$ than seawater (Eickmann *et al*, 2014). Combined, these observations give strong indications for a deep subsurface sulfate reduction zone.

The key determining factor that controls the distribution of ANME is the partial pressure of CH_4 (*e.g.* Girguis *et al*, 2003; Valentine and Reeburgh, 2007; Knittel and Boetius, 2009). AOM rates tend to decrease significantly, when methane concentrations decrease below 0.5 mM (Knittel and Boetius, 2009), which can explain the low density of ANME in GS15-AGR09-PC2 and absence in GS14-GC14. However, previous studies on the distribution of AOM in diffuse venting hydrothermal sediments are scarce (Proskurowski *et al*, 2008). Only a few sites have been studied, including the sediments at Guaymas Basin vent field in the Gulf of California and Lost City hydrothermal field on the mid-Atlantic Ridge (*e.g.* Teske *et al*, 2002; Brazelton *et al*, 2006; Proskurowski *et al*, 2008; Holler *et al*, 2011; Merkel *et al*, 2013). These studies confirm the possibility of methanotrophy in hydrothermal settings, with some studies demonstrating increased activity at temperatures in excess of 30 °C (Schouten *et al*, 2002; Holler *et al*, 2011; Merkel *et al*, 2013). In fact, laboratory studies show optimum condition at 30-60 °C (Kallmeyer and Boetius, 2004). These results also support the assumption that AOM could be of biochemical relevance in habitats of elevated temperatures like the interior of the barite field where the mixing ratio is lower and partial pressure of methane is higher (Holler *et al*, 2011; Merkel *et al*, 2013; Dahle *et al*, 2015). Nevertheless, the temperature is only of minor importance for the ΔG of the reaction (Nauhaus *et al*, 2002), which suggests that the ANME that inhabit the system are thermophilic. The temperature, mixing ratio (fig. 24) and low methane concentrations indicate that GS14-GC14 is sampled from parts of the barite field with low flow rate.

Furthermore, microbial communities are shaped by their chemical surroundings, where the change in chemical composition of a system is accompanied by a change in free-energy of a reaction (McCollom and Schock, 1997). In hydrothermal sediments with seawater mixing, the dilution of the vent fluid by seawater modifies the chemical composition of the vent fluid and changes the energy landscape of the system. The mixing ratio between seawater and hydrothermal fluid in the sediments is therefore important in constraining the distribution of functional groups in hydrothermal sediment (*e.g.* Holden *et al*, 2012; Dahle *et al*, 2015). The microbial community can thus be modelled by taking into account the standard free energy of a reaction (ΔG°), and the change in free energy (ΔG) of the reactions with changing chemical composition of the fluid during mixing (McCollom and Schock, 1997):

$$3) \Delta\text{G} = \Delta\text{G}^\circ + \text{RT} \ln \text{Q}$$

Thermodynamic models of the LCVF suggest that this vent field represents an extremity in terms of its energetic potential for hosting anaerobic methane oxidizers (Dahle et al., 2015; Steen et al, 2016), which contrasts studies on other basalt hosted systems where AOM were anemic. This difference in energy availability of AOM in LCVF is attributed to the sediment influence from the Bear Island Fan (Dahle et al, 2015). Microbial community models based on modelled energy availabilities from chemical compound suggest that around a dilution factor of approximately 9:1 between seawater and hydrothermal fluids (SW:HF), there is a transition from growth conditions favourable for anaerobic methane oxidizers to those favourable for aerobic sulfide and methane oxidizers (Dahle et al., 2015).

Consequentially, parts of the mound with lower mixing ratios (i.e. less seawater influence) favour metabolism based on reductive reactions (i.e. reduction of sulfate and CO₂), which include methanogenesis and sulfate reduction, while seawater-dominated parts of the hydrothermal system, where there is an abundance of electron acceptors, will favour aerobic oxidation of H₂S, CH₄ etc. (McCollom and Schock, 1997). The transition from oxidative reactions to reductive reactions in LCVF, is therefore assumed to take place at the 9:1 mixing ratio (Dahle et al, 2015). This mixing ratio generally marks the shift from oxidized conditions with high seawater influence, to reducing conditions with a more EM signature and increasing temperatures. The geochemistry and thermodynamic models strongly suggest that AOM occurs in the mound at more reducing condition and are possibly the dominant sulfate sink in the mound (Dahle et al, 2015). The difference between GS14-GC14 and the chimney fluid effluent, which represents the part of the mound with high flow rate, indicates that fluid with long residence time are more depleted in both methane and hydrogen. We attribute this depletion to microbial sulfate reduction in the deep subsurface. The sulfate penetration depth is difficult to determine, but hydrothermal mixing zones contain sulfate at all habitable temperatures (Nakamura and Takai, 2014), which means that temperature constrains the spatial distribution of sulfate reduction. The depth probably varies, where areas with high flow rates can accommodate AOM up to the surface. However, the occurrence of AOM is also affected by other interenvironmental differences, including pH, salinity and pressure, differences in thermodynamics and kinetics may affect the energy output in either way (Valentine and Reeburgh, 2007).

Table 4. Metabolic reactions for chemolithoautotrophy. Compiled and modified from Nakamura and Takai, 2014. ^aStandard-state Gibbs free energy at 2 °C and ~250 atm

Energy metabolism	Overall chemical reaction	ΔG_r° (kJ) ^a
Hydrogenotrophic methanogenesis	$H_2 + 1/4CO_2 \rightarrow 1/4CH_4 + 1/2H_2O$	-49.2
Hydrogenotrophic sulfate reduction	$H_2 + 1/4SO_4^{2-} + 1/2H^+ \rightarrow 1/4H_2S + H_2O$	-74.9

Anoxic methanotrophy (AOM)	$\text{CH}_4 + \text{SO}_4^{2-} \rightarrow \text{HCO}_3^- + \text{HS}^- + \text{H}_2\text{O}$	-30.1
-------------------------------	--	-------

6.4.2. H₂ consumption

Studies from several sites have shown greater H₂ loss with longer subsurface residence time, which suggests that there is an additional abiotic or biotic sink in the mound (*e.g. Wankel et al, 2011*). Any abiotic reactions involving H₂ are potentially very exergonic, but due to the sluggish nature of the reaction, the oxidation of H₂ in hydrothermal sediments often proceeds with the aid of enzyme catalysts (*Reysenbach and Schock, 2002*). Consequentially, most of the H₂ consumption is caused by microbial activity in the hydrothermal mound. The consumption can be coupled to sulfate, iron, Mn and nitrate, but also to methanogenesis (*Proskurowski et al, 2008; Holden et al, 2012*). The latter has been suggested based on isotope data, but not yet directly measured (*Wankel et al, 2011*). Several types of bacteria and archaea are able to accommodate oxidation of H₂, in which methanogenic archaea and chemoautotrophic sulfate reducing bacteria are the most important metabolisms (*Schwartz and Friedrich, 2006*). Microbially mediated methanogenesis is a strictly archaeal trait which involves the oxidation of H₂ with CO₂ (*see table 4*) to form methane. Some of these groups are also associated with extremophiles, like *methanopyrus*, that are capable of growth at 122 °C (*Madigan et al, 2013*), which is the current upper limit for life and considerable higher than any observed AOM (*e.g. Merkel et al, 2013*). Several autotrophic sulfur reducers also display hyperthermophilic capabilities where the hydrogen consuming archaea, *Pyrolobus Fumarii*, have been grown at 113 °C (*Bløchl et al, 1997; Jaenicke and Sterner, 2006*). The robustness of both methanogens and sulfate reducers has been observed in previous studies in Guaymas Basin vent field, where SRR have been measured at temperatures of up to 102 °C (*Jørgensen et al, 1992; Stetter 1996; Elsgaard et al, 1994a*). However, while the latter example was heterotrophs, several hydrogen consuming sulfate reducers have been obtained from hydrothermal field. Two obligate H₂-oxidizing, sulfate-reducing archaea, *Ignicoccus islandicus* and *Ignicoccus pacificus*, affiliated with the Crenarchaeota phylum, were enriched from hot marine sediments and from the orifice of a deep-sea vent, respectively (*Huber et al., 2000*). In addition, hydrogen consuming bacteria have also been detected from hydrothermal systems (*Alain et al, 2010; Alazard et al, 2003*).

Consequentially, at some point the temperature exceeds viable conditions for ANME and will be replaced by the thermophilic and hyperthermophilic SRB and methanogens. This means that the H₂ consumption is probably situated deeper than the AOM zone, which is probably situated closer to the surface or along conduits with higher fluid flow. However, the role of sulfate as a H₂ sink depends on the penetration depth and at what the temperature it is depleted. In sediments with abundance of CO₂, H₂ and sulfate, the key determining factor of which one that prevails in a given system is the sulfate concentration (*Schwartz and Friedrich, 2006*). Autotrophic sulfate reduction is normally the most

thermodynamically favourable (*table 4*), which is demonstrated by studies in marine sediments where methane concentrations do not start to increase until the sulfate concentration is below 1 mM (*Sivan et al, 2007*). This is attributed to the higher substrate affinities and energy yield of autotrophic DSR. The battle for the hydrogen between SRB and methanogens will in most cases shift towards the SRB, due to the difference in energy yield. The higher hydrogen affinity of chemoautotrophic sulfate reducers would favour sulfate reducers over methanogens. Thus, in any system containing sulfate, the SRB will outcompete and inhibit the growth of methanogens (*Kristjansson and Schönheit, 1983; Schwartz and Friedrich, 2006*). However, which of them that prevails are dependent of the complex relationship between the reactants and products. The redox conditions deeper into the barite field at LCVF are difficult to assess due to both abiotic and biotic consumption of hydrogen, methane and sulfate. It requires a substantial amount of seawater mixing to lower the vent fluid temperature down to the biological window (*Reysenbach and Schock, 2002*), which would cause the sulfate levels to increase and sulfate reduction would be favoured as a H₂ sink. Moreover, energy modelling by Dahle et al (*2015*) demonstrates the increasing dominance of methanotrophy above a SW:HF mixing ratio of 9:1, which means that AOM could be the dominant sulfate sink in the subsurface. How this affects the sulfate concentration is difficult to assess, but in a system low on sulfate, methanogenesis could be the preferred H₂ sink. Nevertheless, hydrogen consumption by methanogens and sulfate reducers seems to increase in dominance with increasing temperature. The battle between these two metabolic pathways can also be affected by the high methane concentration in the solution that may hamper the methane formation. If so, chemoautotrophic sulfate reduction becomes the dominant hydrogen sink.

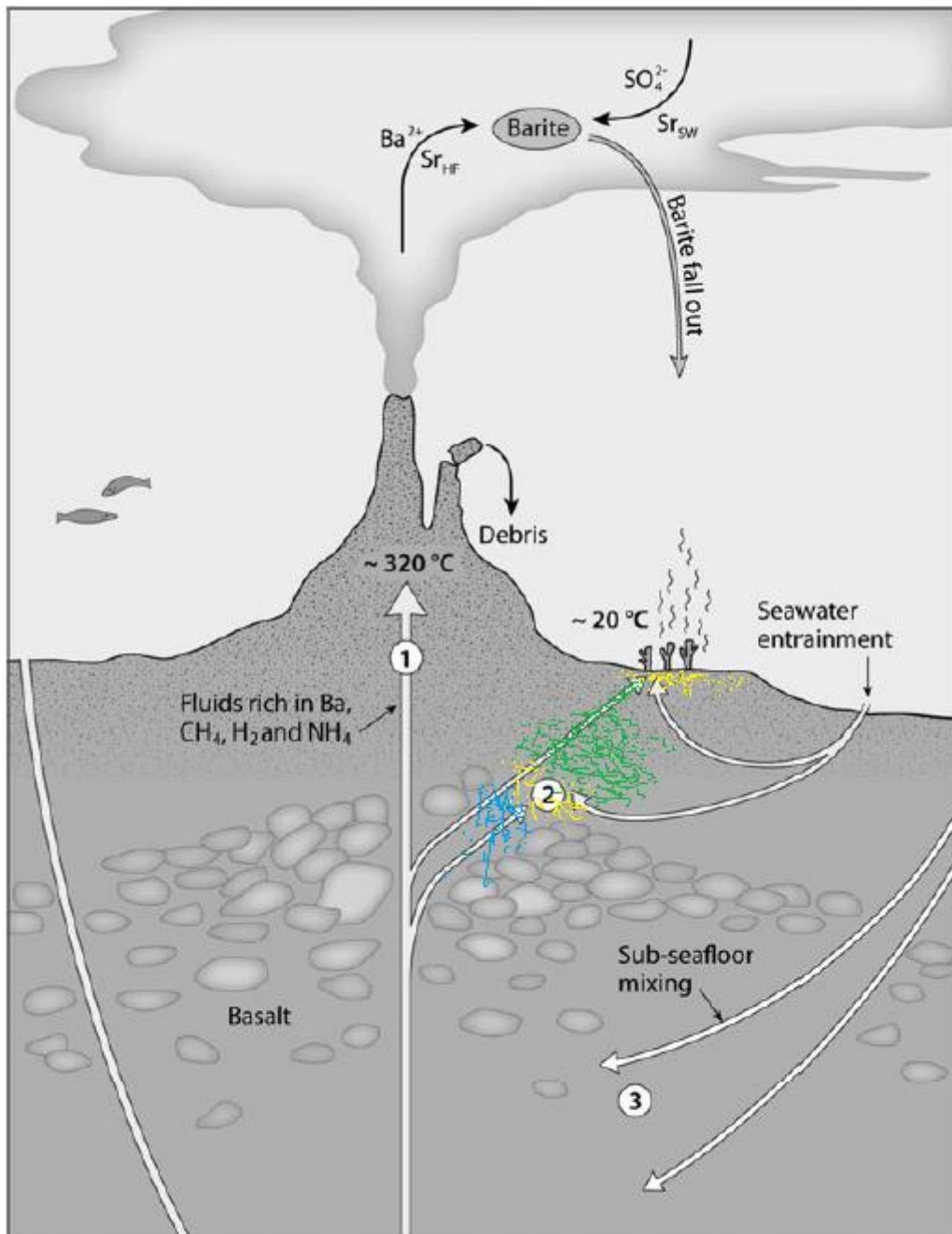


Figure 28. Simplified model modified from Eickmann et al, 2014. (1) Undiluted hydrothermal fluid rich in reduced compounds. (2) Hydrothermal fluid is mixed with seawater with the subsequent consumption of H_2 and CH_4 . Heterotrophic sulfate reduction (yellow) occur close to the surface preferentially where the highest primary production takes place. When the liable carbon is consumed, methanotrophy (green) takes over. Since SRB and methanogens (blue) are more tolerant to heat the consumption of H_2 occur below methanotrophy where there is too hot for ANME.

7. Conclusion

The results obtained in this study provide constraints on the distribution of microbial sulfate reduction in diffuse venting sediments at Loki's Castle Vent Field, by integrating direct measurement of sulfate reduction rates, geochemical measurements from the pore fluids and analyses of the microbial community.

- The distribution of sulfate reducing community seems to be constrained by the flow pattern and fluid composition. The highest sulfate reduction rates were measured close to the surface in an area of high primary production. The rates in less active areas showed lower relative density and lower reduction rates.
- The main electron donor on the surface seems to be organic carbon that is supplied by primary producers. H_2 and CH_4 can also function as a substrate in areas with evolved fluids in the chimney effluent.
- The consumption of CH_4 and H_2 in the subsurface is attributed to a deep sulfate reduction zone, where AOM is the primary sulfate sink in the mound. Both methanogens and autotrophic sulfate reducers could mediate the hydrogen consumption, but the presence of sulfate at all viable temperatures, along with the high methane concentration favours autotrophic sulfate reducers as the main hydrogen sink.
- Desulfobacterales was the dominant sulfate reducing order in all samples, followed by Desulfuromonadales and Desulfarculales. All belong to Deltaproteobacteria class. No thermophilic sulfate reducers were found, but GS14-GC14 contained SEEP-SRB1 and *Desulfobaba gelida*, a known psychrophilic sulfate reducer affiliated with Desulfobacterales.

8. Future work

While this study managed to measure and constrain the distribution of microbial sulfate reduction on the surface, several improvements of the methods can be done. First of all, the incubation temperature for the sediment samples probably didn't represent the in situ conditions, which means that the in situ rate is probably higher than measured. Performing incubations at more temperatures can give a better impression of the optimum rates of the sulfate reducing community and the in situ rates. The chimney effluent contained higher concentrations of possible substrates for sulfate reduction bacteria (CH_4 , H_2), which probably affected the growth rate and respiration rates. Incubation of the barite slurries in fluid more similar to the effluent will give a better constraint on the in situ rates. In addition, the prokaryotic density in the sediments and chimney measurement of the abundance of functional genes (*dsrB*) can give a better idea of the activity of the sulfate reducers.

Additional investigation is needed to characterize the putative deep sulfate reduction zone in the barite field. Isotope measurements of the methane in the effluent can give insight into what processes are consuming hydrogen, whether it is methanogenesis or autotrophic sulfate reduction.

9.1. References

- Alain, K.; Postec, A.; Grinsard, E.; Lesongeur, F.; Prieur, D.; and Godfroy, A. (2010). *Termodesulfatator atlanticus* sp. Nov., a thermophilic, chemolithoautotrophic, sulfate reducing bacterium isolated from a Mid-Atlantic Ridge hydrothermal vent. *International journal of Systematic and Evolutionary microbiology*, Vol. 60, pp. 33-38. DOI 10.1099/ijs.0.009449-0.(LES!!)
- Alazard, D.; Dukan, S.; Urios, A.; Verhè, F.; Bouabida, N.; Morel, F.; Thomas, P.; Garcia, J-L. and Ollivier, B. (2003). *Desulfovibrio hydrothermalis* sp. Nov., a novel sulfate-reducing bacterium isolated from hydrothermal vents. *International Journal of Systematic and Evolutionary Microbiology*, Vol. 53, pp. 173-178. DOI 10.1099/ijs.0.02323-0.
- Alt, J. 1995. *Subseafloor processes in mid-ocean ridge hydrothermal systems*. Pp. 85–114. in *Seafloor Hydrothermal Systems: Physical, Chemical, Biological, and Geological. Interactions*. S.E. Humphris, R.A. Zierenberg, L.S. Mullineaux, and R.E. Thomson. Geophysical monograph 91. American geophysical union
- Amend, J. P.; McCollom, T. M.; Hentscher, M.; Bach, W. (2011). *Catabolic and anabolic energy for chemolithoautotrophs in deep-sea hydrothermal systems hosted in different rock types*. *Geochimica et Cosmochimica Acta*, Vol. 75, pp. 5736-5748. doi:10.1016/j.gca.2011.07.041
- Baumberger T. 2011. *Volatiles in Marine Hydrothermal Systems*. Diss. ETH No. 20061.
- Blöchl, E., R. Rachel, S. Burggraf, D. Hafenbradl, H. W. Jannasch, and K. O. Stetter. 1997. *Pyrolobus fumarii* represents a novel group of archaea, extending the upper temperature limit for life to 113°C. *Extremophiles* 1:14-21.
- Bowles, M. W.; Mogollón, J. M.; Kasten, S.; Zabel, M.; Hinrichs, K-U. (2014). *Global rates of marine sulfate reduction and implications for sub-sea-floor metabolic activities*. *Science mag*, VOL 344 ISSUE 6186.
- Brazelton, W. J.; Schrenk, M. O.; Kelley, D. S.; Baross, J. A. (2006). *Methane- and sulfur-metabolizing microbial communities dominate the Lost City hydrothermal field ecosystem*. *Applied and environmental microbiology*, Vol. 72, No. 9, pp. 6257-6270.
- Bruvoll, V; Breivik, A. J.; Mjelde, R; Pedersen, R.B. (2009). *Burial of the Mohn-Knipovich seafloor spreading ridge by the Bear Island fan: Time constraints on tectonic evolution from seismic stratigraphy*. *Tectonics*, VOL. 28, TC4001, doi:10.1029/2008TC002396.
- Burdige, D. J. (1993). *The biogeochemistry of manganese and iron reduction in marine sediments*. *Earth-Science Reviews*, Vol.35, pp.249-284. Elsevier.
- Canfield, D (1991). *Sulfate reduction in deep- sea sediments*. *American journal of science*, Vol. 291, pp. 177-188.
- Canfield, D. E. and Thamdrup, B (2009). *Towards a consistent classification scheme for geochemical environments or, why we wish the term 'suboxic' would go away*. *Geobiology*, vol. 7, pp. 385-392. Blackwell publishing

- Canfield, D. E.; Jørgensen, B. B.; Fossing, H.; Glud, R.; Gundersen, J.; Ramsing, N. B.; Thamdrup, B.; Hansen, J. W.; Nielsen, L. P.; Hall, P. O. J. (1993). *Pathways of organic carbon oxidation in three continental margin sediments*. Marine Geology, Vol. 113, pp.27-40. Elsevier.
- Corliss, J. B.; Dymond, J.; Gordon, L. I.; Edmond, J. M.; von Herzen, R. P.; Ballard, R. D.; Green, K.; Williams, D.; Bainbridge, A.; Crane, K.; Van Andel, T. H. (1979). *Submarine thermal springs on the Galapagos rift*. Science Magazine, Vol. 203, No. 4385, pp. 1073-1083.
- D'Hondt, S.; Rutherford, S.; Spivack, A. J. (2002). *Metabolic activity of subsurface life in deep-sea sediments*. science, vol. 295. Pp. 2067-2070.
- Dahle, H.; Økland, I.; Thorseth, I. H.; Pedersen, R. B.; Steen, I. H. (2015). *Energy landscape shape microbial communities in hydrothermal systems on the Arctic Mid-Ocean Ridge*. The ISME journal, Vol. 9, pp. 1593-1606.
- De Beer, D; Sauter, E.; Niemann, H.; Kaul, N.; Foucher, J-P.; Witte, U.; Schluter, M.; Boetius, A. (2006). *In situ fluxes and zonation of microbial activity in surface sediments of the Håkon Mosby Mud Volcano*. Limnology and Oceanography, 51 (3), pp. 1315-1331. DOI: 10.2307/3841179.
- Eickmann, B.; Thorseth, I. H.; Peters, M.; Strauss, H.; Brocker, M. and Pedersen, R. B. (2014). *Barite in hydrothermal environments as a recorder of seafloor processes: a multiple-isotope study from the Loki's Castle vent field*. Geobiology (2014), 12, 308–321
- Elderfield, H. and Schultz, A. (1996). *Mid-Ocean Ridge hydrothermal fluxes and the chemical composition of the ocean*. Annu. Rev. Vol. 24, pp. 191-224.
- Elsgaard, L.; Prieur, D.; Mukwaya, G. M.; and Jørgensen, B. B. (1994b). *Thermophilic sulfate reduction in hydrothermal sediments of Lake Tanganyika, East Africa*. Applied and Environmental Microbiology, Vol. 60, No. 5, pp.1473-1480.
- Elsgaard, L; Isaksen, M. F.; Jørgensen, J. J.; Alayse, A-M.; jannasch, H. W. (1994a). *Microbial sulfate reduction in deep-sea sediments at the Guaymas Basin hydrothermal vent area: influence of temperature and substrates*. Geochimica et Cosmochimica Acta, Vol. 58, No. 16, pp. 3335-3343.
- Gerard Muyzer and Alfons J.M. Stams (2008). *The ecology and biotechnology of sulphate-reducing bacteria*. Nature publishing group. Volume 6, p. 441-454
- German, C. R. and Seyfried, Jr., W. E. (2014). *Hydrothermal processes*. Elsevier.
- Girguis, P. R.; Orphan, V. J.; Hallam, S. J.; DeLong, E. F. (2003). Growth and methane oxidation rates of anaerobic methanotrophic archaea in a continuous-flow bioreactor. Applied and environmental microbiology, Vol. 69, No. 9. Pp.5472-5482. DOI: 10.1128/AEM.69.9.5472–5482.2003.
- Glasby, G. P. (2006). *Manganese: predominant role of nodules and crusts*. In: Horst D Schultz, Mathias Zabel eds., *Marine geochemistry* (chp. 11), 2. utgåve. Springer - Verlag Berlin Heidelberg.
- Govenar, B. 2012. *Energy transfer through food webs at hydrothermal vents: Linking the lithosphere to the biosphere*. *Oceanography* 25(1):246–255, DOI <http://dx.doi.org/10.5670/oceanog.2012.23>.
- Haese, R. R. (2006). *The biogeochemistry of iron*. In: Horst D Schultz, Mathias Zabel eds., *Marine geochemistry* (chp. 7), 2. utgåve. Springer - Verlag Berlin Heidelberg.
- Hannington, Mark D.; Jonasson, Ian R.; Herzig, Peter M.; Petersen, Sven (1995). P115-157. Physical and chemical processes of seafloor mineralization at mid-ocean ridges. in *Seafloor Hydrothermal Systems: Physical, Chemical, Biological, and Geological Interactions*. Eds: S.E. Humphris, R.A.

Zierenberg, L.S. Mullineaux, and R.E. Thomson. Geophysical monograph 91. American geophysical union

Hansen, T. H. (1994). *Metabolism of sulfate-reducing prokaryotes*. Kluwer Academic Publishers. Antoine van Leeuwenhoek 66: 165-185.

Hedges, J. I. (1992). *Global biogeochemical cycles: progress and problems*. *Marine Chemistry*, Vol. 39, pp. 67-93. Elsevier.

Holden, J. F., J.A. Breier, K. L. Rogers, M. D. Schulte, and B. M. Toner. (2012). *biogeochemical processes at hydrothermal vents: Microbes and minerals, bioenergetics, and carbon fluxes*. *Oceanography* 25(1):196–208, <http://dx.doi.org/10.5670/oceanog.2012.18>.

Holler, T.; Widdel, F.; Knittel, K.; Amann, R.; Kellermann, M. Y.; Hinrich, K-U.; Teske, A.; Boetius, A.; Wegener, G. (2011). *Thermophilic anaerobic oxidation of methane by marine microbial consortia*. *The ISME Journal*, Vol. 5, pp. 1946-1956.

Huber, H.; Burggraf, S.; Mayer, T.; Wyschkony, I.; Rachel, R.; Stetter, KO. (2000). *Ignicoccus gen. nov., a novel genus of hyper-thermophilic, chemolithoautotrophic Archaea, represented by two new species, Ignicoccus islandicus sp. nov. and Ignicoccus pacificus sp. nov.* *Int J Syst Evol Microbiol* Vol. 50, pp. 2093–2100

Isaksen, M. F. and Jørgensen, B. B. (1996). *Adaption of psychrophilic and psychrotrophic sulfate reduction bacteria to permanently cold marine environments*. *Applied and Environmental Microbiology*, Vol. 2, No. 2, pp. 408-414.

Jaenicke, R. and Sterner, R. (2006). *Life at high temperatures*. In: *The Prokaryotes*, Vol 2: An evolving electronic resource for the microbiological community, 3rd edition. Eds. Dworkin, M.; Falkow, S.; Rosenberg, E.; Schleifer, K-H.; Stackebrandt, E. chp. 1.7, pp. 167-209. Springer Verlag. DOI: 10.1007/0-387-30742-7_7.

Jaeschke, A.; Jørgensen, S. L.; Bernasconi, S. M.; Pedersen, R. B.; Thorseth I. H. and Fruh-Green. G. L. (2012). *Microbial diversity of Loki's Castle black smokers at the arctic mid-ocean ridge*. *Geobiology* (2012), 10, 548–561.

Johnson, K. S; Childress, J. J.; Hessler, R. R; Sakamoto-Arnold, C. M.; Beehler, C. L. (1988). *Chemical and biological interactions in the Rose garden hydrothermal vent field, Galapagos spreading center*. *Deep-Sea Research*, Vol. 35, No. 10/11, pp. 1723-1744.

Jonkers, H. M.; Koh, I-O.; Behrend, P.; Muyzer G. and de Beer, D. (2005). *Aerobic carbon mineralization by sulfate-reducing bacteria in the oxygen saturated photic zone of a hypersaline microbial mat*. *Microbial Ecology*, Vol 49, No.2 pp.291-300.

Jørgensen, B. B and Boetius, Antje (2007). *Feast and famine-microbial life in the deep-sea bed*. *Nature publishing group*, vol. 5. Pp. 770-781.

Jørgensen, B. B. (2006). *Bacteria and marine biogeochemistry*. In: Horst D Schultz, Mathias Zabel eds., *Marine geochemistry* (s. 275) 2. utgåve. Springer - verlag Berlin Heidelberg.

Jørgensen, B. B. and D'Hondt, S (2006). *A starving majority deep beneath the seafloor*. *Science*, co. 314. Pp. 932-934.

Jørgensen, B. B.; Isaksen, M. F.; Jannasch, H. F. (1992). *Bacterial sulfate-reduction above 100 °C in deep-sea hydrothermal vent sediments*. *Science*, New Series, Vol. 258, No. 5089. pp. 1756-1757

- Jørgensen, S. L.; Hannisdal, B.; Lanzen, A.; Baumberger, Tamara; Flesland, K.; Fonseca, R.; Øvreås, L.; Steen, I. H.; Thorseth, I. H.; Pedersen, R. B., and Schleper, C. (2012). *Correlating microbial community profiles with geochemical data in highly stratified sediments from the Arctic Mid-Ocean Ridge*. PNAS, E2846-E2855.
- Kallmeyer, J. and Boetius, Antje (2004). *Effects of temperature and pressure on sulfate reduction and anaerobic oxidation of methane in hydrothermal sediments of Guaymas Basin*. Applied and Environmental Microbiology. Vol. 70, No. 2, pp.1231-1233. DOI: 10.1128/AEM.70.2.1231-1233.2004
- Kallmeyer, J.; Ferdelman, T. G.; Weber, A.; Fossing, H. and Jørgensen, B. B. (2004). *A cold chromium distillation procedure for radiolabeled sulfide applied to sulfate reduction measurements*. *Limnol. Oceanogr.: Methods 2, 2004, 171–180*, the American Society of Limnology and Oceanography, Inc.
- Kasten, S and Jørgensen, B. B. (2006). *Sulfur cycling and methane oxidation*. In: Horst D Schultz, Mathias Zabel eds., *Marine geochemistry* (s. 275) 2nd edition, Springer – Verlag, Berlin Heidelberg.
- Kelley D. S, Baross J. A, Delaney J.R. (2002). *Volcanoes, fluids, and life at mid-ocean ridge spreading centers*. Earth Planet. Sci 30:385-491
- Klingelhøfer, F.; Geli, L.; Matias, L.; Steinsland, N. and Mohr, J. (2000). *Crustal structure of a super-slow spreading centre: a seismic refraction study of Mohns Ridge, 720N*. Geophys. J. Int. (2000) 141, 509-526.
- Knittel, K. and Boetius, A. (2009). *Anaerobic oxidation of methane: progress with an unknown process*. Annu Rev Microbiol. Vol.63, pp.311-34. doi: 10.1146/annurev.micro.61.080706.093130.
- Knoblauch, C. Jørgensen, B. B. and Harder, J. (1999). *Community size and metabolic rates of psychrophilic sulfate reducing bacteria in Arctic marine sediments*. Applied and environmental microbiology. Vol. 65, No. 9 p. 4230-4233
- Knoblauch, C.; Sahm, K. and Jørgensen, B. B. (1999). *Psychrophilic sulfate-reducing bacteria isolated from permanently cold Arctic marine sediments : description of oceanense gen. nov., nov., Desulfofaba gelida gen. nov., sp. Desulfotalea gen. nov., . nov. and Desulfotalea arctica sp.* International Journal of Systematic Bacteriology, Vol. 49, pp.1631-1643.
- Konhauser, K. (2007). *Introduction to geomicrobiology*. Blackwell Publishing
- Kristjansson, J. K and Schönheit, P. (1983). *Why do sulfate-reducing bacteria outcompete methanogenic bacteria for substrates?* Oecologia, Vol. 60, pp. 264-266. Springer-Verlag.
- Laberg, J. S. and Vorren, T. O. (1995). *Late Weichselian submarine debris flow deposits on the Bear Island Trough Mouth Fan*. Marine Geology, Vol. 127 pp. 45-72.
- Laberg, J. S.; Vorren, T. O. (1996). *The middle and late Pleistocene evolution of the Bear island Through Mouth Fan*. Global and Planetary Change, Vol. 12. pp. 309-330. Elsevier.
- Löwemark, L.; März,C; O'Regan M.; Gyllencreutz, R. (2013). *Arctic Ocean Mn-stratigraphy: genesis, synthesis and inter-basin correlation*. *Quaternary science reviews* 92. Pp.97-111. Elsevier.
- Madigan, M.; Martinko, J.; Stahl, D.; Clark, D. (2013). *Biology of microorganisms*. Global edition 13th edition. Pearson.
- Martin, W.; Baross, J.; Kelley, D. and Russel, M. J. (2008). *Hydrothermal vents and the origin of life*. Nature Reviews. Microbiology, Vol. 6, pp. 805-814. doi:10.1038/nrmicro1991.

McCollom, T. M. and Schock, E. L. (1997). Geochemical constraints on chemolithoautotrophic metabolism by microorganisms in seafloor hydrothermal systems. *Geochimica et Cosmochimica Acta*, Vol. 61, No. 20, pp. 4375-4391.

Merkel, A. Y.; Huber, J.A.; Chernyh, N.A.; Bonch-Osmolovskaya, E.A., Lebedinsky, A.V. (2013). *Detection of putatively thermophilic anaerobic methanotrophs in diffuse hydrothermal vent fluids*. *Applied and Environmental microbiology*. Vol. 79, Nr.3. pp. 915-923.

Nakamura, K.; Takai, K. (2014). *Theoretical constraints of physical and chemical properties of hydrothermal fluids on variations in chemolithotrophic microbial communities in seafloor hydrothermal systems*. *Progress in Earth and Planetary Science*, 1:5.
<http://www.progearthplanetosci.com/content/1/1/5>. Springer Open Journal

Nauhaus, K.; Boetius, A.; Kruger, M. and Widdel, F. (2002). *In vitro demonstration of anaerobic oxidation of methane coupled to sulfate reduction in sediments from marine gas hydrate area*. *Environmental Microbiology*, Vol. 4, No. 5, pp. 296-305.

Orcutt, Beth N.; Sylvan, Jason B.; Knab, Nina J. and Edwards, Katrina J. (2011). *Microbial Ecology of the Dark Ocean above, at, and below the Seafloor*. *Microbiology and molecular biology review*. Vol. 75, No.2, p. 361-422.

Orphan, V. J.; House, C. H.; Hinrich, K-U.; Mckeegan, K. D. and DeLong, E. F. (2002). Multiple archaeal groups mediate methane oxidation in anoxic cold seep sediments. *PNAS*, VOL. 99; No. 11, pp. 7663-7668. www.pnas.org/cgi/doi/10.1073/pnas.072210299.

Pedersen, R. B.; Rapp, H. T.; Thorseth, I. H.; Lilley, M. D.; Barriga, F. J. A. S.; Baumberger, T.; Flesland, K.; Fonseca, R.; Früh-Green G. L. & Jørgensen, S. L. (2010). *Discovery of a black smoker vent field and vent fauna at the Arctic Mid-Ocean Ridge*. *Nature communications*: DOI: 10.1038/ncomms1124.

Pedersen, R. B; Thorseth, I. H; Nygård, T. E.; Lilley, M. D.; Kelley, D. S. (2010). *Hydrothermal activity at the Arctic Mid-Ocean Ridges*. Geophysical monograph series 188. American Geophysical Union.

Pernthaler, A.; Dekas, A. E.; Titus Brown, C.; Goffredi, S. K.; Embaye, T.; Orphan, V. J. (2008). *Diverse syntrophic partnership from deep-sea methane vents revealed by direct cell capture and metagenomics*. *PNAS*, Vol. 105, No.19, pp. 7052-7057.

Plugge, C. M; Zhang, W.; Scholten, J. C. M and Stams, A. J. M. (2011). *Metabolic flexibility of sulfate-reducing bacteria*. *Frontiers in Microbiology*. Volume 2. Article 81. doi: 10.3389/fmicb.2011.00081

Proskurowski, G.; Lilley, M. D.; Olson, E. J. (2008). Stable isotopic evidence in support of active microbial methane cycling in low-temperature diffuse flow vents at 9°50'N East Pacific rise. *Elsevier. Geochimica et Cosmochimica Acta*, Vol. 72, pp. 2005-2023.

Rabus, R.; Hansen, T. A.; Widdel, F. (2006). *Dissimilatory sulfate- and sulfur- reducing prokaryotes*. In: *The Prokaryotes, Vol 2: An evolving electronic resource for the microbiological community*, 3rd edition. Eds. Dworkin, M.; Falkow, S.; Rosenberg, E.; Schleifer, K-H.; Stackebrandt, E. chp. 1.22, pp. 659-768. Springer Verlag. DOI: 10.1007/0-387-30742-7_22.

Reeburgh, W. S. (2007). *Oceanic methane biogeochemistry*. *Chem. Rev.* Vol. 107, pp. 486-513.

Reysenbach, A-L. and Schock, E. (2002). *Merging genomes with geochemistry in hydrothermal ecosystems*. *Sciencem* Vol. 296, pp. 1077-1082.

- Robador, Alberto; Jungbluth, Sean P.; LaRowe, Douglas E.; Bowers, Robert M.; Rappé, Michael S.; Amend, Jan P.; Cowen, James P. (2015). *Activity and phylogenetic diversity of sulfate reducing microorganisms in low-temperature subsurface fluids within the upper oceanic crust*. *Frontiers in microbiology*. Vol 5, article 748.
- Roerdink, D. L.; Mason, P. R. D.; Farquhar, J.; Reimer, T. (2012). *Multiple sulfur isotopes in Paleoproterozoic barite identify an important role for microbial sulfate reduction in the early marine environment*. *Earth and Planetary Science Letters*, vol. 331-332, p. 177-186.
- Roerdink, D. L.; Mason, P. R. D.; Whitehouse, M. J.; Reimer, T. (2013). *High-resolution quadruple sulfur isotope analyses of 3.2 Ga pyrite from the Barberton Greenstone Belt in South Africa reveal distinct environmental controls on sulfide isotopic arrays*. *Geochimica et Cosmochimica Acta*, Vol. 117, pp. 203-215.
- Sageman, J.; Jørgensen, B. B.; Greff, O. (1998). *Temperature dependence and rates of sulfate reduction in cold sediments of Svalbard, Arctic Ocean*. *Geomicrobiology Journal*, Vol. 15, pp. 85-100. Taylor and Francis.
- Sarmiento, J. L. and Gruber, N. (2006). *Ocean biogeochemical dynamics*. Princeton University Press.
- Sawicka, J. E.; Jørgensen, B. B. and Bruchert, V. (2012). *Temperature characteristics of bacterial sulfate reduction in continental shelf and slope sediments*. *Biogeoscience*, 9, 3425-3435.
- Schander, C.; Rapp, H. T.; Kongsrud, J. A.; Bakken, T.; Berge, J.; Cochrane, S.; Oug, E.; Byrkjedal, I.; Todt, C.; Cedhagen, T.; Fosshagen, A.; Gebrek. A.; Larsen, K.; Levin, L.; Obst, M.; Pleijel, F.; Støhr, S.; Warèn, A.; Mikkelsen, N. T.; Hadler-Jacobsen, S.; Keuning, R.; Petersen, K. H.; Thorseth, I. H. and Pedersen, R. B. (2010). *The fauna of hydrothermal vents on the Mohn Ridge (North Atlantic)*, *Marine Biology Research*, Vol. 6, No. 2, pp. 155-171, DOI: 10.1080/17451000903147450
- Schouten, S.; Wakeham, S. G.; Hopmans, E. C. and Dampsè, J. S. S. (2002). *Biogeochemical evidence that thermophilic Archaea mediate the anaerobic oxidation of methane*. *Applied and Environmental Microbiology*, Vol. 69, No. 3, pp. 1680-1686.
- Swartz, E and Friedrich, B. (2006). *The H₂-metabolizing prokaryotes*. In: *The Prokaryotes*, Vol 2: An evolving electronic resource for the microbiological community, 3rd edition. Eds. Dworkin, M.; Falkow, S.; Rosenberg, E.; Schleifer, K-H.; Stackebrandt, E. chp. 1. 17, pp. 496-563. Springer Verlag
- Shen, Y and Buick, R. (2003). *The antiquity of microbial sulfate reduction*. *Earth-Science Reviews*. Vol. 64, pp. 243-272. Elsevier.
- Shen, Y.; Buick, R.; and Canfield, D. E. (2001). *Isotopic evidence for microbial sulphate reduction in the early Archaean era*. *Nature*, vol. 410, p. 77-81.
- Sivan, O.; Schrag, D.P.; Murray, R. W. (2007). *Rates of methanogenesis and methanotrophy in deep-sea sediments*. *Geobiology*, Vol. 5, pp. 141-151. DOI: 10.1111/j.1472-4669.2007.00098.x.
- SØRENSEN, K. B.; LAUER A. AND TESKE A. (2004). *Archaeal phylotypes in metal-rich and low activity deep surface sediment of the Peru basin, ODP leg 201, site 1231*. *Geobiology*, 2, pp. 151-161.
- Steen, I. H.; Dahle, H.; Stokke, R.; Roalkvam, I.; Daae, F-L.; Rapp, H. T.; Pedersen, R. B.; Thorseth, I. H. (2016). *Novel barite chimneys at the Lokis Castle vent field shed light on key factors shaping microbial communities and functions in hydrothermal system*. *Frontiers in Microbiology*, Vol. 6, No 1510. doi: 10.3389/fmicb.2015.01510
- Stetter, K. O. (1996). *Hyperthermophilic prokaryotes*. *FEMS Microbiology Reviews*. 18, 149-158
ELSEVIER

- Tarasov, V. G.; Gebruk, A. V.; Mirnov, A. N. and Moskalev, L. I. (2005). *Deep-sea and shallow-water hydrothermal vent communities: two different phenomena?* Chemical Geology, Vol. 224, pp. 5-39. Elsevier.
- Teske, A.; Hinrichs, K-U.; Edgcomb, V.; Gomez,ADV.; Kysela, D.; Sylva, S. P.; Sogin, M. L.; Jannasch, H.W. (2002). *Microbial Diversity of Hydrothermal Sediments in the Guaymas Basin: Evidence for Anaerobic Methanotrophic Communities*. Applied and Environmental Microbiology, Vol. 68, No. 4, pp. 1994-2007. DOI: 10.1128/AEM.68.4.1994-2007.2002.
- Tivey, Margaret k. (2007). *Generation of seafloor hydrothermal vent fluids and associated mineral deposits*. Oceanography, vol. 20, No. 1. The oceanography society.
- Ueno, Y.; Ono, S.; Rumble, D.; and Maruyama, S. (2008). *Quadruple sulfur isotope analysis of ca. 3.5 Ga Dresser Formation: New evidence for microbial sulfate reduction in the early Archean*. Geochimica et Cosmochimica Acta, Vol. 72, pp. 5675-5691
- Valentine, D. L. and Reeburgh, W. S. (2000). *New perspective on anaerobic methane oxidation*. Environmental microbiology, Vol. 2, Nr. 5, pp. 477-484.
- Vogt, C.; Knies, J. (2008). *Sediment dynamics in the Eurasian Arctic Ocean during the last deglaciation-the clay minerals group smectite perspective*. Marine Geology, Vol. 250, pp.211-222 Elsevier. doi:10.1016/j.margeo.2008.01.006.
- Von Damm, K. L. (1995). *Controls on the chemistry and temporal variability of seafloor hydrothermal fluids*. Pp. 222-247. In *Seafloor Hydrothermal Systems: Physical, Chemical, Biological, and Geological Interactions*. Eds: S.E. Humphris, R.A. Zierenberg, L.S. Mullineaux, and R. E. Thomson. Geophysical monograph 91. American geophysical union.
- Wallmann, K. and Aloisi, G. (2013). *The global carbon cycle: geological processes*. In: Knoll, Andrew H., Canfield, Donald E., Konhauser, Kurt O., eds. Fundamentals of geobiology. Wiley-Blackwell chp. 3.
- Wankel, S.D.; Germanovich, L.N.; Lilley, M.D.; Genc, G.; DiPerna, C. J.; Bradley, A.S.; Olson, E.J.; Girguis, P.R. (2011). *Influence of subsurface biosphere on geochemical fluxes from diffuse hydrothermal fluids*. Nature Geoscience. Vol. 4, pp. 461-468. DOI: 10.1038/NGEO1183
- Weber, A. and Jørgensen, B. B. (2002). *Bacterial sulfate reduction in hydrothermal sediments of the Guaymas Basin, Gulf of California, Mexico*. Deep-Sea Research, part 1, Vol. 49, pp. 827-841.
- Welhan, J. A. (1988). *Origins of methane in hydrothermal systems*. Chemical geology, Vol. 71, pp. 183-198. Elsevier.
- Widdel, F.; Boetius, A.; and Jørgensen, B. B. (2006). Anaerobic biodegradation of hydrocarbons including methane. In: *The Prokaryotes, Vol 2: An evolving electronic resource for the microbiological community, 3rd edition*. Eds. Dworkin, M.; Falkow, S.; Rosenberg, E.; Schleifer, K-H.; Stackebrandt, E. chp. 1.33, pp. 659-768. Springer Verlag. DOI: 10.1007/0-387-30742-7_22

9.2. weblink

- 1) <http://www.indiana.edu/~g105lab/1425chap13.htm> (obtained 31.05.16)

Appendix 1

All data are compiled in Google Doc and can be obtained by following the link.

<https://docs.google.com/spreadsheets/u/0/>